TRAF6 prevents autoimmunity by homeostatic suppression of MALT1 paracaspase activity

Dissertation

der Fakultät für Biologie

der Ludwig-Maximilians-Universität München

angefertigt am

Helmholtz Zentrum München

Deutsches Forschungszentrum für Gesundheit und Umwelt

Institut für Molekulare Toxikologie und Pharmakologie

Abteilung Zelluläre Signalintegration

vorgelegt von

Thomas Jerome O'Neill

München, den 12. April 2021

Diese Dissertation wurde angefertigt

unter der Leitung von **Prof. Dr. Daniel Krappmann**

am Helmholtz Zentrum München

Deutsches Forschungszentrum für Gesundheit und Umwelt

Institut für Molekulare Toxikologie und Pharmakologie

Abteilung Zelluläre Signalintegration

Erstgutachter/in: Prof. Dr. Daniel Krappmann

Zweitgutachter/in: Prof. Dr. Michael Boshart

Tag der Abgabe: 12. April 2021

Tag der mündlichen Prüfung: 28. October 2021

Eidesstattliche Erklärung

Ich versichere hiermit an Eides statt, dass meine Dissertation selbstständig und ohne unerlaubte Hilfsmittel angefertigt worden ist.

Die vorliegende Dissertation wurde weder ganz, noch teilweise bei einer anderen Prüfungskommission vorgelegt.

Ich habe noch zu keinem früheren Zeitpunkt versucht, eine Dissertation einzureichen oder an einer Doktorprüfung teilzunehmen.

München, den 12. April 2021 Thomas J. O'Neill

TABLE OF CONTENTS

List of Figures

List of Tables

1 Summary

Balance of immune signaling in T lymphocytes is critical for a functional adaptive immune response. Upon antigen engagement of a T cell receptor (TCR), assembly of the CARD11-BCL10-MALT1 (CBM) complex drives downstream canonical NF-κB signaling pathway activation, which promotes T cell survival, differentiation, and proliferation. Within the CBM complex, MALT1 acts as both a scaffold to induce NF-κB activation and a protease that facilitates optimal T cell responses. Upon antigenic stimulation, MALT1 recruits the E3 ubiquitin ligase TRAF6 to the CBM complex, but the physiological role of this interaction has remained elusive. Therefore, novel murine models lacking interaction between MALT1 and TRAF6 were generated by CRISPR-Cas9 gene editing. Strikingly, abrogation of TRAF6 binding to MALT1 disrupts immune homeostasis and causes fatal, early-onset autoimmune inflammation. While NF-κB activity is completely dependent on TRAF6 expression, as well as MALT1-TRAF6 interaction, constitutive MALT1 cleavage activity was shown to be the direct effect of abolished binding to TRAF6. Secondary genome editing and inactivation of MALT1 protease function in mice completely rescues the fatal phenotype triggered by the disrupted MALT1-TRAF6 interaction, revealing that aberrant MALT1 protease activity is responsible for the autoinflammation caused by defective TRAF6 regulation. Further, autoimmunity in T cell specific TRAF6 knockout mice was ameliorated by therapeutic treatment with a potent MALT1 inhibitor. Thus, TRAF6 acts as both a positive regulator of CBM-dependent NF-κB signaling upon antigen engagement and as a negative regulator of MALT1 protease activity in resting T cells. Indeed, TRAF6 functions as a brake on MALT1 protease activity in resting T cells, essential for the maintenance of peripheral tolerance. By unraveling the complex dual role of TRAF6 in T cells, these data provide a rationale for the use of MALT1 inhibitors for new therapeutic approaches in the treatment of autoimmune disease.

2 Zusammenfassung

Das Gleichgewicht von Immunsignalwegen in T-Lymphozyten ist entscheidend für eine funktionelle adaptive Immunität. Durch die Antigenbindung an einen T-Zell Rezeptor (TZR) wird der CARD11-BCL10-MALT1 (CBM) Komplex gebildet, welcher den kanonischen NF-κB Signalweg aktiviert und damit Überleben, Differenzierung und Proliferation von T-Zellen vermittelt. Als Teil des CBM Komplexes fungiert MALT1 sowohl als Gerüstprotein zur Induktion von NF-κB als auch als Protease, welche eine optimale Immunantwort gewährleistet. Antigenstimulation führt dazu, dass MALT1 die E3-Ubiquitin Ligase TRAF6 an den CBM Komplex rekrutiert, aber die genaue physiologische Relevanz dieser Interaktion ist unklar. Aus diesem Grund wurden neuartige Mausmodelle mit fehlender MALT1-TRAF6 Interaktion mit Hilfe von CRISPR-Cas9 Genom Editierung generiert. Die Zerstörung der MALT1-TRAF6 Interaktion führt zu einer Störung der Immunhomöostase und einer früh einsetzenden und tödlich verlaufenden Autoimmunität bei Mäusen. Während die NF-κB Aktivierung vollständig von TRAF6 und der Rekrutierung von TRAF6 an MALT1 abhängt, führt der Verlust von TRAF6 gleichzeitig zu einer konstitutiven Spaltung von MALT1 Substraten. Sekundäre Genomeditierung und Inaktivierung der MALT1 Proteaseaktivität in Mäusen hebt den tödlichen Phänotyp verursacht durch den Verlust der MALT1-TRAF6 Interaktion vollständig auf, was somit beweist, dass die konstitutive MALT1 Proteaseaktivität verantwortlich für die Autoentzündungen nach fehlender TRAF6 Interaktion ist. Weiterhin mildert sich die Autoimmunität in Mäusen mit spezifischer Ablation von TRAF6 in T Zellen durch gezielte therapeutische Behandlung mit einem potenten MALT1 Inhibitor. Somit ist TRAF6 ein positiver Regulator der CBM Komplex-abhängigen Signalübertragung nach Antigenstimulation in aktivierten T Zellen und gleichzeitig ein negativer Regulator der MALT1 Protease Aktivität in ruhenden T-Zellen. Durch die Unterbindung der Enzymaktivität von MALT1 in ruhenden T-Zellen trägt TRAF6 somit entscheidend zur Aufrechterhaltung einer peripheren Immuntoleranz bei. Diese Daten verdeutlichen die komplexe duale Rolle von TRAF6 und bieten eine Grundlage für die Benutzung von MALT1 Inhibitoren in neuen Therapieansätzen zur Behandlung von Autoimmunerkrankungen.

3 Introduction

Lymphocytes protect the host against various external and internal risks, from pathogenic attack to the proliferation of tumor cells. Induction of the immune system leads to differentiation, proliferation, and survival of lymphocytes to yield a strong, coordinated response. The functions of the immune system are generally separated into two groups: innate and adaptive immunity.

3.1 Innate immunity

The innate immune system acts as the first line of defense against pathogenic invasion (Akira et al., 2006). Innate immunity is dependent upon recognition of a limited number of pathogenic signals via germline encoded pattern-recognition receptors (PRRs). PRRs recognize and bind to pathogenic macromolecules known as pathogen-associated molecular patterns (PAMPs). Various PRRs, many of which are Toll-like receptors (TLRs), recognize different classes of macromolecules, including lipids, nucleic acids, and heat shock proteins (Akira et al., 2006). For example, TLR7 recognizes viral RNA (Diebold et al., 2004), and TLR9 recognizes viral DNA (Krug et al., 2001). Signaling downstream of TLRs leads to activation of transcription factors, including nuclear factor kappa-light-chain-enhancer of activated B cells (NF-κB), activator protein 1 (AP-1), and interferon regulatory factors (IRFs) to induce proinflammatory cytokine and interferon (INF) production (Akira & Takeda, 2004). TLRs are expressed on the surface of diverse cell types, including phagocytes like macrophages and dendritic cells (DC) and antigen presenting cells (APCs) like B cells of the adaptive immune system (Akira et al., 2006). In common with the adaptive immune system, functional innate immunity is dependent upon discrimination of self, facilitated both by evolution of TLR specificity and control of receptor localization (Barton et al., 2006). The mechanisms of innate immunity lead to elimination of a majority of pathogens and induction of the targeted mechanisms of the adaptive immune system.

3.2 Adaptive Immunity

Adaptive immunity is mediated by B and T lymphocytes. Whereas the innate immune system has evolved to recognize a limited set of antigens, adaptive immunity is malleable and generates long-term memory. The receptors expressed on cells of the adaptive immune system therefore have mechanisms for the recognition of novel antigens. Crosstalk is essential between the two systems: innate signaling lead to induction of adaptive immunity, and mechanisms exist in adaptive immunity which affect innate signaling.

3.2.1 Humoral immunity in B cells

B cells are the main component of a humoral immune response. B cells can act as APCs to activate T cells and, upon interaction with a T cell, they secrete antibodies which mark bacteria and other

invaders for targeting by other immune cells, including those of the innate immune system. Indeed, B cell receptors (BCRs) are essentially membrane bound immunoglobulins (Ig) (antibodies) which, once ligated to an antigen induce plasma B cell behavior, secreting antibodies to target and neutralized the offending entity. This process is known as antibody opsonization and is an essential aspect of humoral, antibody-mediated immunity (Kutteh et al., 2014). The immunoglobulins produced by a B cell are tissue-specific, and therefore influenced by the cellular environment (Parkin & Cohen, 2001).

B lymphocyte development and maturation occurs in the bone marrow (Parkin & Cohen, 2001). Pre-B cell receptor (BCR) diversification occurs through mechanisms of gene rearrangement. One of these mechanisms is called V(D)J recombination (Figure 3-1). BCR genes are composed of variable (V), diversity (D), and joining (J) segments of DNA, and association of these segments has evolved to contain aspects of randomness. Not only is the multiplicity of each segment variable, but purposeful inaccuracy in splicing and random insertion of nucleotide bases introduces mutations which induce frame shifts and entirely novel amino acid sequences upon translation. V(D)J recombination is driven by RAG recombinase proteins, which induce dsDNA breaks, and DNA repair enzymes to repair those breaks. In this way, a coherent repertoire of receptors is developed which can recognize the exceptionally large pool of possible antigens confronted by the host. V(D)J recombination is tightly regulated due to the potential for catastrophe in dysregulated dsDNA cleavage, and though infrequent, these errors indeed contribute to development of cancers (Mills et al., 2003). Loss of RAG protein function yields autoimmunity, underscoring the need for a diverse B cell repertoire (Zhang et al., 2005). Following V(D)J recombination, B cells go through enzyme catalyzed Ig gene rearrangement to further diversify the BCR. Unique to BCR diversification is the pro-mutagenic activity of the enzyme AID (activation-induced deaminase), which deaminates and converts random cytosine bases to uracil bases, greatly expanding the BCR repertoire (Maizels, 2005). Following rearrangement, B cells express a BCR composed of one heavy and one light chain which combine for antigen recognition. B cells undergo negative and positive selection to eliminate harmful recognition of self-peptides (Giltiay et al., 2012).

3.2.2 Cell-mediated immunity in T cell

T cells are the main drivers of cell-mediated immunity. Recognition and activation of a T cell by an antigen presented by an APC initiates proliferation and differentiation events, yielding strong, specific immune responses. A functional adaptive immune system therefore requires specific recognition of an enormous number of antigens by T cell receptors (TCRs) (Parkin & Cohen, 2001). Clonal diversity is made possible through gene rearrangement mechanisms which produce novel

TCRs. Early progenitor T cells are produced in the bone marrow (BM), but T cells progenitors migrate out of the BM for maturation and clonal selection in the cortex and medulla of the thymus. T lymphocyte maturation follows a set of well-described changes to surface marker expression which eventually yields mature T cells which can fulfill their roles in defending against an unpredictable array of pathogenic and host-derived challenges (Kumar et al., 2018). T cell receptor (TCR) diversification via V(D)J rearrangement follows roughly the same process as in B cells. These

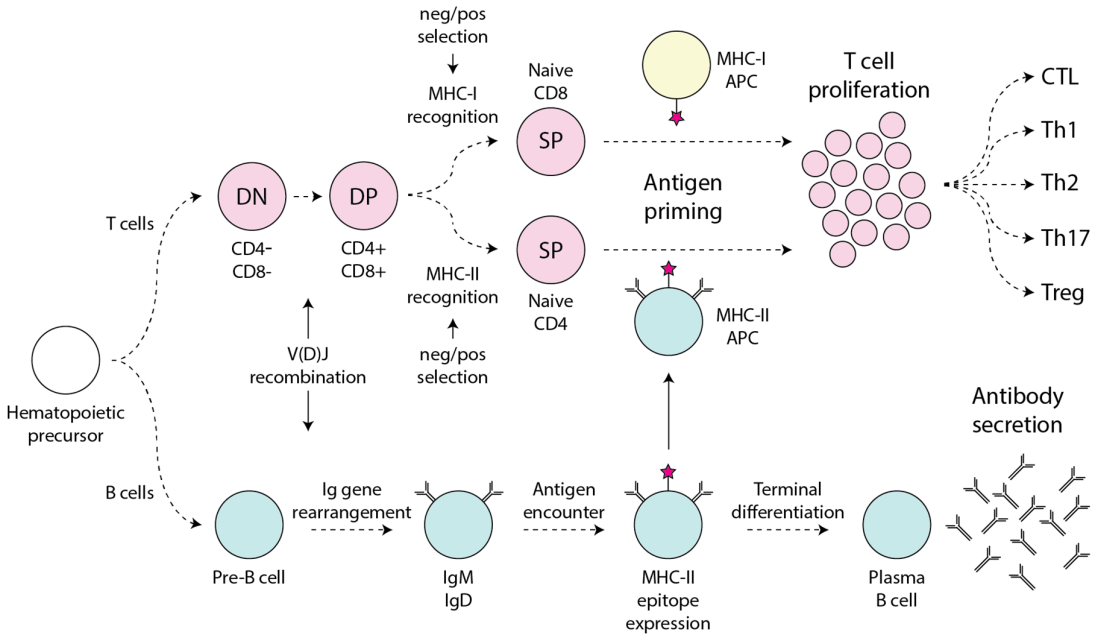

Figure 3-1. Overview of T and B lymphocyte maturation and differentiation.
Lymphocyte differentiation begins in the bone marrow (BM). B cell maturation continues in the BM, while pre-T cells are transported to the thymus early in development. Both B and T cells undergo V(D)J recombination and gene rearrangement to increase variability of their respective antigen receptors. Cells are presented with self-peptide MHC complexes during positive and negative selection, and cells which bind too weakly or strongly are removed from the lymphocyte pool. Mature B cells bind to and internalize antigens where they are processes and expressed on the cell surface bound to MHC-II complexes. These MHC-II antigen-presenting cells (APCs) present their antigens to naïve single-positive (SP) CD4 T cells, leading to T cell proliferation and differentiation into various helper T cell (Th) subclasses and regulatory T cells (Tregs). Following B cell epitope presentation, B cells differentiate into plasma B cells, secreting antibodies to mark antigens for phagocytosis in a process termed antibody opsonization. Naïve CD8 T cells interact with MHC-I APCs giving rise to cytotoxic T lymphocytes (CTLs).

mechanisms yield a theoretical T cell repertoire with specific binding to an estimated 10^{10} epitopes (Arstila et al., 1999), although this is disputed by newer RNA sequencing methods and the true repertoire is likely much lower (Laydon et al., 2015).

T cells progress through an initial double negative (DN) phase of maturation during which they do not express CD4 or CD8 receptors (Figure 3-1) (Parkin & Cohen, 2001). During this phase, the pre-TCR is expressed as a pre-Tα/mature-Tß TCR (von Boehmer & Fehling, 1997). Only upon successful pre-TCR expression and gene recombination will the pre-Tα chain be replaced by a mature, recombined Tα chain and a mature TCRαß receptor is expressed on double positive (DP) cells (CD4+

CD8+). DP cells go through a process of sensitization to self-peptides expressed on thymic epithelial cells (TECs) and dendritic cells (DCs), during which they are introduced to an exhaustive repertoire of self-epitopes bound to major histocompatibility complex (MHC) molecules (Taniuchi, 2018). This process establishes central tolerance. T cells must also be screened against peptides which are expressed in other tissues than the thymus, a process mediated by the transcription factor AIRE (Perniola, 2018). The selection process is essential for eliminating T cells with strong recognition of self-peptides, which would yield autoimmunity. During selection, T cells which are over reactive to self-peptides are killed by apoptosis via negative selection, while cells which have insufficient specificity to the MHC molecules die in a process termed "death by neglect" (Germain, 2002). T cells require constant expression of a CD4 or CD8 co-receptor for binding to epitopes, and loss of co-receptor expression leads to functional T cell inactivation, called anergy (Fathman & Lineberry, 2007).

Each epitope encountered by the TCR, both during and after development, is bound to an MHC moldecule, of which two classes with distinct cellular functions exist (J. Oh & Shin, 2015). MHC class I (MHC-I) molecules are present on all nucleated cells, and express intracellular epitopes to report on changes within the cell, e.g. viral or bacterial infections. Recognition of MHC-I molecules by CD8+ cytotoxic T lymphocytes (CTLs) leads to apoptosis and phagocytosis of the MHC-I-expressing cell. MHC class II molecules are expressed on APCs, which present epitopes from the extracellular environment. APCs collect antigens from the cellular milieu via endocytotic pathways and present them on the cell surface on an MHC-II molecule, where they are recognized by CD4+ helper T (Th) cells. MHC epitope recognition leads to T cell differentiation, yielding CTLs, Th cell specificities (Th1, Th2, and Th17) and regulatory T cells (Tregs) (Figure 3-1) (Raphael et al., 2015).

Th cell sub-types differ in the cytokines which they produce (Swain, 1995), and which cell-type a naïve Th0 cell will differentiate into is in turn influenced by cytokine signaling (Parkin & Cohen, 2001). Accordingly, Each Th cell subtypes has a different effector T (Teff) cell function mediated in part by cytokine production: Th1 cells produce IFNγ and TNFα and are important in cell-mediated responses, Th2 cells produce primarily IL-4, IL-5, IL-10, and IL-13 to promote humoral immune responses, and Th17 cell signaling is IL-17 driven (Raphael et al., 2015). IL-17 activates cells of the innate immune system and induces the release of inflammatory mediators from other cells. IFNγ and TNFα are strong proinflammatory cytokines which are prevalent in autoimmune diseases. Indeed, overproduction of IFNγ can have a pathogenic rather than ameliorative effect in combating disease (Raphael et al., 2015). Different T cell subsets also regulate each other through cytokine signaling. For example, IL-4 production from Th2 cells suppresses IFNγ from Th1 cells. Additionally, crosstalk

with the innate immune system is mediated by cytokines: IFNγ increases expression of TLRs on innate immune cells, IL-4 is essential for DC differentiation, and IL-17 activates innate immune cells (Raphael et al., 2015).

3.3 Regulatory T cells and T cell homeostasis

Central to the maintenance of a functional adaptive immune system is tolerance: the differentiation between host and pathogen. Teff cells are responsible for protection against pathogens and cancer cells but can also drive autoimmunity by self-antigen recognition. Regulatory T cells (Treg) are a subclass of T lymphocytes which act in intricate balance with Teff cells to suppress excessive activity and are essential for peripheral tolerance. An underactive immune system can lead to immunosuppression and cancer, while an immune response with insufficient specificity and regulation can yield autoimmunity. Many common cancers arise from loss of homeostasis in the immune system (Picard et al., 2018).

Differentiation and function of the Treg lineage requires sustained expression of FoxP3 (forkhead box P3), dependent upon signaling by the cytokines IL-2 and IL-5 (Josefowicz & Rudensky, 2009; Sakaguchi et al., 2008).Tregs which lose FoxP3 expression cease to be Tregs, instead acquiring Teff cell function, indicating that FoxP3 expression is necessary and sufficient for Treg identity (Josefowicz & Rudensky, 2009; Williams & Rudensky, 2007). FoxP3+ Treg function is broad and is responsible for tolerance toward self, autologous tumor cells, and the commensal microbes of the host microbiome (Sakaguchi et al., 2008; Swiatczak & Cohen, 2015). To these ends, Tregs have an expansive repertoire, including cell surface marker expression and cytokine production, primarily immunosuppressive IL-35. The essential role of Tregs is apparent in FoxP3 mutant scurfy mice, which develop a severe, spontaneous autoimmune phenotype (Bennett et al., 2001), and in human patients with immune dysregulation polyendocrinopathy enteropathy X-linked (IPEX) syndrome, an autoimmune disease marked by Treg deficiency (Bacchetta et al., 2018). Treg development is unique, in that Tregs are already functional in the thymus, whereas conventional T cells do not become antigen-primed until entering the periphery. This is due to Tregs being primed by self-peptides as a part of immune self-tolerance. Self-peptide recognition allows for Tregs to recognize and suppress Teff cells via direct cell-cell interaction and by secretion of cytokines and other signaling molecules (Sakaguchi et al., 2020).

3.3.1 TCR signaling

Ligation of an epitope presented on an MHC-I or MHC-II molecule to the TCR leads to assembly of supramolecular receptor clusters, involving the binding of an MHC-I or MHC-II molecule to the TCR and its respective CD8 or CD4 glycoprotein (Hayden & Ghosh, 2012). Binding of the TCR alone leads

to weak TCR activation, and full activity requires simultaneous interaction of co-receptors such as B7 (CD80 or CD86) and the T cell coreceptor CD28 (Kane et al., 2002; Schmitz & Krappmann, 2006). Upon TCR complex assembly, intracellular ITAM phosphorylation initiates a cascade of activation events (Figure 3-2). Zeta chain-associated protein kinase 70 kDa (ZAP70) is recruited to the receptor, initiating a phosphorylation cascade involving the linker proteins linker for the activation of T cells (LAT) and SH2-containing leukocyte phosphoprotein 76 kDa (SLP-76) and leading to eventual activation of phospholipase C (PLC) γ (Schulze-Luehrmann & Ghosh, 2006). PLCγ catalyzes the hydrolysis of membrane-associated phosphatidylinositol 4,5-bisphosphate (PIP_2), which splits into the signaling molecules Inositol triphosphate (IP_3) and diacylglycerol (DAG). DAG is hydrophobic, remaining in the plasma membrane and activating protein kinase C (PKC) θ, while IP_3 binds to its cognate receptor on the ER, triggering the release of Ca^{2+} ions for activation of calcineurin, which initiates the NFAT activation pathway. Downstream of PLCγ, mitogen-activated protein kinase kinase (MEK) is activated, leading to extracellular signal-regulated kinase (ERK1/2) activation and AP-1 transcription factor activity (Hayden & Ghosh, 2012). Strong PKCθ activity requires phosphorylation by protein-dependent kinase 1 (PDK-1), which is activated by co-receptor binding. PKCθ phosphorylates caspase recruitment domain 11 (CARD11), which releases from autoinhibition and binds to heterodimers composed of B cell lymphoma/leukemia 10 (BCL10) and mucosa-associated lymphoid tissue lymphoma translocation 1 (MALT1) to form the CARD11-BCL10-MALT1 (CBM) complex (Thome et al., 2010). MALT1 binds to the E3 ligase tumor necrosis factor receptor (TNFR)-associated factor 6 (TRAF6), which polyubiquitinates proximal substrates including MALT1 and IKKß (Oeckinghaus et al., 2007) leading to association of the TAK1-TAB2/3 complex and activation of the downstream IκB kinase (IKK) complex. The IKK complex mediates phosphorylation and ultimately proteasomal degradation of inhibitory nuclear factor of kappa light polypeptide gene enhancer in B-cells inhibitor (IκB) proteins, most prominently IκBα, and NF-κB dimers can enter the nucleus to act as transcription factors (Meininger et al., 2016).

3.3.2 Tonic TCR signaling

Normally, immune cell signaling is initiated by antigen ligation to a receptor (Figure 3-2). For example, only when a T cell encounters a specific antigen-loaded MHC complex on an APC will the cascade of events leading to NF-κB activation begin. However, low level, antigen receptor signaling exists in the absence of a strong cognate antigen, a process known as 'tonic signaling'. The role of tonic signaling in B cells is well described and is essential for B cell maturation and survival. Inducible deletion of the BCR on B cells leads to cell death, but B cells expressing a modified BCR lacking antigen-binding domains still undergo low level tonic signals, indicating independent mechanisms for tonic signaling which are, nevertheless, still dependent upon the BCR (Lam et al., 1997; Myers et al.,

2017). BCR KO cells can be rescued by constitutive activation of PI3K downstream of the BCR (Srinivasan et al., 2009).

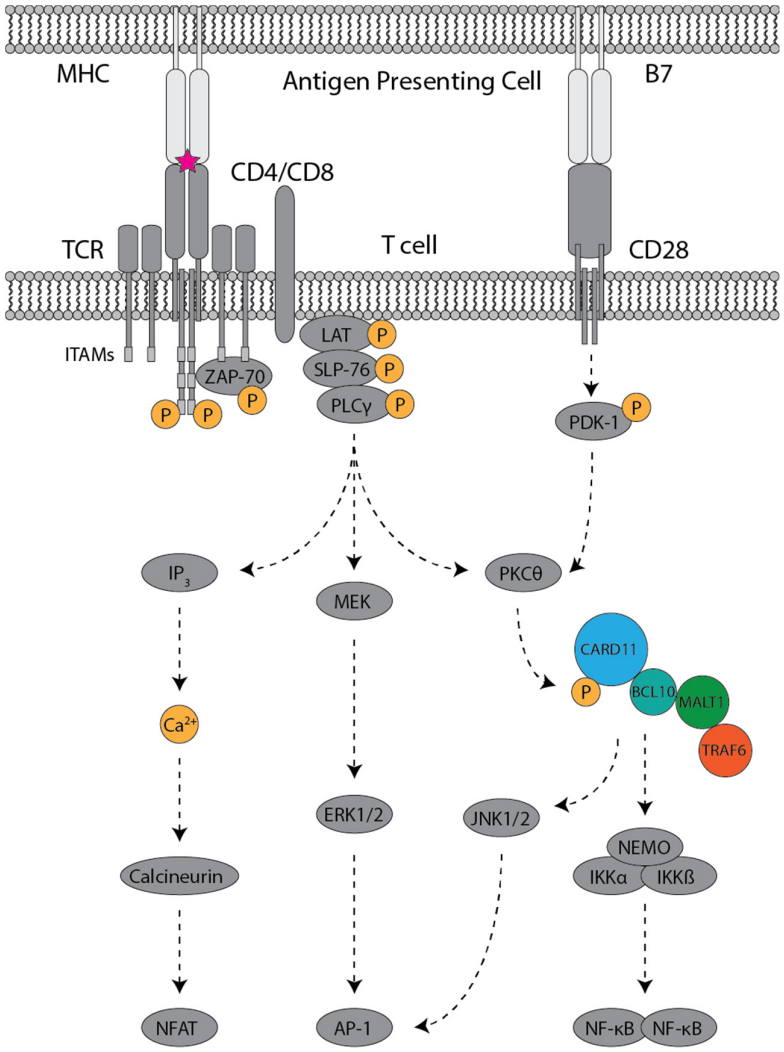

Figure 3-2. Signaling downstream of TCR antigen ligation.
Ligation of an MHC epitope to a T cell receptor in the presence of co-receptor binding leads to initiation of signaling pathways. Upon binding, phosphorylation of intracellular ITAMs leads to association of ZAP70 and subsequent phosphorylation and assembly of LAT and SLP-76. SLP-76 activates the growth factor and lipase PLCγ by phosphorylation, which catalyzes hydrolysis of the phospholipid PIP_2 to IP_3 and DAG. IP_3 induces ER-dependent Ca^{2+} signaling and NFAT activation, while DAG is essential for activation of the transcription factors AP-1 via ERK signaling and NF-κB via activation of PKCθ. PKCθ and other kinases activate CARD11 by phosphorylation, inducing CBM complex assembly, IKK complex activation, and nuclear transport of NF-κB.

Tonic signaling in T cells is not well defined and its existence and function remains controversial (Myers et al., 2017). In contrast to B cells, loss of TCR expression does not lead to cell death but does contribute to lower lifespan of T cells. This argues that tonic signals do not play a central role in T cell maturation, but instead are important for maintenance of T cell homeostasis (Polic et al., 2001). Furthermore, it is clear that resting T cells come into contact with self-peptide MHC complexes in the

periphery, and that these interactions generate TCR-dependent, low-level signals that nevertheless initiate downstream pathways (Stefanová et al., 2002). Such sub-threshold signals were apparent in phosphorylation events downstream of the TCR which could no longer be detected upon blocking of MHC-II signals or removing cells from the peripheral tissue (Stefanová et al., 2003). Therefore, it has been hypothesized that tonic signaling is dependent upon some of the same mechanisms as strong, antigen ligation dependent TCR signaling, but its relevance requires further clarification.

3.4 NF-κB signaling

The NF-κB family of transcription factors is central to immune regulation and has broad implications in survival, differentiation, and proliferation of immune cell populations (Meininger & Krappmann, 2016). Accordingly, NF-κB activity is tightly controlled, and loss of proper regulation can have severe consequences, leading to autoimmune disease or immune suppression.

The NF-κB protein family is composed of five members: RelB, c-Rel, p65 (RelA), p100, and p105 (Hayden & Ghosh, 2012). The NF-κB precursors p100 and p105 are further processed to form the active p50 and p52, respectively. In resting cells, NF-κB proteins are maintained as inactive dimers in the cytosol by inhibitory IκB proteins which shield their nuclear localization signals (Figure 3-3). The primary IκB protein in signaling downstream of T cell and B cell receptors is IκBα, which primarily targets p65:p50 NF-κB heterodimers (Hayden & Ghosh, 2012). IκBα is phosphorylated by the upstream IKK complex, composed of the subunits IKKα, IKKß, and IKKγ (also known as NF-kappa-B essential modulator (NEMO)). Following phosphorylation, IκBα is modified with K48-linked ubiquitin chains and subsequently degraded by the proteasome, and captive NF-κB proteins are released for nuclear import (Figure 3-3). Following release, NF-κB proteins bind to DNA sequences and promote the transcription of essential factors for cell survival and proliferation (Meininger & Krappmann, 2016). The IKK complex is activated by phosphorylation and ubiquitination events from upstream signaling complexes. Diverse upstream signaling pathways converge to activate the IKK complex but signaling downstream of the IKK complex is common to all pathways. Upstream signals include TNF receptors (TNFR), Toll-like receptors (TLR), interleukin (IL) receptors, and antigen receptors (TCR and BCR) (Hayden & Ghosh, 2008).

3.5 The CBM complex and the E3 ligase TRAF6

The CBM complex acts as a switch in the NF-κB pathway, directing receptor-dependent signals from TCR and BCR to IKK complex activation. Further, CBM complex assembly activates the enzymatic function of MALT1 (Ruland & Hartjes, 2019). Neither the scaffolding nor the enzymatic activities of

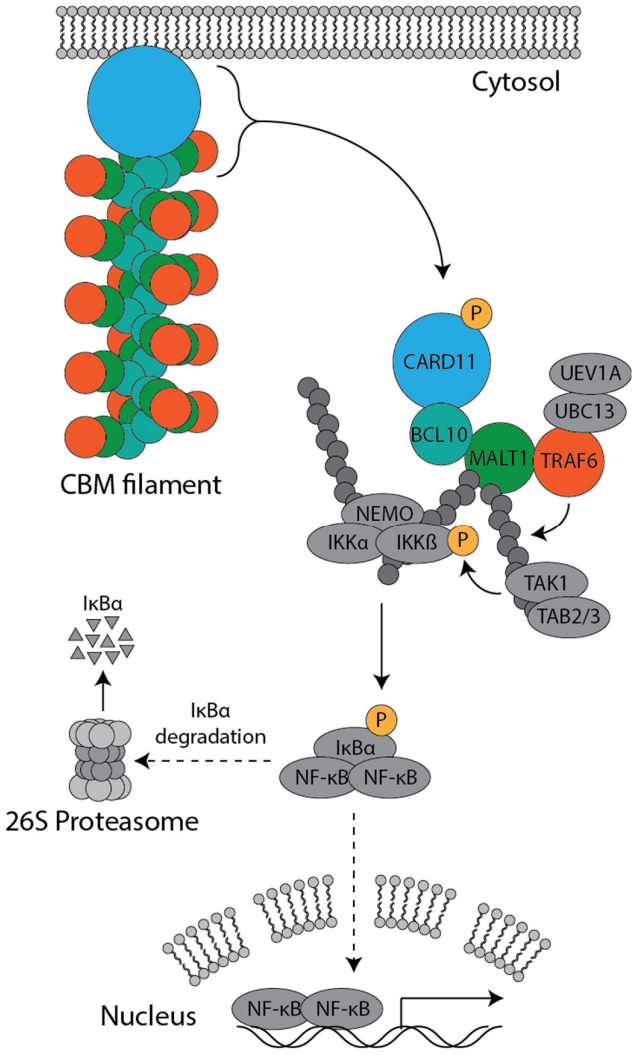

Figure 3-3. NF-κB signaling via CBM complex assembly
TCR ligation leads to formation of the CBM complex. As a protein scaffold, MALT1 binds to the E3 ligase TRAF6, leading to ubiquitination of MALT1 and the IKK complex member NEMO. Polyubiquitination of MALT1 leads to association of the TAB2/3-TAK1 complex, which activated IKKß by phosphorylation. IKKß in turn phorphorylates IκBα, marking it for ubiquitination and proteasomal degradation. NF-κB proteins move to the cell nucleus and act as transcription factors for transcription of genes required for cellular survival and proliferation.

MALT1 can occur without CBM complex association. Upon antigenic stimulation, CARD11, BCL10, and MALT1 form a supramolecular complex in which CARD11 acts as a membrane-bound seed, and MALT1-BCL10 dimers form a spindle which elongates from the membrane (David et al., 2018; Qiao et al., 2013; Schlauderer et al., 2018). This spindle acts as an extended surface area for docking of

other molecular factors, most significantly the E3 ligase TRAF6, which binds to MALT1 and ubiquitinates downstream members of the pathway. Interestingly, MALT1 activation is dependent upon CBM filament formation, but MALT1 retains activity upon dissociation from the high-order complex (Eitelhuber et al., 2015).

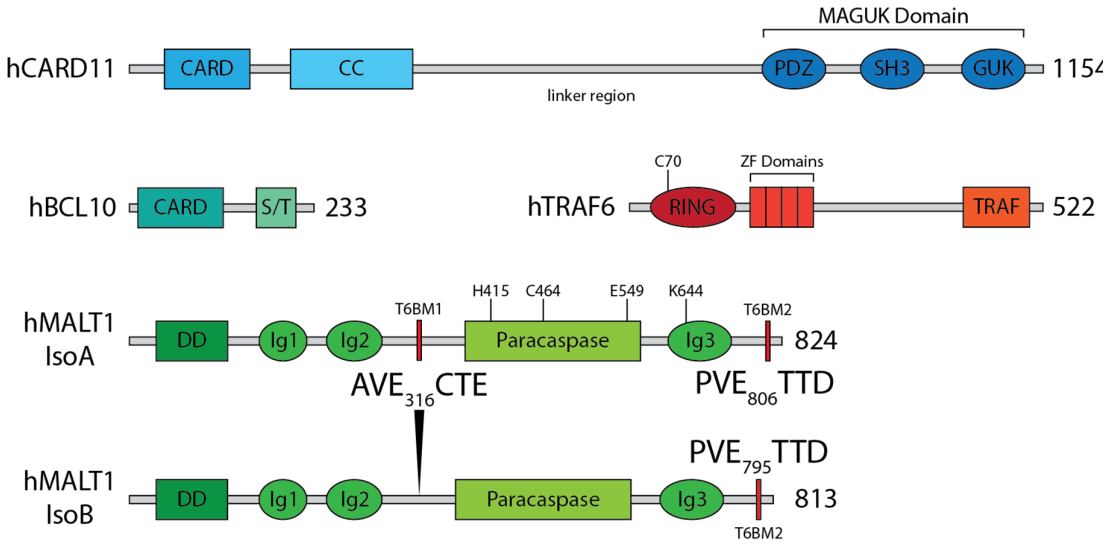

Figure 3-4. CARD11, BCL10, MALT1, and TRAF6 domains and isoforms.
Components of the human CBM complex, composed of CARD11, BCL10, and MALT1, and the E3 ligase TRAF6. The C-terminal caspase recruitment domain (CARD) and coiled-coil (CC) domains of CARD11 bind to the linker region to induce autoinhibition in resting cells. Phosphorylation in the linker region releases autoinhibition, permitting interaction with BCL10-MALT1 heterodimers via CARD-CARD interaction with BCL10. The membrane associated guanylate kinase (MAGUK) domain binds CARD11 to the membrane. The death domain (DD) of MALT1 interacts with the CARD domain of BCL10. MALT1 has additional enzymatic activity through its catalytic diad (H415 and C464) in the paracaspase domain. MALT1 is expressed in two isoforms: MALT1A, containing two binding motifs for interaction with the E3 ligase TRAF6, and MALT1B, containing only the second binding motif. TRAF6 has an N-terminal RING domain with catalytic residue C70, with an N-terminal multimeric zinc-finger domain and the C-terminal TRAF domain for binding to adaptor proteins.

3.5.1 CARD11

Since its discovery in 2001 as a novel caspase recruitment domain (CARD) protein (Bertin et al., 2001; Gaide et al., 2001), CARD11 has been recognized as a central protein in immunological signaling. CARD11, also called CARMA1 (Caspase recruitment domain-containing membrane-associated guanylate kinase protein-1), is a member of the CARD family of scaffold/adaptor proteins which also includes CARD9, CARMA2 (CARD14), and CARMA3 (CARD10) (Juilland & Thome, 2018). Whereas MALT1 and BCL10 are ubiquitously expressed in all cells, CARD protein expression is cell-type specific, and signaling occurs through formation of alternative CARD-BCL10-MALT1 complexes (Ruland & Hartjes, 2019). For example, NF-κB signaling in myeloid and mast cells is mediated by CARD9 (Bertin et al., 2000; Ruland, 2008). Traditionally, the nomenclature “CBM complex” is reserved for CARD11-BCL10-MALT1 complex signaling in T cells, B cells, and natural killer (NK) cells.

CARD11 is composed of an N-terminal CARD domain, a coiled-coil (CC) domain and linker region, and a membrane-associated guanylate kinase (MAGUK) domain for membrane interaction (Figure 3-4) (Bedsaul et al., 2018). CARD11 is maintained inactive in resting cells via intracellular interactions between the inhibitory linker region and CARD/CC domains (Lamason et al., 2010). CARD11 inactivity in resting T cells is vital for maintenance of tolerance, and mutations within the auto-inhibitory linker and CC domains of CARD11 leads to loss of autoinhibition and constitutive lymphocyte signaling, a common characteristic of B cell lymphomas (Lenz et al., 2008). CARD11 is activated following antigen ligation to a T or B cell receptor. Kinases, including PKCθ in T cells and PKCß in B cells, are activated and phosphorylate within the linker region of CARD11, releasing intracellular interactions and repositioning CARD11 into an open, active conformation, whereupon it acts as a seed for binding to preformed BCL10-MALT1 dimers in the cytosol via CARD-CARD interaction to form the CBM filament (Matsumoto et al., 2005; McCully & Pomerantz, 2008; Sommer et al., 2005).

3.5.2 BCL10

BCL10 was first characterized from the translocation t(1;14)(p22;q32) which leads to BCL10 overexpression and MALT lymphoma (Willis et al., 1999). BCL10 contains an N-terminal CARD domain for association with CARD-family proteins via a homotypic CARD-CARD interaction (Figure 3-4). The C-terminal region of the BCL10 CARD domain forms an additional heterotypic interaction with the MALT1 death domain (DD), and MALT1-BCL10 heterodimers exist in the cytosol independent of receptor signaling. Following CARD11 phosphorylation and activation upon antigen ligation to a lymphocyte receptor, MALT1-BCL10 heterodimers associate with CARD11 to form CBM complex filaments (Oeckinghaus et al., 2007; Qiao et al., 2013). Aggregation of the BCL10-MALT1 filament core is dependent upon BCL10-BCL10 interactions via R42 (Schlauderer et al., 2018). Due to its critical role in CBM complex assembly, BCL10 is an important target of post-translational modifications which dictate its assembly, disassembly, and proteasomal degradation (Gehring et al., 2018). To control signaling duration, BCL10 phosphorylation by downstream IKKß leads to its proteasomal degradation (Lobry et al., 2007; Wegener et al., 2006). Further, BCL10 is the target of K63 polyubiquitination for association with NEMO of the IKK complex (Wu & Ashwell, 2008).

3.5.3 MALT1

MALT1 was discovered in the recurrent translocation t(11;18)(q21;q21), which leads to fusion of the N-terminal BIR domain of the anti-apoptotic protein API2 to MALT1 (Dierlamm et al., 1999). The API2-MALT1 oncoprotein has elevated NF-κB signaling due to increased signaling downstream of receptor ligation (Rosebeck et al., 2016). MALT1 contains an N-terminal DD, a paracaspase domain, and 3 immunoglobulin-like (Ig) domains (Figure 3-4). MALT1 forms heterodimers with BCL10 via

interactions between the DD of MALT1 and the CARD regions of BCL10, relying upon residues V81 and L104 in MALT1 and BCL10, respectively (Schlauderer et al., 2018). Mutation of either of these residues to arginine leads to reduced *in vitro* MALT1-BCL10 binding. As a scaffolding protein, MALT1 is reliant upon binding to BCL10 for CBM complex assembly, and binding to the E3 ligase TRAF6 via the two TRAF6 binding motifs (T6BM) in exon 7 and 17 (Figure 3-4) (Kutukculer et al., 2020; Meininger et al., 2016; Noels et al., 2007; L. Sun et al., 2004). An additional T6BM was previously proposed to reside in MALT1 exon 16 based on sequence similarity to other motifs, but mutation of this site has no effect on TRAF6 binding efficiency (Meininger et al., 2016).

MALT1 has a unique role in humans as the only known Eukaryotic paracaspase, homologous to mammalian caspases and the metacaspases found in plants, fungi, and protazoa (Uren et al., 2000). Despite early recognition of the paracaspase domain of MALT1, nearly a decade passed before identification of the first MALT1 cleavage substrates BCL10 and A20 (Figure 3-5) (Coornaert et al., 2008; Rebeaud et al., 2008). Unlike canonical caspases, which cleave following aspartic acid residues, MALT1 cleaves on the C-terminal side of arginine residues in the P1 position (Hachmann et al., 2012). MALT1 cleavage activity is dependent upon the catalytic diad composed of histidine-415 and cysteine-464 (Figure 3-4). The paracaspase function of MALT1 is tightly regulated in resting cells, and MALT1 only becomes active following monoubiquitination at residue K644 (Pelzer et al., 2013). Additionally, residue 549 in the MALT1 dimerization interface is a prerequisite for monoubiquitination and enzymatic activity (Figure 3-4) (Cabalzar et al., 2013).

MALT1 substrates can be categorized as NF-κB pathway regulators, transcriptional regulators, and post-transcriptional regulators (Figure 3-5). NF-κB pathway regulators include BCL10, A20, CYLD, HOIL-1, and MALT1. BCL10 cleavage is essential for regulation of TCR-induced cell adhesion for targeting of T cells to sites of inflammation and for cell-cell interaction with APCs (Rebeaud et al., 2008). The deubiquitinase (DUB) A20 regulates the duration of TCR-dependent IKK complex signaling by catalyzing the cleavage of K63-linked polyubiquitin chains on MALT1 (Duwel et al., 2009). A20 is cleaved by MALT1 following TCR stimulation with CD3/CD28, and its resynthesis for downregulation of MALT1 signaling is subsequently upregulated by NF-κB. CYLD, like A20, is a DUB targeting polyubiquitin chains which acts as an inhibitor of NF-κB and JNK signaling (Reiley et al., 2007). Cleavage of CYLD by MALT1 is therefore required for downstream NF-κB and JNK signaling upon TCR stimulation (Staal et al., 2011).

The linear ubiquitin chain assembly complex (LUBAC) is composed of SHARPIN, HOIL-1, and HOIP. LUBAC positively regulated NF-κB signaling by polyubiqutination of IKK complex member NEMO via the E3 ligase HOIP, whose activity is dependent upon LUBAC assembly (Tokunaga & Iwai, 2012).

MALT1 cleaves in the N-terminus of HOIL-1, modulating binding to HOIP within LUBAC (Figure 3-5) (Douanne et al., 2016; Klein et al., 2015). Following cleavage, the N-terminal fragement of HOIL-1 is still able to bind to HOIP for ubiquitin ligase activity, while the C-terminal fragment acts to inhibit LUBAC complex activity (Elton et al., 2016). RELB is an NF-κB family member which forms inactive dimers when bound to RELA or REL, instead requiring p50 or p52 binding for activity. Increased expression of RELB therefore inhibits NF-κB activity, and cleavage of RELB by MALT1 leads to increased transcription of RELA and REL dependent genes (Hailfinger et al., 2011).

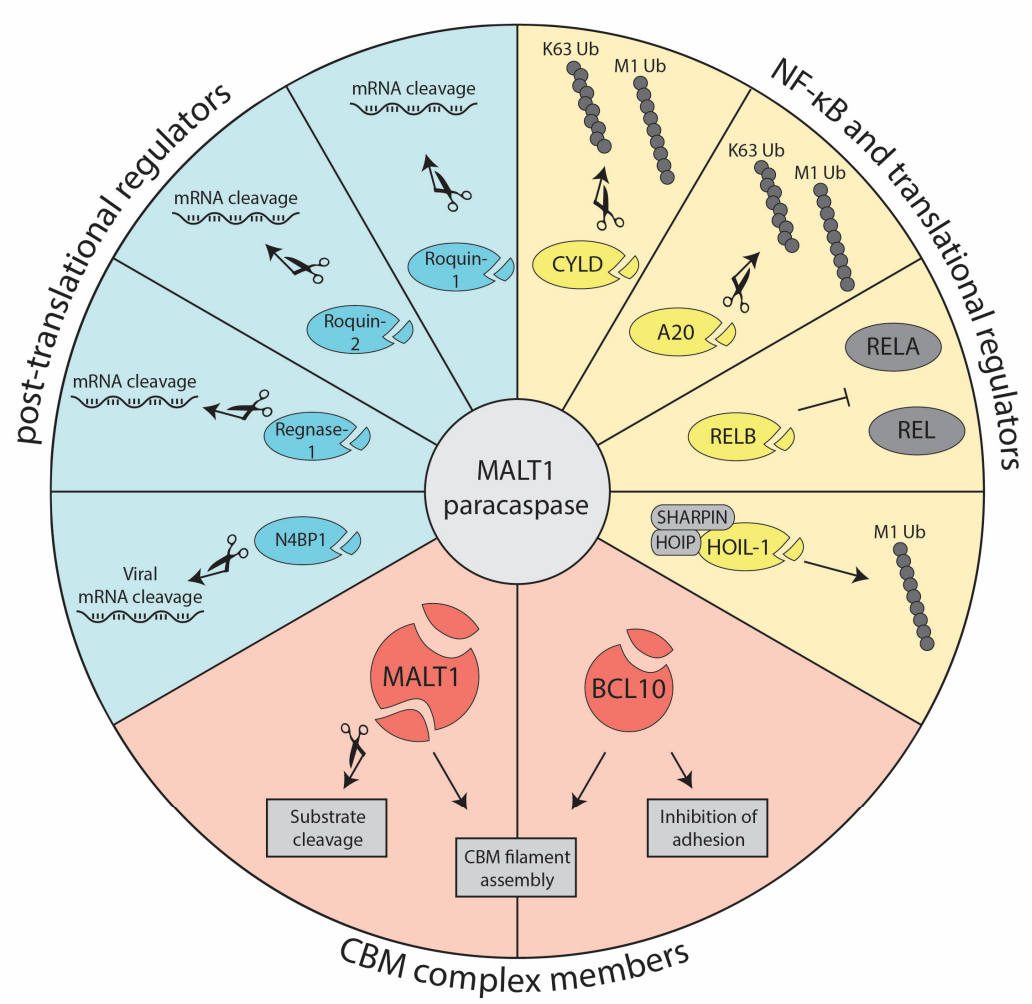

Figure 3-5. MALT1 cleavage substrates.
MALT1 cleavage substrates fall into three groups: CBM complex members, NF-κB and translational regulators, and post-translational regulators. Within the CBM complex, MALT1 cleaves BCL10 and itself, controlling CBM filament dynamics and adhesion. Cleavage of the negative NF-κB regulators CYLD, A20, and RELB induces stronger NF-κB signaling, while cleavage of the positive NF-κB regulator HOIL-1 within LUBAC weakens NF-κB signaling. MALT1 cleaves a number of RNA binding protein (RBP) substrates. Cleavage of Roquin-1, Roquin-2, and Regnase-1 leads to increased translation of RBP target mRNAs and pro-inflammatory signaling. MALT1 also cleaves N4BP1, an RBP which cleaves viral mRNA.

Recent evidence supports MALT1 auto-cleavage as a mechanism for regulation of MALT1 activity via both N- and C-terminal cleavage sites. N-terminal cleavage was shown to be required for induction

of NF-κB target transcription in Jurkat T cells (Baens et al., 2014). C-terminal cleavage removes the second TRAF6 binding motif on MALT1, indicating a possible mechanism for controlling the strength of MALT1-TRAF6 interaction (Ginster et al., 2017). Recently, mice without N-terminal MALT1 autocleavage were shown to have 40% fewer Treg cells, suggesting a role for auto-cleavage in Treg cell development (Baens et al., 2018).

A number of RNA binding proteins (RBPs) and regulators of posttranscriptional RNA metabolism have been shown to be substrates of MALT1 protease in T cells (Figure 3-5). Roquin-1/2 and Regnase-1 are RBPs which target the 3'-untranslated region (UTR) of a set of mRNAs including *Icos*, *Ox40*, and *Ctla-4* (CD278, CD134, and CD152, respectively), the IκB family members *NFkBID* and *NFkBIZ* (encoding IκBNS and IκBζ), and signaling molecules including *Il2*, *Il6*, and *Tnf* (Jeltsch et al., 2014; Vogel et al., 2013). Post-transcriptional regulation by Regnase-1 and Roquin-1/2 represses Th17 differentiation and cytokine production, and cleavage by MALT1 leads to upregulation of pro-inflammatory factors and receptor signaling (Jeltsch et al., 2014; Uehata et al., 2013). Recently, the RBP protein N4BP1, which cleaves viral RNA to inhibit HIV-I replication, was identified as a MALT1 substrate (Yamasoba et al., 2019).

3.5.4 The TRAF6 E3 ligase

The TRAF (TNF receptor associated factor) family of proteins in composed of 7 structurally similar members in humans (TRAF1-TRAF7). TRAF proteins mediate signals from TCRs and BCRs, TNF, and Toll/Interleukin-1 receptors, influencing cell survival, differentiation and proliferation (Inoue et al., 2000). All TRAF proteins (except TRAF1) have an N-terminal RING domain classifying them as E3 ligases, and all (except TRAF7) have a C-terminal TRAF domain for protein-protein interaction (Park, 2018). Therefore, TRAF proteins have both catalytic and scaffolding functions. TRAF6 is an E3 ligase which, together with the heterodimeric E2 conjugating enzyme Ubc13/Uev1A, catalyzes the proximity-dependent addition of K63-linked polyubiquitin chains to substrates (Shi & Sun, 2018). TRAF6 activity is essential in NF-κB signaling downstream of various receptor families, including TLRs, IL-1R, and lymphocyte receptors. In lymphocyte signaling, TRAF6 associates with MALT1 in the CBM complex following TCR or BCR ligation. C-terminal MALT1 polyubiquitination by TRAF6 is essential for recruitment of both NEMO of the IKK complex and the protein kinase TAK1 (Oeckinghaus et al., 2007; L. Sun et al., 2004).

TRAF6 is recruited to MALT1 via two TRAF6 binding motifs (T6BMs), one each in exons 7 and 17 (Meininger et al., 2016; Noels et al., 2007; L. Sun et al., 2004). MALT1 has two splice isoforms which depend upon the activity of the ribonucleoprotein heterogenous nuclear ribonucleoprotein U (hnRNP U) which inhibits inclusion of the 11 amino acid exon 7 via an alternative splicing mechanism

(Figure 3-4) (Meininger et al., 2016). Interestingly, exon 7 contains T6BM1 for interaction with TRAF6, and splicing therefore regulates the strength of MALT1-TRAF6 interaction and the extent of NF-κB activation. *In vitro* studies in Jurkat T cells have described the essential role of TRAF6 in NF-κB signaling pathways. Knockdown of TRAF6 using siRNAs yields a loss in IκBα phosphorylation and degradation, with a concomitant reduction in NF-κB activation (Bidere et al., 2006; Oeckinghaus et al., 2007). Further, mutation of glutamic acid residues in the T6BMs of MALT1 leads to complete abrogation of IKK complex and NF-κB activation (Meininger et al., 2016). The importance of MALT1 signaling by isoform expression is underlined by the highly conserved sequences of T6BMs across species (Kutukculer et al., 2020; Meininger et al., 2016).

3.6 CBM complex mutations and deficiency

3.6.1 Murine models

The CBM complex acts as a bridge between TCR antigen ligation and downstream signaling and activation events. In resting T cells of wildtype mice, the CBM complex does not assemble and MALT1 is inactive. Only upon TCR antigen ligation will complex assembly yield NF-κB signaling and cleavage of MALT1 substrates. Accordingly, murine models with abrogated expression of CARD11 (Egawa et al., 2003; Hara et al., 2003; Jun et al., 2003), BCL10 (Ruland et al., 2001), or MALT1 (Ruefli-Brasse et al., 2003; Ruland et al., 2003) yield immune suppressive phenotypes, with strongly diminished NF-κB activation, cytokine upregulation, and lymphocyte proliferation (Thome et al., 2010; Turvey et al., 2014).

CARD11-deficient mice exhibit defective thymocyte maturation and absence of B1 B cells, with compromised NF-κB activation following TCR stimulation. Abrogated activation in CARD11$^{-/-}$ mice leads to deficient cytokine production and an overall suppressed immune system (Egawa et al., 2003). Interestingly, Treg cell specific ablation of CARD11 in mice leads to conversion of Treg cells to pathogenic, IFNγ-secreting cells, indicating that stability of Tregs is dependent upon CBM complex assembly and downstream signaling (Di Pilato et al., 2019). Knockout of BCL10 in mice leads to an embryonal lethal neural tube-closure phenotype in one-third of homozygous mice, likely due to the role of BCL10 in development (Ruland et al., 2001). Surviving BCL10-deficient mice show normal development, but with an immune suppressive phenotype (Ruland et al., 2001). Due to the essential role of NF-κB signaling in B cell development, deficient mice have severely decreased mature follicular (Tfh), marginal zone (MZ), and B1 B cell populations (Xue et al., 2003). Mice which completely lack MALT1 expression (*Malt1* KO) are not competent for scaffolding or paracaspase activity and have a suppressed immune system, with loss of both Teff and Treg populations (Figure 3-6) (Ruefli-Brasse et al., 2003; Ruland et al., 2003). MALT1 is required for differentiation of B1 and

MZ B cells in the bone marrow, and KO mice additionally lose these populations (Ruefli-Brasse et al., 2003; Ruland et al., 2003). Despite immune suppression, *Malt1* KO mice are healthy and viable under clean housing conditions. Overall, mice deficient in CBM complex members have an immune suppressive phenotype as a result of defective signaling downstream of TCR and BCR signaling.

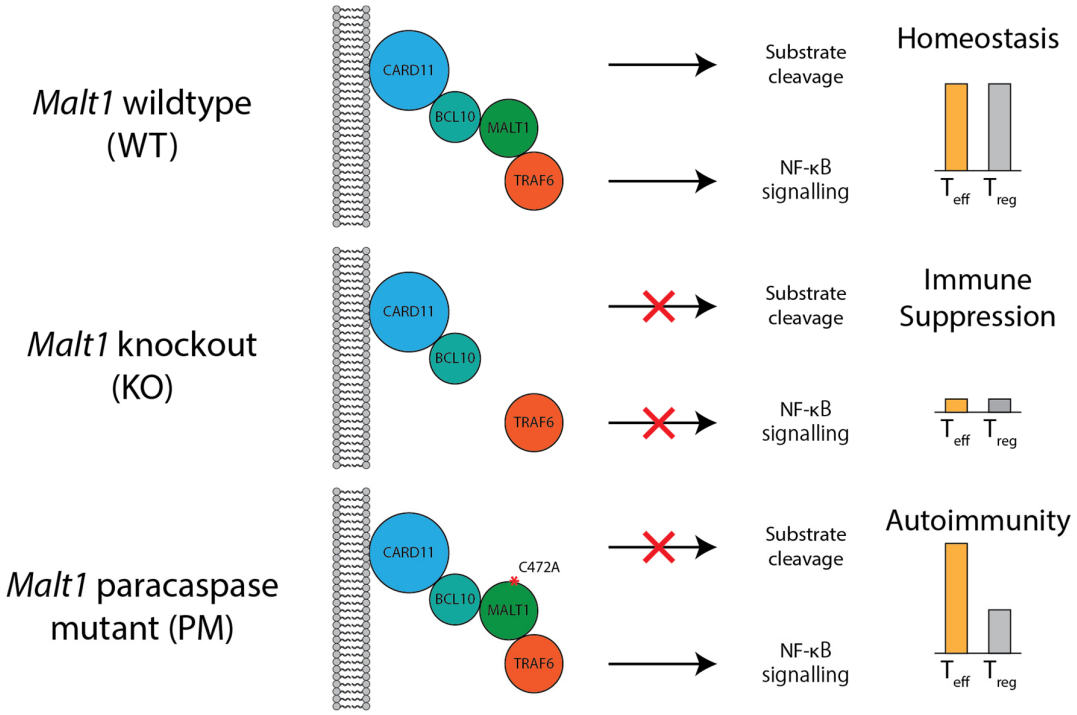

Figure 3-6. Murine models modulating MALT1 function.
In *Malt1* wildtype (WT) mice, CBM complex assembly and TRAF6 binding to MALT1 leads to activation of MALT1 substrate cleavage and NF-κB activation. Loss of MALT1 expression in *Malt1* knockout (KO) mice yields loss of both Teff and Treg cell populations and immune suppression. Mutation of exclusively the paracaspase active site cysteine C472 (C464 in humans) in *Malt1* paracaspase mutant (PM) mice leads to autoimmunity due to Teff cell expansion and inhibition of Treg maturation.

To investigate the specific role of MALT1 paracaspase function, mice have been developed which have intact scaffolding function but lack paracaspase activity via mutation of the active site cysteine 472 (human MALT1A C464). So-called *Malt1* PD mice (henceforth referred to as *Malt1* PM mice) exhibit weight loss and ataxia, a degenerative disease of the nervous system, with strong reduction in FoxP3+ Treg populations and expansion of Teff cells (Figure 3-6) (Bornancin et al., 2015; Gewies et al., 2014; Jaworski et al., 2014). *Malt1* PM mice have only partially intact NF-κB signaling, showing that NF-κB signaling is in part dependent upon MALT1 cleavage activity. Despite strong dependence of Tregs maturation on MALT1 paracaspase function, reduction in Tregs of *Malt1* PM mice is less severe than in *Malt1* KO mice, indicating that intact NF-κB signaling is sufficient for partial Treg development. Thus, a loss in homeostatic balance between Teff and Treg cells drives autoimmunity

in *Malt1* PM mice. Interestingly, T cell-specific PM mice (*Malt1*$^{PM/fl}$; *CD4-Cre*$^{Cre+}$) show identical disease onset, stressing that the PM phenotype is primarily T cell drive (Demeyer et al., 2019).

TRAF6 is essential for development and its ablation leads to early mortality (Kobayashi et al., 2003; Lomaga et al., 1999; Naito et al., 2002). *Traf6* KO mice exhibit splenomegaly, lymph node deficiency, and strong inflammatory organ infiltration (Chiffoleau et al., 2003). TRAF6-deficient mice have defective signaling downstream of TLR and TNFR (CD40) signaling in DCs, showing the need for TRAF6 in DC development and activation (Kobayashi et al., 2003). Defective signaling in the development of TRAF6 knockout mice leads to osteopetrosis, with poor bone and tooth growth (Lomaga et al., 1999; Naito et al., 1999; Ruland et al., 2001). Further, TRAF6 is essential for the maturation of the TECs important in the negative selection of T cells, and TRAF6-deficiency was accompanied by loss of expression of the protein AIRE (Akiyama et al., 2005).

The specific role of TRAF6 in T cells was investigated via mice with T cell-specific ablation of TRAF6 (*Traf6*-ΔT mice). *Traf6*-ΔT mice are viable but develop an autoimmune inflammatory phenotype after 10-12 weeks of age, with splenomegaly, lymphadenopathy, and increased production of inflammatory cytokines, indicating that TRAF6 is essential for maintenance of immune homeostasis (King et al., 2006). *Traf6*-ΔT mice had normal number of Tregs, showing that the dependence of Treg development on TRAF6 expression is not intrinsic to conventional T cells. Rather, recent murine studies with Treg-specific ablation of TRAF6 have shown that Treg cells themselves require TRAF6 expression for development, localization, and identity (Muto et al., 2013; Ni et al., 2019). This is due to the dependence of Treg development on NF-κB signaling, which requires TRAF6 ligase activity (Schmidt-Supprian et al., 2004). Specifically, the importance of c-Rel in Treg development has been shown (Isomura et al., 2009; Long et al., 2009). Interestingly, although TRAF6 activity is indispensable for IKK complex activation in the NF-κB pathway in Jurkat T cells, *Traf6*-ΔT mice reportedly had no mitigation of NF-κB activation levels (King et al., 2006).

3.6.2 Human CBMopathies

Genetic diseases commonly have roots within immune regulatory pathways, and approximately 350 of these so-called primary immunodeficiency diseases (PID) have been characterized and subcategorized. These diseases are described according to whether they have normal (Combined Immunodeficiency Disease, CID) or abnormal (Severe Combined Immunodeficiency Disease, SCID) numbers of T and B cells (Picard et al., 2018). Interestingly, a number of these disorders relate to loss of homeostatic regulation within the NF-κB pathway, and genetic disorders which specifically affect CBM complex members are classified as CBMopathies (Lu et al., 2018). Loss-of-function (LoF) mutations have been found in CARD11, BCL10, and MALT1, leading primarily to diminished protein

expression and CID. This includes three SCID patients with CARD11 CC or GUK domain mutations (Fuchs et al., 2015; Greil et al., 2013; Stepensky et al., 2013) and one CID patient with a splice site mutation in intron 1 of BCL10 (Torres et al., 2014). There is also a growing list of patients with heterozygous LoF (CID) and gain-of-function (GoF) (BENTA: B cell expansion with NF-κB and T cell anergy) mutations in CARD11, again highlighting the consequence of dysregulated CARD11 signaling (Lu et al., 2018).

To date, 9 human patients have been described in the literature with MALT1 mutations (Charbit-Henrion et al., 2017; Frizinsky et al., 2019; Jabara et al., 2013; Kutukculer et al., 2020; McKinnon et al., 2014; Punwani et al., 2015). These MALT1 mutations overwhelmingly lead to LoF and CID, with either complete loss or severe reduction in MALT1 expression levels or stability. Human MALT1-deficiency is characterized by symptoms of immune suppression, with recurrent infection and failure to thrive. Interestingly, one patient was recently characterized with a MALT1 mutation which does not lead to lower MALT1 protein expression levels (Kutukculer et al., 2020). Instead, the single base-pair mutation c.2418G>C, leading to expression of MALT1A E806D protein, lies within one of the T6BMs (T6BM2) which have been shown to be essential for MALT1-TRAF6 interaction (Meininger et al., 2016; Noels et al., 2007). The MALT1B isoform, which lacks T6BM1 in exon 7, was predominantly expressed in the patient, and MALT1B E806D cannot interact with TRAF6. Therefore, the preponderance for MALT1B expression clearly defines the severity of the patient phenotype. In contrast to other MALT1 CID patients, the MALT1 E806D patient has, in addition to immune suppressive symptoms, signs of autoimmunity, including dermatitis, splenomegaly, and cervical lymphadenopathy (Kutukculer et al., 2020). The exact mechanisms driving autoimmunity upon loss of MALT1-TRAF6 interaction *in vivo* remain to be determined.

3.7 Aims of the study

The purpose of this study was to determine the *in vivo* function of the MALT1-TRAF6 interaction (Figure 3-7). Previous studies have described the role of TRAF6 as a positive regulator of NF-κB signaling *in vitro* (Meininger et al., 2016; Noels et al., 2007; L. Sun et al., 2004). However, conflicting reports on the effects of abrogated MALT1-TRAF6 interaction in mice have made clear that the physiological relationship between these two signaling molecules is incompletely resolved, as TRAF6 was suggested to be dispensable for TCR-induced NF-κB signaling in murine CD4 T cells (King et al., 2006; Muto et al., 2013). Recently, a human patient was described with a mixed phenotype involving immune suppression and autoimmunity arising from mutation in the second T6BM of MALT1, further inspiring interest in this interaction.

To elucidate the physiologic function of the MALT1-TRAF6 interaction, we generated a murine model in which we specifically introduced missense mutations in the two functional TRAF6 binding motifs (T6BMs) in the *Malt1* gene, rendering MALT1 incapable of interacting with TRAF6 (*Malt1* TBM (TRAF6 binding mutant) mice). Based on cellular models, we hypothesized that selective destruction of MALT1 scaffolding with TRAF6 should abrogate NF-κB activation and yield a similar phenotype to that of complete MALT1 deficiency (Meininger et al., 2016; Noels et al., 2007; Ruefli-Brasse et al., 2003; Ruland et al., 2003). Surprisingly, *Malt1* TBM mice succumb to an early onset fatal autoimmune and inflammatory disease, prompting us to investigate the cellular and molecular causes of this unexpected phenotype. To clarify the reasons for autoimmunity in *Malt1* TBM mice, we utilized Cre-recombinase mice for expression of TBM mutations only in T cells (*Malt1* TBM-T and *Malt1* TBM-Treg mice), comparing them with T cell-specific TRAF6 KO mice (*Traf6*-ΔT). Importantly, we clarify that MALT1-TRAF6 association and TRAF6 expression are essential for TCR-dependent NF-κB activation in T cells. Further, both genetic manipulations lead to a highly similar autoimmune phenotype, leading us to speculate that MALT1 protease activation in the absence of NF-κB activation may be the cause of autoimmunity. Indeed, loss of TRAF6 or defective MALT1-TRAF6 interaction leads to spontaneous and unopposed MALT1 protease activation and constitutive substrate cleavage dependent upon tonic TCR signaling. By developing a heterologous system in Jurkat T cells, we show that constitutive MALT1 activity as a consequence of defective MALT1-TRAF6 interaction is also present *in vitro* and is dependent upon CBM complex formation and a functional TCR, strongly implicating a tonic signaling mechanism.

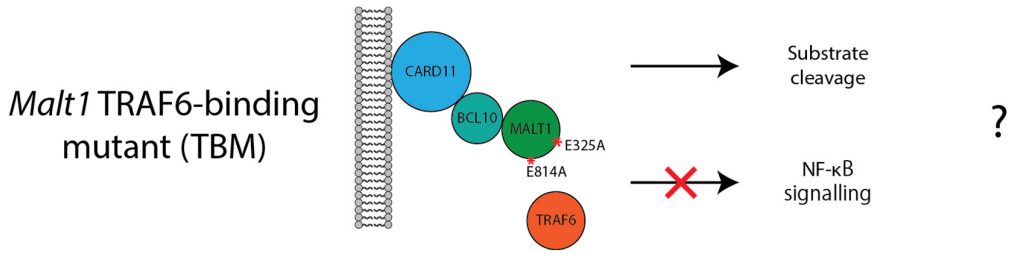

Figure 3-7. *Malt1* TBM model for investigation of MALT1-TRAF6 interaction *in vivo*
Jurkat T cells with maintained MALT1 paracaspase function but loss of scaffolding function for assembly with TRAF6 are no longer competent for NF-κB signaling, but consequences of these mutations have not been shown *in vivo.*

We decided to investigate this notion of constitutive MALT1 activity by performing an *in vivo* CRISPR-Cas9 rescue experiment by mutating and inactivating MALT1 enzyme activity in *Malt1* TBM mice (*Malt1* TBMPM (MALT1 TRAF6-binding/paracaspase mutant) mice). Indeed, *Malt1* TBMPM mice show complete reversion of autoimmunity, proving that dysregulation of protease activity in *Malt1* TBM mice causes fatal immune activation. To show that constitutive MALT1 protease activation in T

cells also drives autoimmunity upon loss of TRAF6, we performed genetic and therapeutic reversion experiments with *Traf6*-ΔT mice. Inactivation of the paracaspase domain in *Traf6*-ΔT mice led to reversion of autoimmunity, proving that the phenotype upon loss of TRAF6 expression is driven by aberrant MALT1 activity. Similarly, pharmacological treatment of *Traf6*-ΔT mice with the low-nanomolar MALT1 inhibitor MLT-985 reverts autoimmunity, again linking the *Traf6*-ΔT phenotype to aberrant MALT1 activity. Thus, using *in vivo* and *in vitro* experiments, we elucidated a completely new and unexpected function of TRAF6 in counteracting MALT1 protease activation to prevent the induction of autoimmunity in resting cells.

4 Results

4.1 Generation and characterization of a mouse line expressing MALT1 with TRAF6 Binding Mutations (TBM)

4.1.1 Targeted mutation of Malt1 T6BMs in M. musculus

Mutation of TRAF6 binding motifs (T6BMs) on MALT1 abrogates NF-κB activation *in vitro* (Meininger et al., 2016). However, these effects have not been shown *in vivo*. To determine the effect of T6BM mutation *in vivo*, missense mutations were introduced into the *Malt1* gene of murine embryonic stem (mES) cells via CRISPR-Cas9 gene editing. Two single-guide RNAs (sgRNAs) were designed, one each at proximity to the first (T6BM1) and second (T6BM2) T6BM in *Malt1*, located within Exons 7 and 17, respectively (Figure 4-1A). Taking advantage of homologous repair mechanisms for targeted mutation, homology directed repair (HDR) templates were introduced together with sgRNAs, each spanning the targeted site. HDR templates were designed with E-to-A point-mutations for loss of TRAF6 binding and additional silent mutations, both to prevent recurrent sgRNA targeting events in correctly modified loci and for insertion of artificial cleavage sites for downstream clonal selection (MlyI for T6BM1, AlwI for T6BM3) (Figure 4-1B).

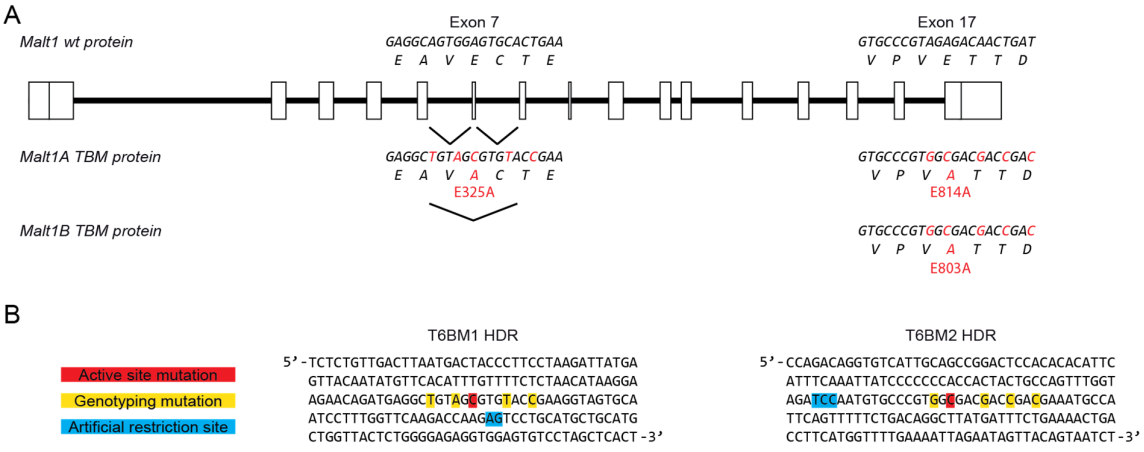

Figure 4-1. *Malt1* T6BM targeting strategy
A) *Malt1* genomic locus with schematic exon-intron structure and indication of the wildtype sequence (above the scheme) and the mutated sequence (below the scheme) after successful modification of the locus. Two mutations, E325A within exon 7 and E814A (E803A for MALT1 isoform B) within exon 17 were introduced by CRISPR-Cas9 and homology directed repair (HDR) templates into the *Malt1* gene. Modifications to DNA and amino acid sequences are indicated in red. B) Sequences of HDR templates for T6BM1 and T6BM2 including functional E-to-A point mutations (red), additional silent mutations for screening and inhibition of repeated cleavage after successful insertion of the homology template (yellow), and insertion of artificial restriction sites proximal to T6BM1 (MlyI) and T6BM2 (AlwI) (blue). Guide RNA and HDR template sequences are shown in section 7.1.7.2.

An overview of the strategy for targeted mutation in mES cells is shown in Figure 4-2A. Prior to mES cell transfection, cell quality was checked based on growth (Figure 4-2B, top) and expression of alkaline phosphatase (Figure 4-2B, bottom, dark staining), a marker used for verifying pluripotency in stem cells. Following transfection with sgRNAs and HDR templates, cells were sorted and enriched

on EGFP expression from the sgRNA-expression pX458 vectors (Figure 4-2C) and enriched cells were grown on a murine embryonic feeder (MEF) cell layer. Monoclonal colonies were picked and screened using real-time (RT)-PCR with mutation-specific primers to identify genetic alterations (Figure 4-2D) and potential double mutants (alterations in T6BM1 and T6BM2), which amplified at lower Ct values in RT-PCR (Figure 4-2E), were sequenced. Of approximately 800 monoclonal colonies screened, two clones were found containing all targeted loss-of-function mutations homozygously inserted (Figure 4-2F).. Clone #3-3E10 was used for creation of chimeric mice.

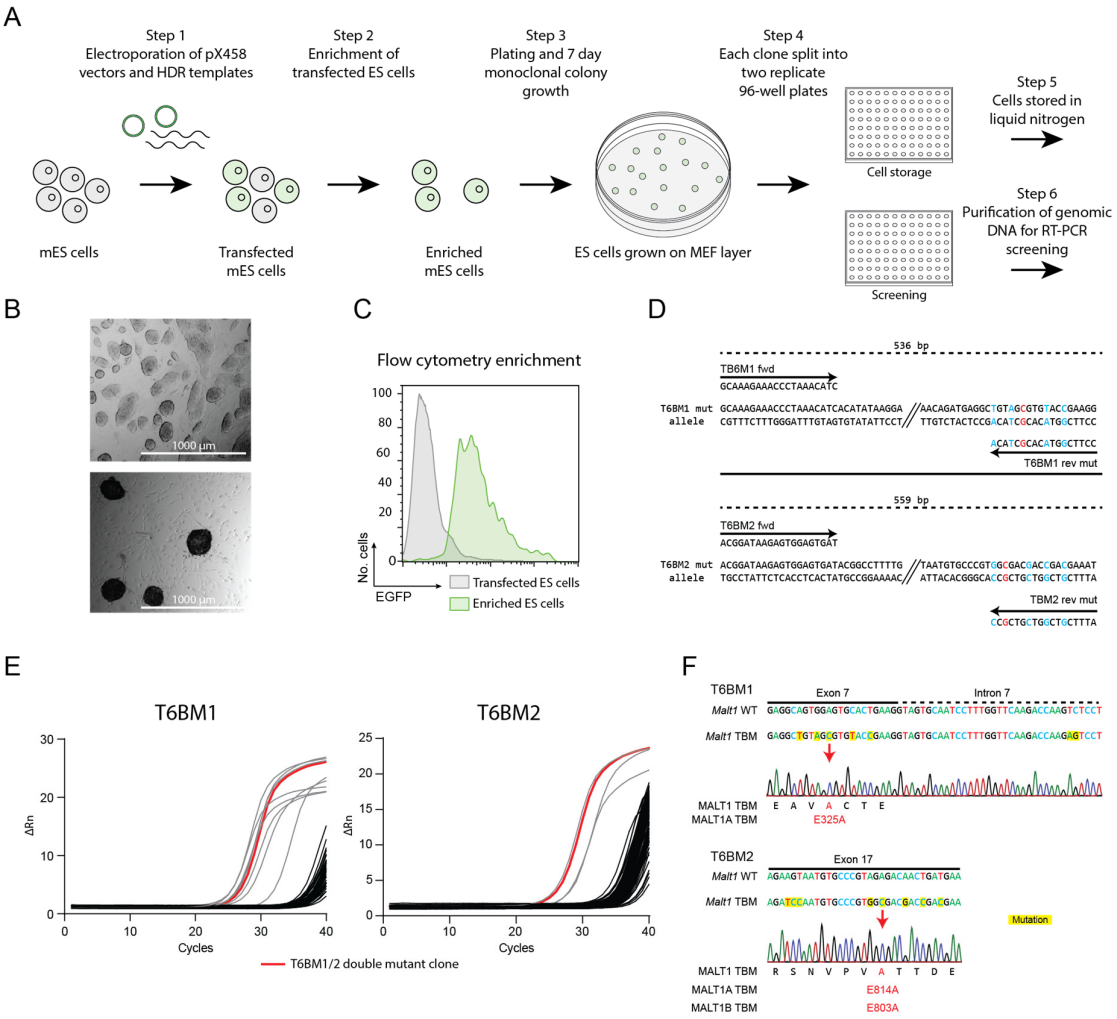

Figure 4-2. Induction and screening of *Malt1* T6BM mutations in murine ES cells.
A) Workflow for targeting of T6BM sites and screening of monoclonal murine embryonic stem (mES) cell colonies. mES cells were electroporated and enriched by sorting on EGFP. Monoclonal colonies were grown and used for RT-PCR screening and mutation verification using mutation specific primers. B) Healthy mES cells prior to electroporation (top) and monoclonal colonies stained (dark) with alkaline phosphatase to verify pluripotency (bottom). C) Histogram depicting the EGFP expression profile of transfected cells before (grey) and after (green) sorting. D) Mutation-specific primers to detect modification of T6BMs via real-time (RT) PCR. E) RT-PCR screening results showing potentially modified clones (grey curves with lower Ct values) compared to negative clones (black curves with higher Ct values). The homozygous double-positive clone (homozygous for T6BM1 and T6BM2 mutations) used for generation of mice is highlighted by red curves. F) Sequencing of genomic DNA spanning T6BM1 and T6BM2 to verify correct mutagenesis in *Malt1* TBM mES cells. Mutated nucleotide residues are highlighted in yellow, altered amino acid residues are shown in red.

ES cells from clone #3-3E10 were injected into morulae of C57BL/6 mice, which after implantation into foster mice yielded chimeric offspring (90% brown chimerism). Crossing of chimeric mice to C57BL/6 resulted in offspring with either black fur (negative for germ line transmission) or brown fur (indicating successful germ line transmission) (Figure 4-3A). Sequence analyses demonstrated that all brown germline offspring indeed carried both T6BM mutations and thus constituted *Malt1*$^{TBM/+}$ founder mice. All *Malt1*$^{TBM/+}$ mice were viable, healthy, and fertile. Unexpectedly, chimeric mice eventually showed signs of disease, with 5 of 9 mice dying or reaching a humane endpoint at approximately 3-5 months of age (Figure 4-3B). One mouse was taken for necropsy at 5 months, showing signs of severe splenomegaly (Figure 4-3C). Thus, expression of *MALT1* T6BM mutations in chimeric mice appears to lead to a disruptive immune phenotype with signs of hyperplasia in the spleen.

A

B

Mouse ID	Age of death (days)	Cause of death
80008922	120	Sacrificed
80008923	108	Found dead
80008924	157	Sacrificed
80008925	157	Found dead
80008926	191	-
80008992	228	-
80009374	107	Found dead
80009375	176	-
80009376	145	-

C

Mouse: 80008924
Spleen weight: 1.34 g

Figure 4-3. Chimeric mice derived from T6BM mES cell clone.
A) Brown male chimeric founder mouse #80008992 with first litter containing color selected *Malt1*$^{+/+}$ (black) and *Malt1*$^{TBM/+}$ (brown) mice. B) Age and cause of death for the 9 *Malt1* TBM chimeric mice obtained. Mice without an indicated cause of death had no visible phenotype at time of sacrifice. C) Spleen and lymph nodes of *Malt1* TBM chimera showing advanced splenomegaly in chimeric mouse #80008924 at age 5 months. Morulae injection was performed by Ronald Naumann, Max Planck Institute of Molecular Cell Biology and Genetics, Dresden.

4.1.2 *Malt1*$^{TBM/TBM}$ mice exhibit a massive inflammatory phenotype

Malt1$^{TBM/+}$ heterozygous mice were intercrossed to yield *Malt1*$^{TBM/TBM}$ mice. Wildtype, heterozygous, and homozygous *Malt1* TBM mice were born at Mendelian ratio and could be distinguished from tissue using the differential PCR that was established for screening of mES cell clones, with additional wildtype-specific primers for identification of the wildtype *Malt1* allele (Figure 4-4A). MALT1 protein expression in purified CD4 T cells was equivalent in *Malt1*$^{TBM/TBM}$ mice compared to *Malt1*$^{TBM/+}$ and *Malt1*$^{+/+}$ littermates (Figure 4-4B). *Malt1*$^{TBM/TBM}$ mice appeared normal at birth but stopped thriving at 3-4 weeks of age and had to be sacrificed at a mean age of 27 days (Figure 4-4C). Histological analyses of organs showed signs of severe inflammatory cell infiltration in all tissues tested, with notable thickening of the intestine wall, collapse of lung alveoli, and infiltration of tissue

surrounding vasculature of the liver and kidney (Figure 4-4D). Additionally, *Malt1*$^{TBM/TBM}$ showed signs of hemophilia and loss of bone marrow density, indicating potential depletion of hematopoietic stem cell numbers and differentiation (data not shown). In conclusion, *Malt1*$^{TBM/TBM}$ mice show an advanced autoimmune phenotype stemming from loss of MALT1-TRAF6 interaction.

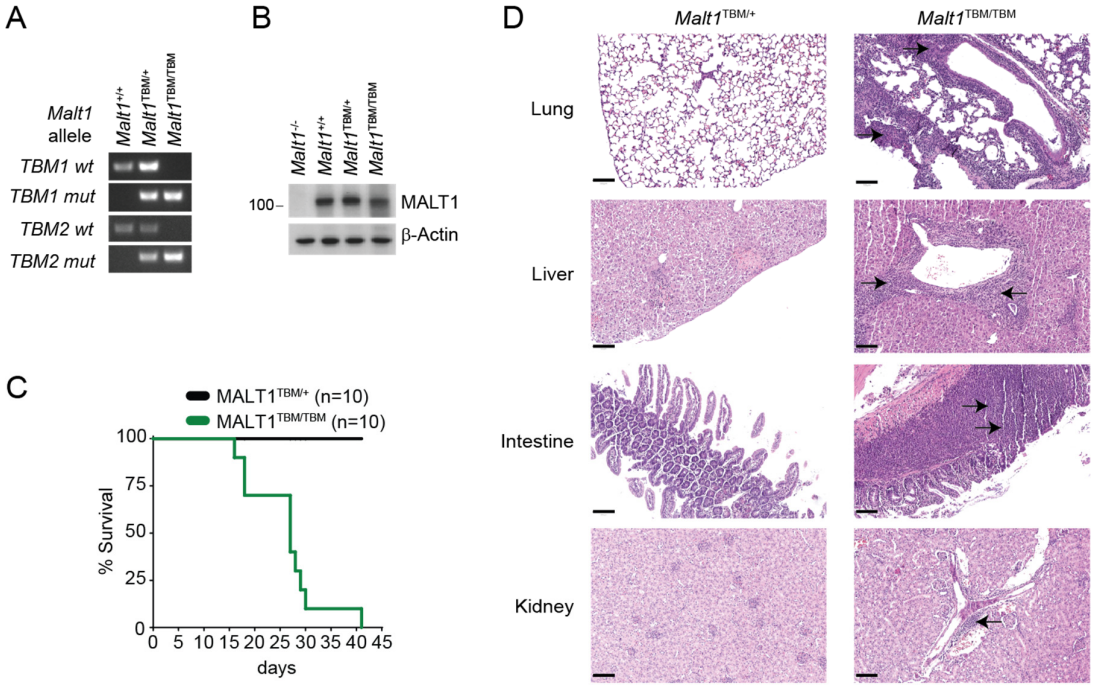

Figure 4-4. *Malt1* TBM survival and inflammation.
A) Genotyping of *Malt1* TBM mice to distinguish *Malt1*$^{TBM/TBM}$, *Malt1*$^{TBM/+}$, and *Malt1*$^{+/+}$ genotypes. B) Analysis of MALT1 protein expression by Western Blot in lysates of CD4+ T cells from *Malt1*$^{TBM/TBM}$, *Malt1*$^{TBM/+}$, and *Malt1*$^{+/+}$ mice. A *Malt1*$^{-/-}$ sample was also analyzed as a negative control to prove specificity. C) Survival of *Malt1*$^{TBM/TBM}$ and *Malt1*$^{TBM/+}$ mice, with a mean *Malt1*$^{TBM/TBM}$ survival of 27 days. D) Representative histological analyses showing hematoxylin and eosin staining of lung, liver, intestine, and kidney tissue from *Malt1*$^{TBM/TBM}$ and *Malt1*$^{TBM/+}$ between 25 and 29 days of age. Examples of infiltration are indicated by arrows. Scale bar: 100 µM. Histological sections were prepared at the Helmholtz Zentrum, München, staining and imaging was performed in the lab of Dr. Mark Kriegsmann at the University Hospital Heidelberg.

Due to the severity of the phenotype in homozygous TBM mice, all mice for subsequent analyses were sacrificed at age 18 days to reduce burden and to study the immune phenotype at disease onset. 18 day old *Malt1*$^{TBM/TBM}$ mice showed no significant weight loss (Figure 4-5A) but already exhibited splenomegaly and lymphadenopathy, whereas *Malt1*$^{TBM/+}$ mice were phenotypically normal at this age (Figure 4-5B,C). Multiorgan inflammation, apparent from histology and increased peripheral lymph organ size, was accompanied by increased cytokine production regarding IFNγ, IL-6, IL-10, IL-17, and TNFα, indicating systemic inflammation (Figure 4-5D). The *Malt1*$^{TBM/TBM}$ phenotype was persistent through 6 generations of backcrossing to C57BL/6, indicating that the observed phenotype is specific to the targeted *Malt1* mutations and not the result of potential off-target effects from CRISPR-Cas9 targeting.

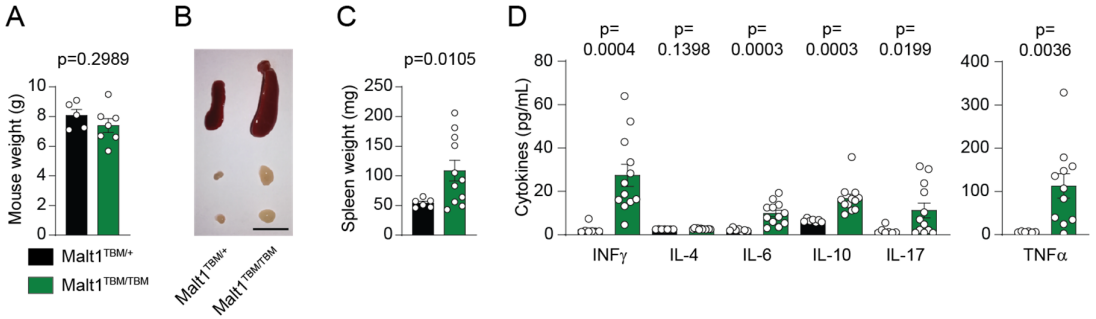

Figure 4-5. Immune phenotyping of 18 day old *Malt1* TBM mice.
A) Mouse weight of *Malt1*$^{TBM/TBM}$ and *Malt1*$^{TBM/+}$ mice. B) Representative images of spleen and lymph nodes in *Malt1*$^{TBM/TBM}$ and *Malt1*$^{TBM/+}$ mice. Scale bar: 1 cm. C) Spleen weight in *Malt1*$^{TBM/TBM}$ and *Malt1*$^{TBM/+}$ mice. D) Blood serum levels of indicated cytokines in *Malt1*$^{TBM/TBM}$ and *Malt1*$^{TBM/+}$ mice. A-D) Mice were analyzed at 18 days after birth. Unaffected control *Malt1*$^{TBM/+}$ littermates (black) were compared to *Malt1*$^{TBM/TBM}$ mice (green). Each dot represents one mouse. All bars show means ± SEM, and p-values were calculated by unpaired t-test with Welch's correction.

4.1.3 *Malt1*$^{TBM/TBM}$ mice show massive loss of B cells

Using flow cytometry, T and B lymphocyte populations were analyzed in *Malt1*$^{TBM/TBM}$ mice. *Malt1*$^{TBM/TBM}$ mice showed a severe loss of CD45RA+ (B220+) B cells in spleen and lymph nodes, but not bone marrow (Figure 4-6A,B). Loss of B cells led to a relative increase in the CD3+ T cell population in spleen, but not lymph nodes or thymus (Figure 4-6A,C). CD4+ T helper (Th) and CD8+ cytotoxic T lymphocyte (CTL) populations were increased in spleen, but not lymph nodes of *Malt1*$^{TBM/TBM}$ mice compared with *Malt1*$^{TBM/+}$ when gated on CD3+ T cells (Figure 4-6D,E). No changes were seen in thymic T cell populations (Figure 4-6F,G). Overall, 18 day old *Malt1*$^{TBM/TBM}$ mice showed strong changes in lymphocyte populations, occurring most prominently in the peripheral lymph organs spleen and lymph nodes, while central lymphoid tissue remained unaffected.

4.1.4 Upregulation of activated lymphocytes in *Malt1*$^{TBM/TBM}$

To investigate the cause of the observed severe autoimmune and inflammatory disorder seen in *Malt1*$^{TBM/TBM}$ mice, in depth immune phenotyping was performed. Upon antigen stimulation, naïve T cells ($T_{Naïve}$) differentiate to effector and memory cell subsets, including central memory (T_{CM}) and effector memory (T_{EM}) T cells, which are essential for defending against infection. While the precise nature of effector and memory subset differentiation is contentious (Lefrancois & Marzo, 2006; Omilusik & Goldrath, 2017), an increasein these populations can be correlated with immune upregulation and inflammation.

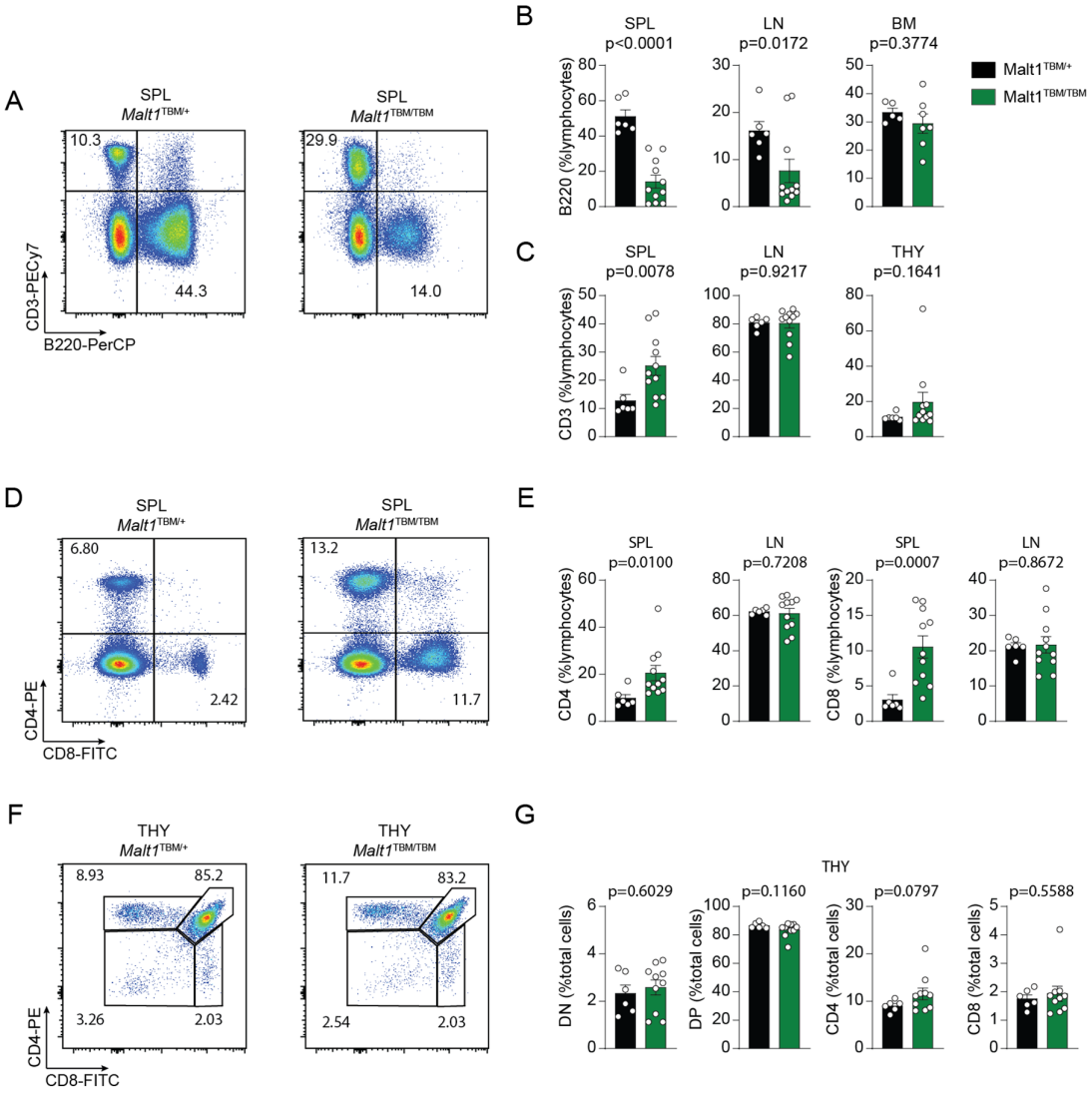

Figure 4-6. Immune phenotyping of T and B cell populations in *Malt1* TBM mice.
A-C) Relative populations of CD3+ T and B220+ B cells in spleen (SPL), lymph nodes (LN), bone marrow (BM), and thymus (THY) of *Malt1*$^{TBM/TBM}$ and *Malt1*$^{TBM/+}$ mice. D-E) Relative populations of CD4+ and CD8+ T cells in spleen and lymph nodes of *Malt1*$^{TBM/TBM}$ and *Malt1*$^{TBM/+}$ mice. F-G) Relative populations of CD4+ and CD8+, as well as CD4 CD8 double negative (DN) and double positive (DP), T cells in thymus of *Malt1*$^{TBM/TBM}$ and *Malt1*$^{TBM/+}$ mice. A-G) Mice were analyzed at 18 days after birth. Unaffected control *Malt1*$^{TBM/+}$ littermates (black) were compared to *Malt1*$^{TBM/TBM}$ mice (green). Each dot represents one mouse. All bars show means ± SEM, and p-values were calculated by unpaired t-test with Welch's correction.

To determine the activation status of peripheral T cells in spleen and lymph nodes, we co-stained CD4+ T cells with the surface marker CD44 and CD62L, which distinguishes between naïve ($T_{Naïve}$: CD44^{lo}CD62L^{hi}), central memory (T_{CM}: CD44^{hi}CD62L^{hi}), and effector memory (T_{EM}: CD44^{hi}CD62L^{lo}) T cell populations (Figure 4-7A). Compared with controls, *Malt1*$^{TBM/TBM}$ mice show massive accumulation of T_{EM} cells, indicative of excessive T cell activation and response (Figure 4-7A,B). Concomitant with this increase in T_{EM} cells, we observed a strong decline in naïve T cells from spleen and lymph nodes, while the T_{CM} population remained unchanged compared with controls (Figure 4-7A,C). A comparable, if not stronger shift towards T_{EM} cells was seen in CD8+ T cells (Figure 4-7D-

F), revealing a strong T effector memory response upon abrogation of MALT1-TRAF6 interaction in T cells of young *Malt1* TBM mice. Additionally, expression of the early lymphocyte activation marker CD69 on CD3+ T cells was increased in spleen and lymph nodes of *Malt1*$^{TBM/TBM}$ mice compared with *Malt1*$^{TBM/+}$ (Figure 4-7G,H). Thus, mutation of T6BM sites on *Malt1* leads to spontaneous T lymphocyte activation and accompanying loss of naïve T cells in peripheral lymphoid tissues.

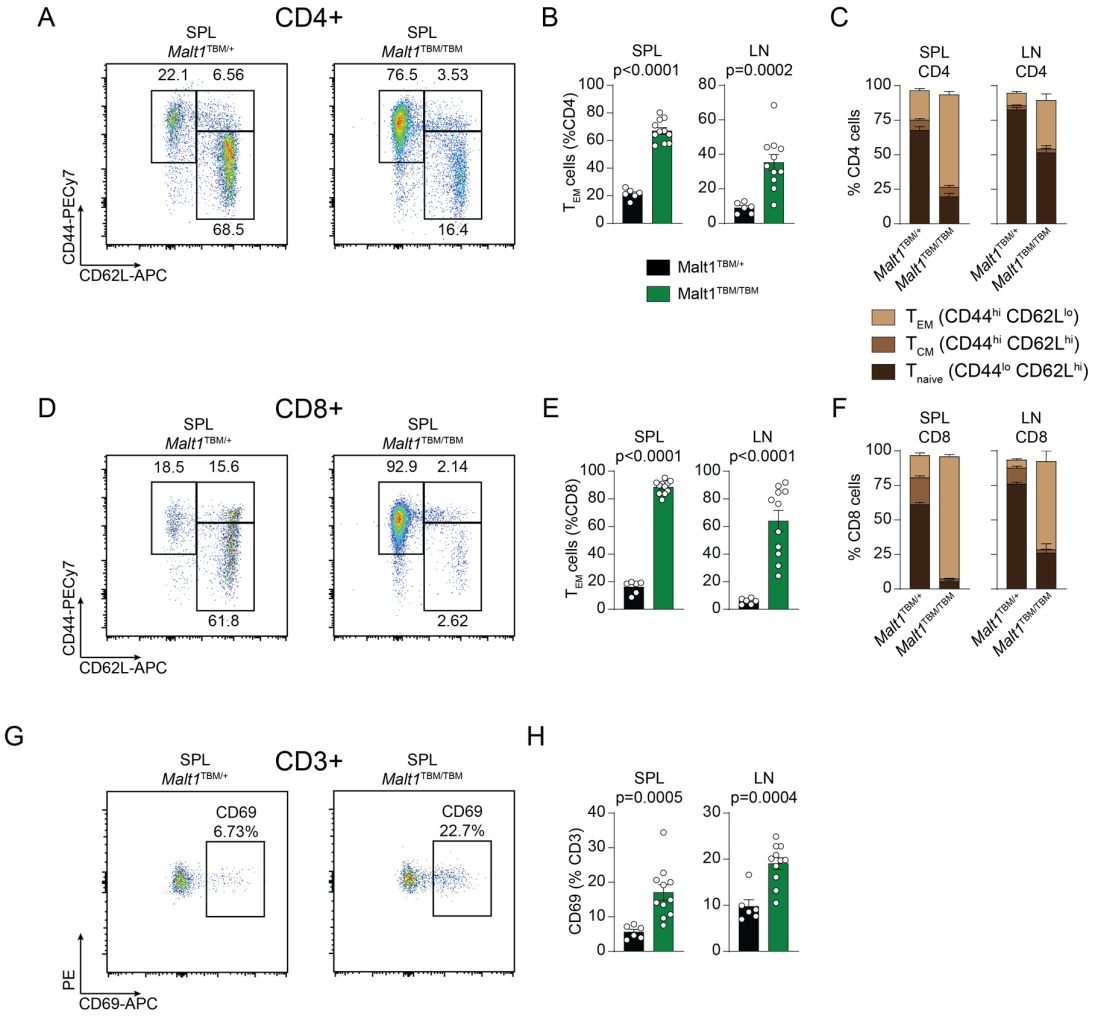

Figure 4-7. Activation phenotype of T cells in *Malt1* TBM mice.
A-C) Relative populations of CD4+ naïve T cells ($T_{naïve}$: CD44^{lo} CD62L^{hi}), central memory T cells (T_{CM}: CD44^{hi} CD62L^{hi}) and effector memory T cells (T_{EM}: CD44^{hi} CD62L^{lo}) in spleen (SPL) and lymph nodes (LN) of *Malt1*$^{TBM/TBM}$ and *Malt1*$^{TBM/+}$ mice. D-F) Relative populations of CD8+ $T_{naïve}$,T_{CM} and T_{EM} cells in spleen and lymph nodes of *Malt1*$^{TBM/TBM}$ and *Malt1*$^{TBM/+}$ mice. G-H) Relative populations of CD3+ CD69+ T cells in spleen and lymph nodes of *Malt1*$^{TBM/TBM}$ and *Malt1*$^{TBM/+}$ mice. A-H) Mice were analyzed at 18 days after birth. Unaffected control *Malt1*$^{TBM/+}$ littermates (black) were compared to *Malt1*$^{TBM/TBM}$ mice (green). Each dot represents one mouse. All bars show means ± SEM, and p-values were calculated by unpaired t-test with Welch's correction.

Despite a strong reduction in the relative number of peripheral B lymphocytes, we next assessed the activation status of B cells in *Malt1*$^{TBM/TBM}$ mice. Activated antigen presenting cells (APCs) like macrophages and B cells have upregulated expression of CD69 and CD86. As was the case in T cells, expression of CD69 was increased strongly on B cells in spleen and lymph nodes (Figure 4-8A,B).

Similarly, a higher percentage of B220+ B lymphocytes in *Malt1*$^{TBM/TBM}$ mice showed increased expression of CD86 compared with controls, in line with general immune activation (Figure 4-8C-D). Moreover, remaining B cells in *Malt1*$^{TBM/TBM}$ mice showed a tendency towards increased anti-dsDNA autoantibody production compared with controls (Figure 4-8E), a further indication of autoimmune activation.

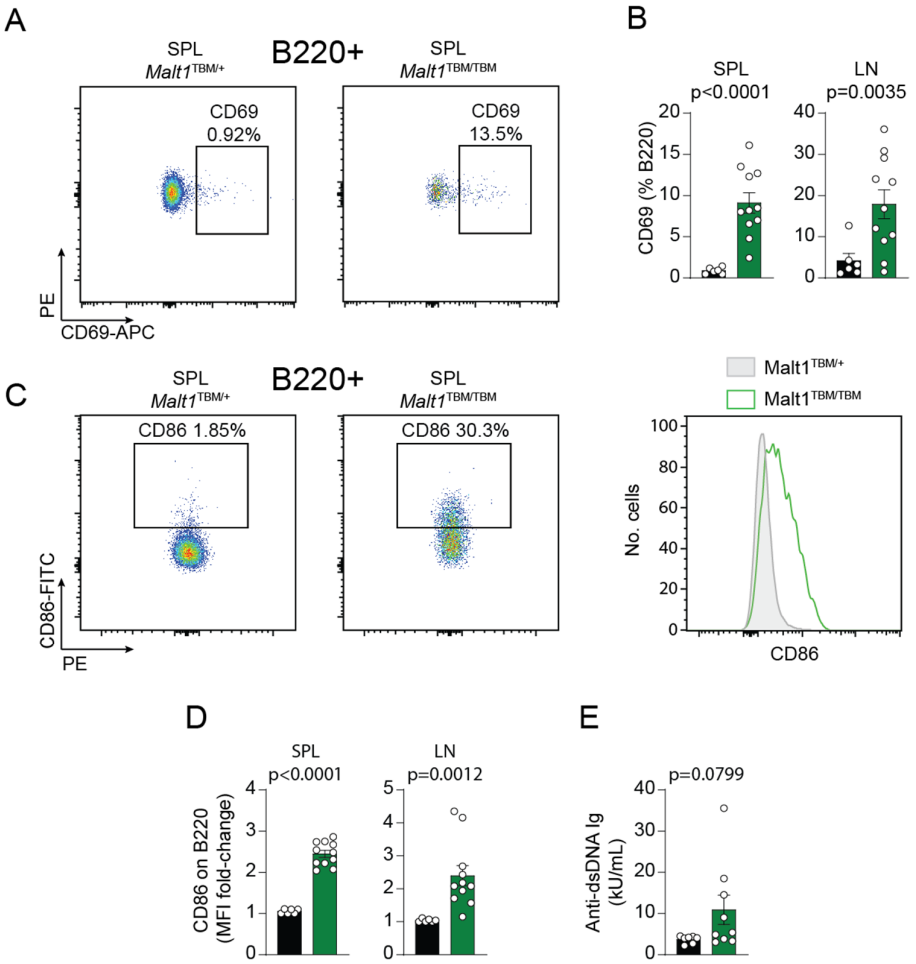

Figure 4-8. Activation phenotype of B cells in *Malt1* TBM mice.
A-B) Relative populations of B220+ CD69+ B cells in spleen (SPL) and lymph nodes (LN) of *Malt1*$^{TBM/TBM}$ and *Malt1*$^{TBM/+}$ mice. C-D) Relative populations of B220+ CD86+ B cells in spleen and lymph nodes of *Malt1*$^{TBM/TBM}$ and *Malt1*$^{TBM/+}$ mice shown as percentage and histogram (C), and MFI fold-change (D). E) Blood serum concentration (10^3 units per mL) of anti-dsDNA Ig antibodies in *Malt1* TBM mice. A-D) Mice were analyzed at 18 days after birth. Unaffected control *Malt1*$^{TBM/+}$ littermates (black) were compared to *Malt1*$^{TBM/TBM}$ mice (green). Each dot represents one mouse. All bars show means ± SEM, and p-values were calculated by unpaired t-test with Welch's correction.

4.1.5 *Malt1*$^{TBM/TBM}$ mice have increased regulatory T cell populations and function

Immune-suppressive regulatory T (Treg) cells are important regulators of peripheral tolerance, antagonizing and balancing conventional T cell activity to prevent autoinflammation (Teh et al., 2015). MALT1 paracaspase function is essential for the maturation of regulatory T cells in the thymus. In line with this, mice carrying destructive mutations in the MALT1 paracaspase domain

(*Malt1* paracaspase mutant (PM) mice) have severe autoimmune activation and severe loss of suppressive CD4+FoxP3+ Tregs (Bornancin et al., 2015; Gewies et al., 2014; Jaworski et al., 2014). Moreover, conditional expression of the paracaspase mutation in Tregs was reported to give rise to defective Tregs (Rosenbaum et al., 2019). In contrast, *Malt1*$^{TBM/TBM}$ mice show an increase in CD4+FoxP3+ Tregs (Figure 4-9A,B), as well as a higher frequency of peripherally differentiated Tregs expressing T_{EM} activation markers (effector Tregs (eTregs): CD4+FoxP3+CD44^{hi}CD62L^{lo}) compared with controls (Figure 4-9C). *Malt1* TBM Tregs still express the suppression markers Ox40 and CTLA-4, indicating that they should still be able to suppress effector T cells (Teh et al., 2015). Expression of CTLA-4 was unchanged in eTregs, while Ox40 expression was significantly elevated in *Malt1*$^{TBM/TBM}$ compared to controls, another marked difference from the decreased expression in *Malt1* PM mice (Figure 4-9D,E). Thus, inhibition of MALT1-TRAF6 binding leads to a severe immune pathology with accumulation of activated T and B cells and an increase in Treg and eTreg populations, in direct contrast to the phenotype of *Malt1* PM mice.

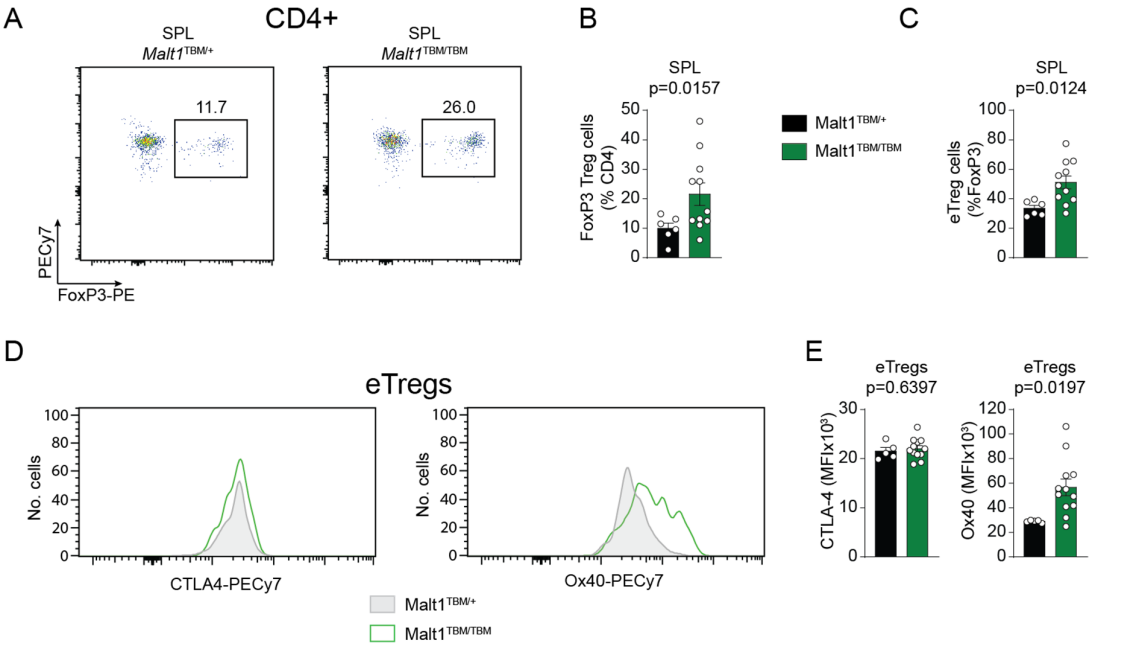

Figure 4-9 Regulatory T cell phenotype in *Malt1* TBM mice.
A-B) Relative populations of CD4+ FoxP3+ Treg cells in spleen (SPL) of *Malt1*$^{TBM/TBM}$ and *Malt1*$^{TBM/+}$ mice. C) Relative populations of CD4+ FoxP3+ CD44^{hi} CD62L^{lo} effector Tregs (eTregs) in spleen of *Malt1*$^{TBM/TBM}$ and *Malt1*$^{TBM/+}$ mice. D-E) Expression of Ox40 and CTLA-4 on eTregs in spleen of *Malt1*$^{TBM/TBM}$ and *Malt1*$^{TBM/+}$ mice shown as MFI. A-E) Mice were analyzed at 18 days after birth. Unaffected control *Malt1*$^{TBM/+}$ littermates (black) were compared to *Malt1*$^{TBM/TBM}$ mice (green). Each dot represents one mouse. All bars show means ± SEM, and p-values were calculated by unpaired t-test with Welch's correction.

4.1.6 Heterozygous *Malt1*$^{TBM/+}$ mice have late-onset inflammation

Heterozygous *Malt1*$^{TBM/+}$ mice were used as controls and did not show any signs of inflammation during the first 4-6 weeks after birth (see Figure 4-4D, Figure 4-5D). However, due to the severe

immune disorder of *Malt1*$^{TBM/TBM}$ mice, we wanted to explore whether TBM mutations on one allele in heterozygous animals could have a dominant effect and be sufficient to cause a delayed immune phenotype. *Malt1*$^{TBM/+}$ mice appeared healthy and did not show any change in body weight up to one year of age (Figure 4-10A). However, necropsy at 3, 6, and 12 months of age showed that at one year, spleen weight is significantly increased in heterozygous mice compared to wildtype (Figure 4-10B). CD4+ T_{EM} cells were significantly increased after 6 months, and CD8+ T_{EM} cells after one year, showing that the effector T cell phenotype seen in *Malt1*$^{TBM/TBM}$ is also present in heterozygous mice, though with strongly delayed onset (Figure 4-10C). CD4+FoxP3+ Treg cells were increased after one year, again showing the same tendencies as in homozygous mice (Figure 4-10D). Thus, expression of a single *Malt1* TBM allele in *Malt1*$^{TBM/+}$ mice is sufficient to cause a delayed T cell activation phenotype reminiscent of *Malt1* TBM chimeras, arguing for a dominant phenotype.

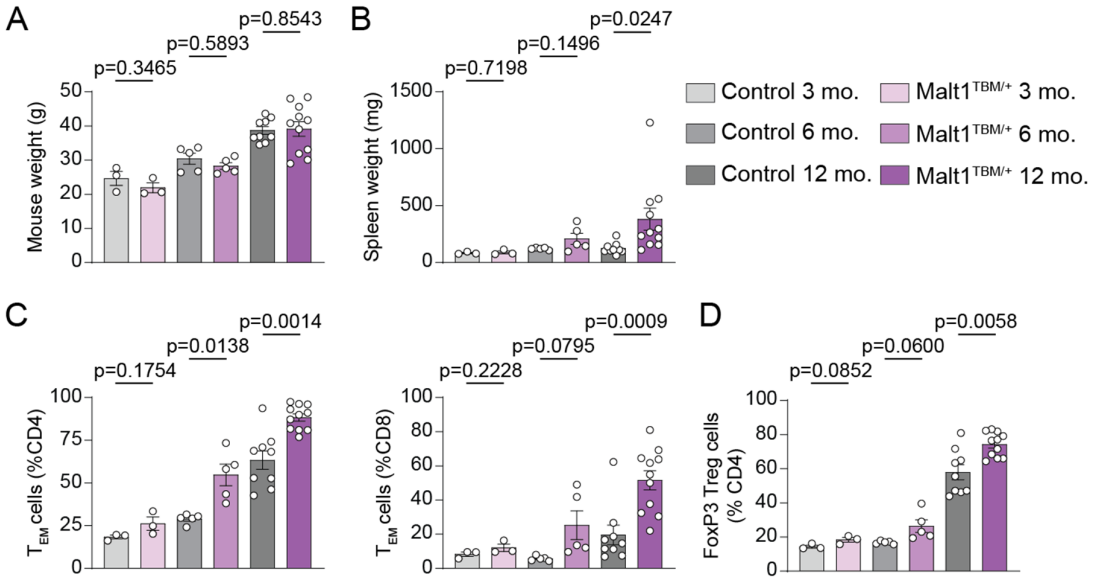

Figure 4-10 Immune phenotyping of *Malt1* TBM heterozygous mice.
A,B) Mouse (A) and spleen (B) weight in *Malt1*$^{TBM/+}$ and *Malt1*$^{+/+}$. C) Relative populations of CD4+ and CD8+ T_{EM} cell in spleen of *Malt1*$^{TBM/+}$ and *Malt1*$^{+/+}$ mice. D) Relative populations of CD4+ FoxP3+ Tregs in spleen of *Malt1*$^{TBM/+}$ and *Malt1*$^{+/+}$ mice. A-D) Mice were analyzed at approximately 3, 6, and 12 months after birth. Unaffected control *Malt1*$^{+/+}$ littermates (grey shades) were compared to *Malt1*$^{TBM/+}$ mice (purple shades). Each dot represents one mouse. All bars show means ± SEM, and p-values were calculated by unpaired t-test with Welch's correction.

4.2 Impairment of MALT1-TRAF6 interaction in T cells is sufficient to cause lymphocyte activation

Analysis of *Malt1*$^{TBM/TBM}$ mice demonstrated that mutation of *Malt1* T6BMs in all somatic cells results in severe autoinflammation with prominent activation of T cells. To clarify the contribution of T cells to the phenotype of *Malt1* TBM mice, expression of the *Malt1* TBM mutations needed to be restricted specifically to T cells utilizing Cre-recombinase mouse lines. All T cells express the glycoprotein CD4 early in thymic T cell development (Parkin & Cohen, 2001). Therefore, to express

TBM mutations in total T cells, *Malt1* TBM mice were crossed with CD4-cre recombinase mice. To this end, CD4-Cre was expressed heterozygously in *Malt1*$^{TBM/+}$ mice, and these mice were subsequently crossed with Malt1$^{flox/flox}$ mice to yield *Malt1*$^{TBM/flox}$*;CD4-Cre*$^{Cre+}$ mice (*Malt1* TBM-T mice). *Malt1* TBM-T mice express the TBM mutations heterozygously in all cell types but lose expression of the floxed endogenous allele in T cells to yield *Malt1*$^{TBM/-}$.

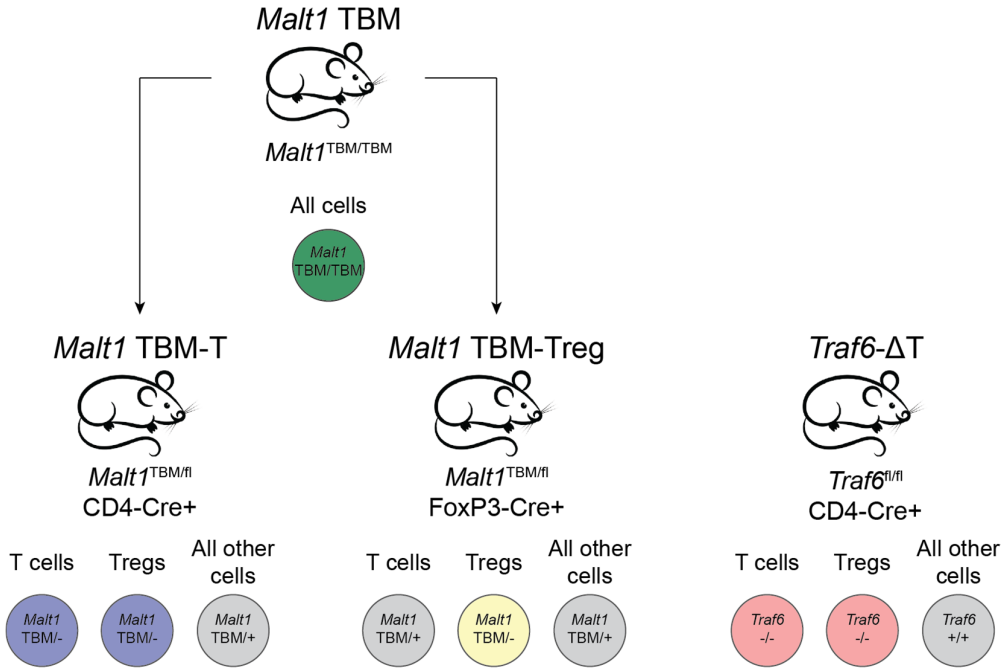

Figure 4-11 Breeding overview of mice utilizing the Cre-Lox recombination system for conditionally interrupting MALT1-TRAF6 interaction.
Breeding overview for establishment of T cell conditional (TBM-T mice: *Malt1*$^{TBM/fl}$; *CD4-Cre*$^{Cre+}$) and Treg conditional (TBM-Treg mice: *Malt1*$^{TBM/fl}$; *FoxP3-Cre*$^{Cre+}$) lines from *Malt1* TBM mice. For comparison, T cell conditional loss of TRAF6 (*Traf6*-ΔT mice: *Traf6*$^{fl/fl}$; *CD4-Cre*$^{Cre+}$) was established in parallel. Affected cell populations are shown in color for each line, unaffected populations are shown in grey.

MALT1 has been shown to be essential for Treg development and function (Gewies et al., 2014; Jaworski et al., 2014; Rosenbaum et al., 2019; Ruland et al., 2003), and given the increased expression and suppressive features of Tregs in *Malt1* TBM mice, we wanted to investigate the specific impact of the TBM mutations on Treg cells. Treg lineage is defined by expression of the transcription factor FoxP3 (Josefowicz & Rudensky, 2009). Therefore, *Malt1*$^{TBM/+}$ mice were crossed with transgenic FoxP3-Cre mice, which were then crossed with *Malt1*$^{flox/flox}$ mice to give *Malt1*$^{TBM/flox}$;*FoxP3-Cre*$^{Cre+}$ (*Malt1* TBM-Treg), which express *Malt1*$^{TBM/-}$ in FoxP3+ Tregs.

Mice with loss of TRAF6 expression in T cells have an autoimmune phenotype milder than, but with similarities to, the phenotype of *Malt1* TBM mice (King et al., 2006). Therefore, for direct comparison of TBM-mediated loss of MALT1-TRAF6 interaction to complete loss of TRAF6 expression, T cell conditional TRAF6 knockout mice were generated: *Traf6*$^{flox/flox}$*;CD4-Cre*$^{Cre+}$ (*Traf6*-ΔT

mice). All Cre-specific models and their affected cell populations are shown in Figure 4-11. All conditional mouse lines have Cre recombinase expression under control of endogenous promotors. Therefore, to avert loss of function of endogenous genes downstream of these promotors, mice were not bred with homozygous Cre expression.

4.2.1 Destruction of MALT1-TRAF6 interaction drives immune activation by a T cell intrinsic mechanism

All three conditional mouse models with impaired MALT1-TRAF6 interaction proved to be viable and were analyzed at an age of 12 weeks when no obvious signs of disease were observed. *Malt1* TBM-T mice showed similar MALT1 protein expression compared to controls (Figure 4-12A). As described previously for *Traf6*-ΔT mice (King et al., 2006), *Malt1* TBM-T developed signs of dermatitis on the tail and ears starting at 12 weeks of age compared with controls (Figure 4-12B,C). However, dermatitis in *Traf6*-ΔT mice, which were verified to lack TRAF6 expression in T cells (Figure 4-12H), was not reproduced, even in mice up to 6 months of age. *Malt1* TBM mice showed a strong increase in the serum cytokines IFNγ, IL-6, IL-10, IL-17, and TNFα. However, *Malt1* TBM-T and *Traf6*-ΔT mice had cytokine levels similar to relative controls, with slight significant increases in the anti-inflammatory cytokines IL-10 in *Malt1* TBM-T mice and IFNγ in *Traf6*-ΔT mice (Figure 4-12E,F). In line with this, histologies of lung, liver, intestine, and kidney from *Malt1* TBM-T and *Traf6*-ΔT were similar to control mice, showing no signs of immune cell infiltration and inflammation (data not shown). Mouse weight was unchanged in TBM-T, *Traf6*-ΔT, and TBM-Treg mice at 12 weeks of age (Figure 4-12G). As in *Malt1* TBM mice, TBM-T and *Traf6*-ΔT mice exhibited splenomegaly and lymphadenopathy, while TBM-Treg mice did not (Figure 4-12H). Relative numbers of T and B lymphocytes were largely unchanged in all three Cre models (Figure 4-12I,J). When gated on CD3+ cells, CD4+ lymphocytes were increased in TBM-T mice, and CD8+ lymphocytes decreased in TBM-T and *Traf6*-ΔT (Figure 4-12K,L). TBM-Treg mice showed no changes in lymphocyte populations and spleen weight. Overall, modulation of T and B cell cell populations was less severe in Cre models than in *Malt1* TBM mice.

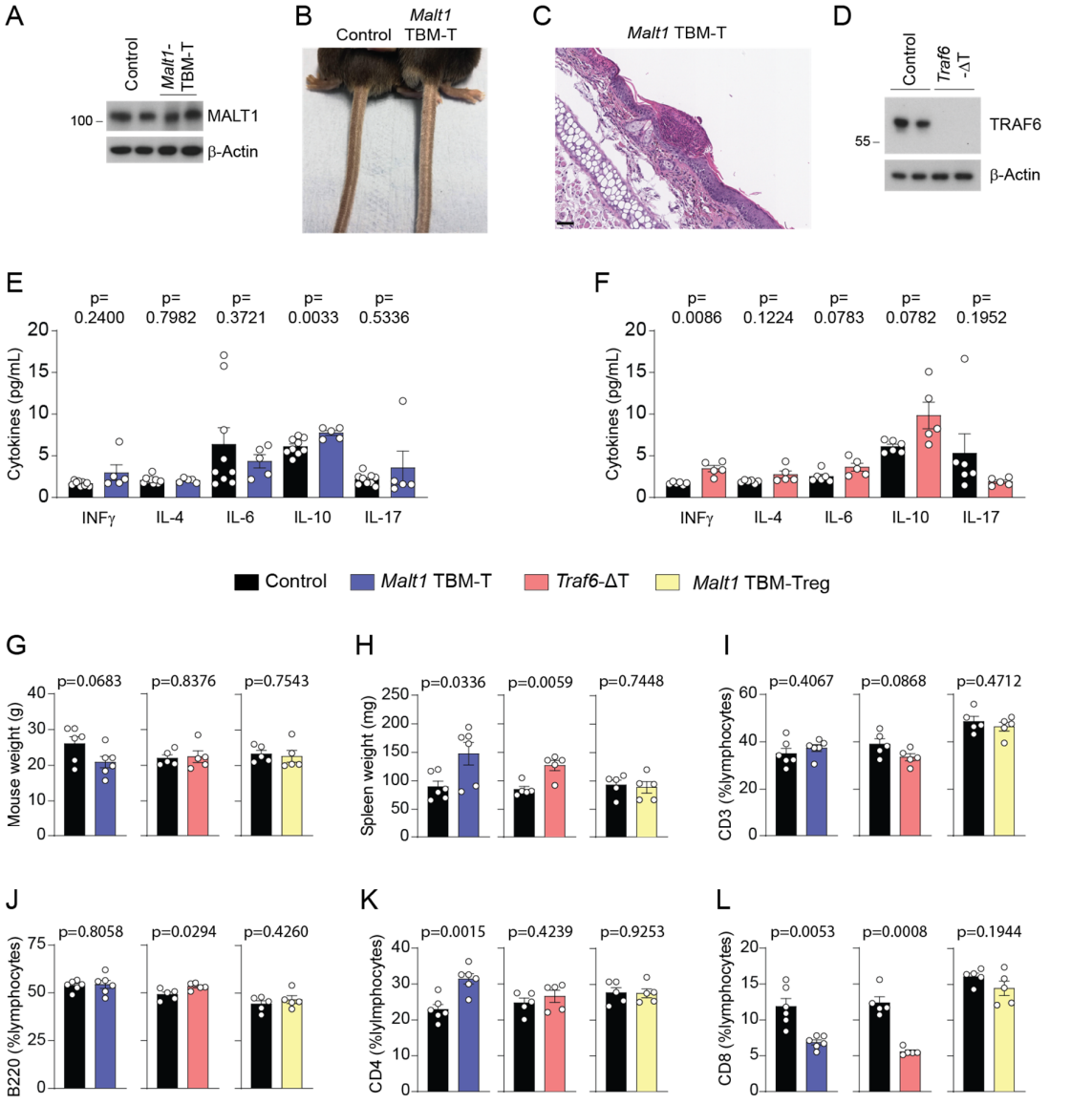

Figure 4-12. Cytokine production and lymphocyte populations in Cre models.
A) Immunoblot showing relative MALT1 protein expression in *Malt1* TBM-T and control mice (each two mice). B) Representative pictures showing dermatitis on the tail of TBM-T compared with control mice. C) Representative histological analysis of tail tissue from *Malt1* TBM-T. D) Immunoblot showing loss of TRAF6 protein expression in *Traf6*-ΔT compared to control mice (each two mice). E,F) Blood serum levels of indicated cytokines in *Malt1* TBM-T (E) and*Traf6*-ΔT (F) mice. G-H) Mouse body (G) and spleen (H) weight in TBM-T, *Traf6*-ΔT, and TBM-Treg mice. I-J) Relative populations of CD3+ T cells (I) and B220+ B cells (J) in spleen of TBM-T, *Traf6*-ΔT, and TBM-Treg mice. K-L) Relative populations of CD4+ (K) and CD8+ (L) T cells in spleen of TBM-T, *Traf6*-ΔT, and TBM-Treg mice. G-L) All stains were performed on splenocytes. Littermate control mice were *Malt1*$^{fl/+}$*;CD4-Cre-,* *Malt1*$^{fl/+}$;CD4-Cre+ and *Malt1*$^{TBM/fl}$*;CD4-Cre-* or *Malt1*$^{fl/+}$*;FoxP3-Cre-,* *Malt1*$^{fl/+}$;FoxP3-Cre+ and *Malt1*$^{TBM/fl}$*;FoxP3-Cre-* or *Traf6*$^{-fl/+}$*;CD4-Cre+,Traf6*$^{fl/fl}$*;CD4-Cre-* and *Traf6*$^{fl/+}$*;CD4-Cre-* (black) for *Malt1* TBM-T (blue), *Traf6*-ΔT (pink), and *Malt1* TBM-Treg (yellow), respectively. Each dot represents one mouse. All bars show means ± SEM, and p-values were calculated by unpaired t-test with Welch's correction.

Next, we determined peripheral lymphocyte activation in *Malt1* TBM-T, *Traf6*-ΔT, and *Malt1* TBM-Treg mice. Both *Malt1* TBM-T and *Traf6*-ΔT mice showed strong increases in CD4+ and CD8+ T_{EM} cells, with a corresponding reduction of $T_{naïve}$ cells (Figure 4-13A-F). CD3+ CD69+ cells were also increased in *Malt1* TBM-T and *Traf6*-ΔT mice, again indicating T cell activation (Figure 4-13G). *Malt1*

TBM-Treg mice did not show any signs of T cell activation, either in T_{EM} cells or expression of CD69, again indicating that loss of MALT1-TRAF6 interaction in regulatory T cells does not drive the phenotype seen in *Malt1* TBM mice (Figure 4-13A-G).

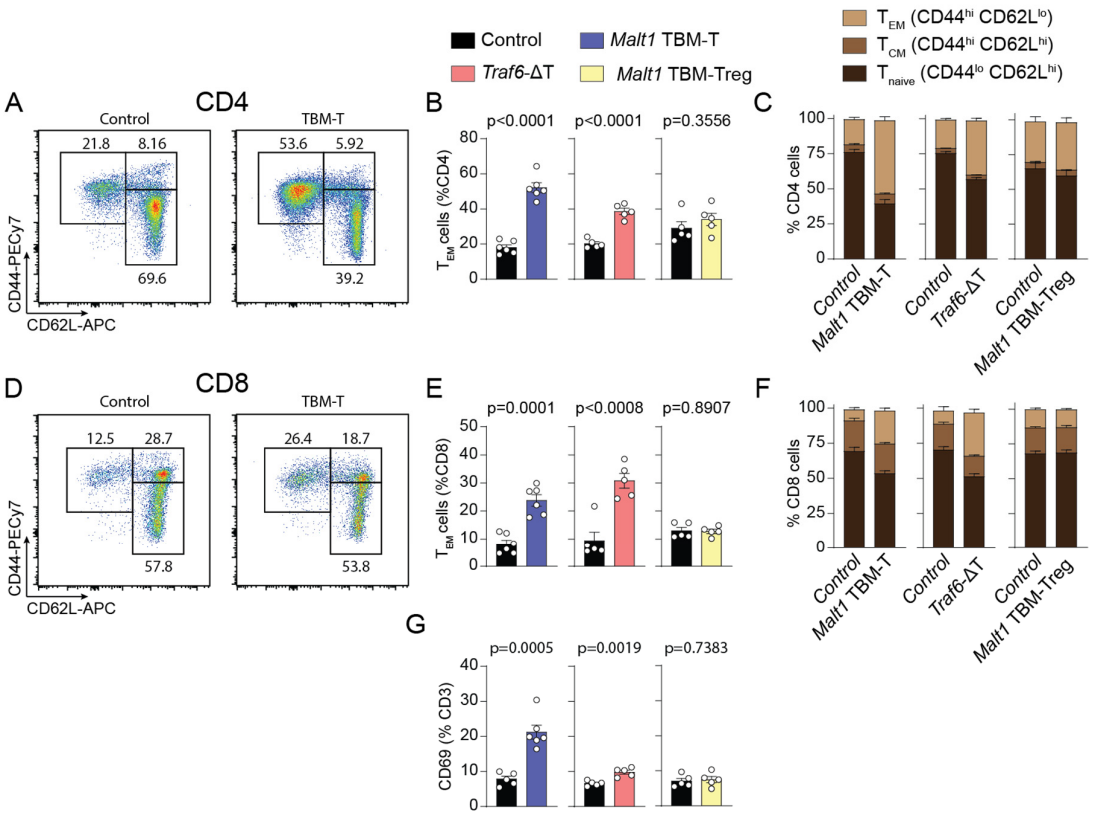

Figure 4-13. Activation phenotype of T cells in Cre models.
A,D) Representative plots showing T_{EM}, T_{CM}, and $T_{naïve}$ CD4+ (A) and CD8+ (D) T cells in TBM-T mice. B,E) Relative populations of CD4+ (B) and CD8+ (E) T_{EM} cells in TBM-T, *Traf6*-ΔT, and TBM-Treg mice. C-F) Relative distribution of T_{EM}, T_{CM}, and $T_{naïve}$ CD4+ (C) and CD8+ (F) T cells in spleen of TBM-T, *Traf6*-ΔT, and TBM-Treg mice. G) Relative populations of CD3+ CD69+ T cells in spleen of TBM-T, *Traf6*-ΔT, and TBM-Treg mice. A-G) All stains were performed on splenocytes. Littermate control mice were *Malt1*$^{fl/+}$*;CD4-Cre-*, *Malt1*$^{fl/+}$;CD4-Cre+ and *Malt1*$^{TBM/fl}$*;CD4-Cre-* or *Malt1*$^{fl/+}$*;FoxP3-Cre-*, *Malt1*$^{fl/+}$;FoxP3-Cre+ and *Malt1*$^{TBM/fl}$*;FoxP3-Cre-* or *Traf6*$^{-fl/+}$*;CD4-Cre+,Traf6*$^{fl/fl}$*;CD4-Cre-* and *Traf6*$^{fl/+}$*;CD4-Cre-* (black) for *Malt1* TBM-T (blue), *Traf6*-ΔT (pink), and *Malt1* TBM-Treg (yellow), respectively. Each dot represents one mouse. All bars show means ± SEM, and p-values were calculated by unpaired t-test with Welch's correction.

Further, CD69+ and CD86+ cell expression was increased on B220+ cells of both *Malt1* TBM-T and *Traf6*-ΔT (Figure 4-14A,B). Increased B cell activation contributed to an increase in dsDNA-specific autoantibodies, a strong sign of autoimmunity in TBM-T and *Traf6*-ΔT (Figure 4-14C). As was the case in T cells, B cells of *Malt1* TBM-Treg mice showed no upregulation of activation markers (Figure 4-14A,B).

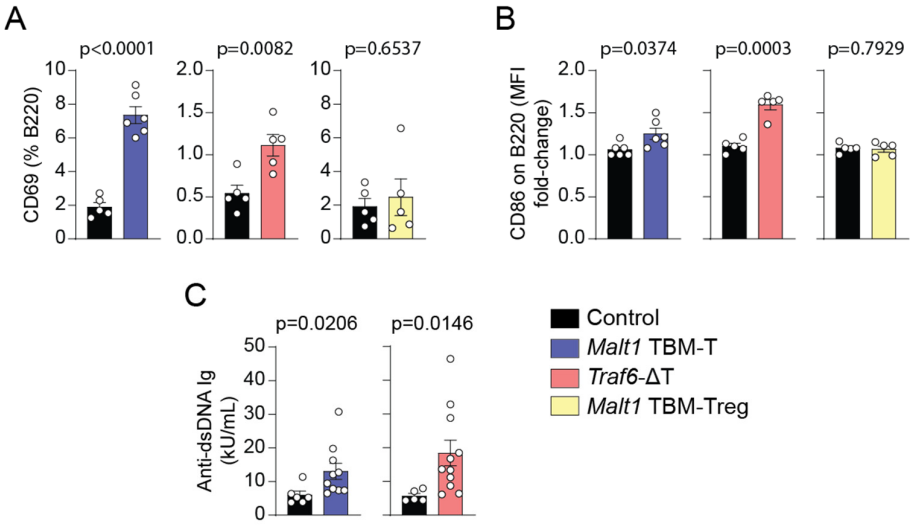

Figure 4-14. Activation phenotype of B cells in Cre models.
A) Relative populations of B220+ CD69+ B cells in spleen of TBM-T, *Traf6*-ΔT, and TBM-Treg mice. B) Relative expression of CD86 on splenic B220+ B cells as MFI fold-change in TBM-T, *Traf6*-ΔT, and TBM-Treg mice. C) Blood serum concentration (10^3 units per mL) of anti-dsDNA Ig antibodies in TBM-T and *Traf6*-ΔT mice. A-C) All stains were performed on splenocytes. Littermate control mice were *Malt1*$^{fl/+}$*;CD4-Cre-*, *Malt1*$^{fl/+}$;CD4-Cre+ and *Malt1*$^{TBM/fl}$*;CD4-Cre-* or *Malt1*$^{fl/+}$*;FoxP3-Cre-*, *Malt1*$^{fl/+}$;FoxP3-Cre+ and *Malt1*$^{TBM/fl}$*;FoxP3-Cre-* or *Traf6*$^{-fl/+}$*;CD4-Cre+,Traf6*$^{fl/fl}$*;CD4-Cre-* and *Traf6*$^{fl/+}$*;CD4-Cre-* (black) for *Malt1* TBM-T (blue), *Traf6*-ΔT (pink), and *Malt1* TBM-Treg (yellow), respectively. Each dot represents one mouse. All bars show means ± SEM, and p-values were calculated by unpaired t-test with Welch's correction.

To determine if MALT1-TRAF6 binding abrogation plays a primary role in the increased Treg populations and function seen in *Malt1* TBM mice, Treg markers were measured in *Malt1* TBM-T, *Traf6*-ΔT, and *Malt1* TBM-Treg mice. CD4+FoxP3+ Tregs were increased in *Malt1* TBM-T and TBM-Treg but not *Traf6*-ΔT (Figure 4-15A). CD4+FoxP3+CD44^{hi}CD62L^{lo} eTregs were significantly elevated in all three Cre lines (Figure 4-15B). Expression of the Treg cell suppression marker Ox40 was significantly increased in all three Cre lines, although the magnitude of increase in *Malt1* TBM-Treg and *Traf6*-ΔT was negligible (Figure 4-15C). Thus, loss of MALT1-TRAF6 interaction in T cells leads to a general increase in FoxP3 Tregs and expression of the Treg suppression marker Ox40.

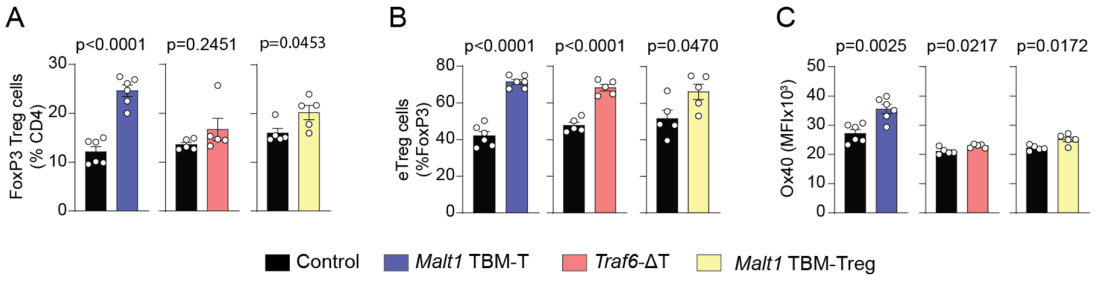

Figure 4-15. Regulatory T cell phenotype in Cre models.
A) Relative populations of CD4+ FoxP3+ Treg cells in spleen of *Malt1* TBM-T, TBM-Treg, and *Traf6*-ΔT mice. B)) Relative populations of CD4+ FoxP3+ CD44hi CD62Llo Tregs in spleen of *Malt1* TBM-T, TBM-Treg, and *Traf6*-ΔT mice. C) Expression of Ox40 on eTregs in spleen of *Malt1* TBM-T, TBM-Treg, and *Traf6*-ΔT mice shown as MFI. A-C) All stains were performed on splenocytes. Littermate control mice were *Malt1*$^{fl/+}$*;CD4-Cre-*, *Malt1*$^{fl/+}$;CD4-Cre+ and *Malt1*$^{TBM/fl}$*;CD4-Cre-* or *Malt1*$^{fl/+}$*;FoxP3-Cre-*, *Malt1*$^{fl/+}$;FoxP3-Cre+ and *Malt1*$^{TBM/fl}$*;FoxP3-Cre-* or *Traf6*$^{-fl/+}$*;CD4-Cre+,Traf6*$^{fl/fl}$*;CD4-Cre-* and *Traf6*$^{fl/+}$*;CD4-Cre-* (black) for *Malt1* TBM-T (blue), *Traf6*-ΔT (pink), and *Malt1* TBM-Treg, respectively. Each dot represents one mouse. All bars show means ± SEM, and p-values were calculated by unpaired t-test with Welch's correction.

4.2.2 MALT1-TRAF6 association drives NF-κB activation in T cells

To unravel the unexpected auto-immune and inflammatory disease caused by the disruption of MALT1-TRAF6 interaction, we wanted to investigate the molecular consequences of MALT1 and TRAF6 mutations on signaling in primary CD4 T cells. *In vitro* data after TCR/CD28 co-stimulation of Jurkat T cells indicates that TRAF6 association to MALT1 is required for downstream ubiquitination and activation of the IKK complex in the NF-κB pathway (Meininger et al., 2016). Therefore, T cells from *Malt1* TBM-T and *Traf6*-ΔT mice were used to test the impact of these mutations on downstream activation and nuclear import of NF-κB transcription factors. EMSA analyses with lysates from CD4 T cells of TBM-T and *Traf6*-ΔT clearly show an almost complete loss of NF-κB DNA binding activity following stimulation with PMA/Ionomycin (P/I) compared with controls, which together with reduction of IκBα phosphorylation and degradation and reduced p65 phosphorylation – as shown by Western Blot analyses – demonstrates strong loss of NF-κB pathway induction downstream of the CBM complex (Figure 4-16A,B). P/I stimulation was used as it yields strong T cells activation independent of receptor signaling complexes, and therefore excludes possible secondary phenotypic alterations to signaling upstream of the CBM complex. To independently verify these results, quantitative flow cytometric imaging analysis was utilized to quantify the extent of NF-κB nuclear translocation in primary CD4 T cells. Stimulated control cells show nuclear translocation of the NF-κB subunit p65, whereas stimulated TBM-T and *Traf6*-ΔT CD4 T cells showed no increase in nuclear p65, showing strong resemblance to unstimulated control cells and indicating a loss of NF-κB activation in these cells (Figure 4-16C). Similarity score is a calculation which compares nuclear and cytosolic localization of p65 staining between images. A higher score indicates an inversion of the unstimulated control image, and therefore nuclear import of p65 from the cytosol. Stimulated CD4 T cells from control mice show a similarity score over 1, indicating nuclear import of p65. However, stimulation of *Traf6*-ΔT and *Malt1* TBM-T T cells gives a similarity score similar to the unstimulated control, indicating an inability to activate NF-κB in these mice (Figure 4-16D-F). Results show that induction of NF-κB activation and translocation is strongly dependent upon both the expression of TRAF6 and TRAF6-MALT1 binding in T cells.

4.2.3 *Malt1* TBM mice have enhanced Malt1 cleavage activity

NF-κB induction is dependent upon MALT1 scaffolding but not MALT1 enzymatic function, and NF-κB is still activated upon stimulation in MALT1 protease defective cells (Bornancin et al., 2015; Gewies et al., 2014; Jaworski et al., 2014; Meininger et al., 2016). However, the effect of abrogated MALT1 scaffolding function on MALT1 paracaspase activity is unknown. Interestingly, TRAF6 binding is not required for activation of MALT1 protease function, and TBM-T and *Traf6*-ΔT CD4 T cells can be stimulated with P/I to induce robust cleavage of MALT1 substrate like CYLD and Regnase-1 (Figure

4-17A,B). In fact, TBM-T and *Traf6*-ΔT cells show cleavage of MALT1 substrates even in unstimulated conditions, indicating that abrogation of MALT1-TRAF6 interaction leads to constitutive MALT1 activity (Figure 4-17A,B).

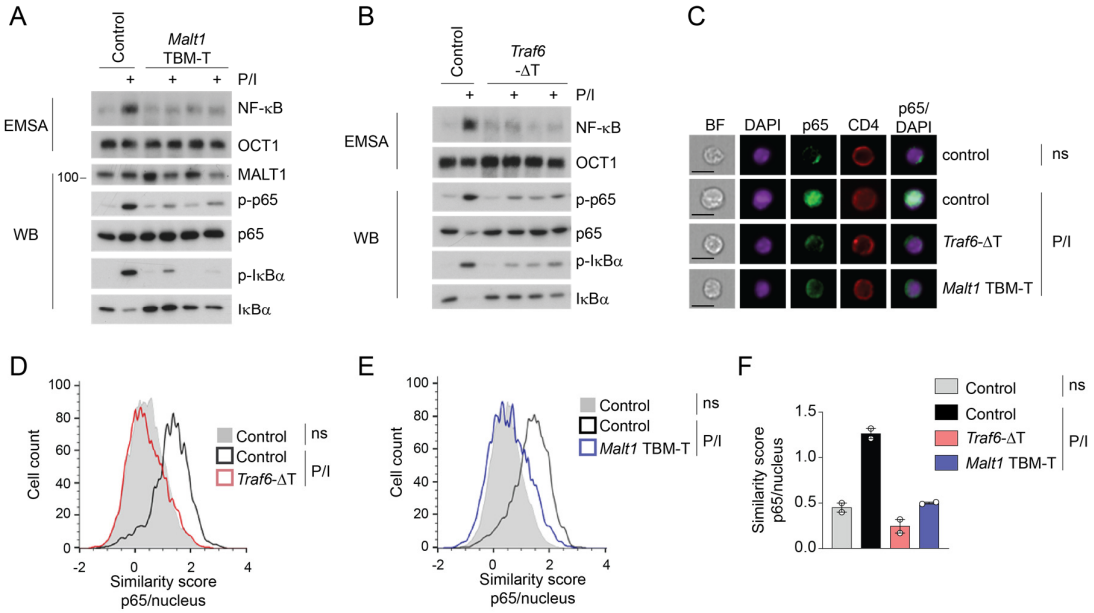

Figure 4-16. NF-κB activation in *Malt1* TBM-T and *Traf6*-ΔT mice.
A,B) Biochemical analysis of NF-κB DNA binding (EMSA) and canonical NF-κB signaling (Western Blot) for TBM-T (A) and *Traf6*-ΔT (B) mice. C) ImageSteam® analyses of nuclear import of the NF-κB subunit p65 in splenic CD4+ T cell of TBM-T and *Traf6*-ΔT mice. Non-stimulated (ns) cells were compared with cells stimulated with PMA/Ionomycin (P/I) for 30 minutes. DAPI is shown for nuclear stain. Scale bars: 10 µm. BF: bright field. D,E) Histograms showing similarity scores for nuclear p65 in TBM-T and *Traf6*-ΔT mice after P/I stimulation. F) Similarity score comparison of control, TBM-T, and *Traf6*-ΔT mice after P/I stimulation. A-F) Littermate control mice were *Malt1*$^{fl/+}$*;CD4-Cre-, Malt1*$^{fl/+}$;CD4-Cre+ and *Malt1*$^{TBM/fl}$*;CD4-Cre-* or *Traf6*-$^{fl/+}$*;CD4-Cre+,Traf6*$^{fl/fl}$*;CD4-Cre-* and *Traf6*$^{fl/+}$*;CD4-Cre-* (black) for *Malt1* TBM-T (blue) or *Traf6*-ΔT (pink), respectively. Each dot represents one mouse. ImageStream® analysis was done in collaboration with Marc Rosenbaum from the group of Jürgen Ruland, TUM school of medicine, München.

We wanted to investigate putative downstream effects of constitutive MALT1 protease activation in CD4 T cells from *Malt1* TBM-T and *Traf6*-ΔT mice. The majority of known MALT1 cleavage substrates act either as positive and negative regulators of NF-κB activation (CYLD, A20, HOIL-1, and RELB), or are themselves members of the CBM complex (BCL10 and MALT1). However, MALT1 cleavage also regulates the expression of the RNA-binding proteins (RBPs) Regnase-1 and Roquin-1/2 which are essential for regulating pro-inflammatory mRNAs and preventing T cell activation and differentiation in resting cells (Essig et al., 2017). Loss of function in Roquin is associated with increased lymphocyte activation via upregulation of *Pten* and hyperactivation of the PI3K-mTOR pathway in T cells (Essig et al., 2017). We therefore predicted that constitutive MALT1 paracaspase activity and cleavage of RBP substrates could yield autoimmunity and should be apparent in increased expression of Regnase-1 and Roquin-1/2 substrates. In line with this hypothesis, IκBNS and ICOS, the mRNAs of which are targets of the MALT1 cleavage substrate Roquin-1, have massively increased expression in CD4+ and

CD8+ T cells of TBM-T and *Traf6*-ΔT mice independent of stimulation (Figure 4-17C-H). These results suggest that dysregulation of MALT1 cleavage via loss of TRAF6 expression or binding strongly impacts downstream regulatory networks, essentially amounting to a partial loss-of-function of MALT1 cleavage substrates.

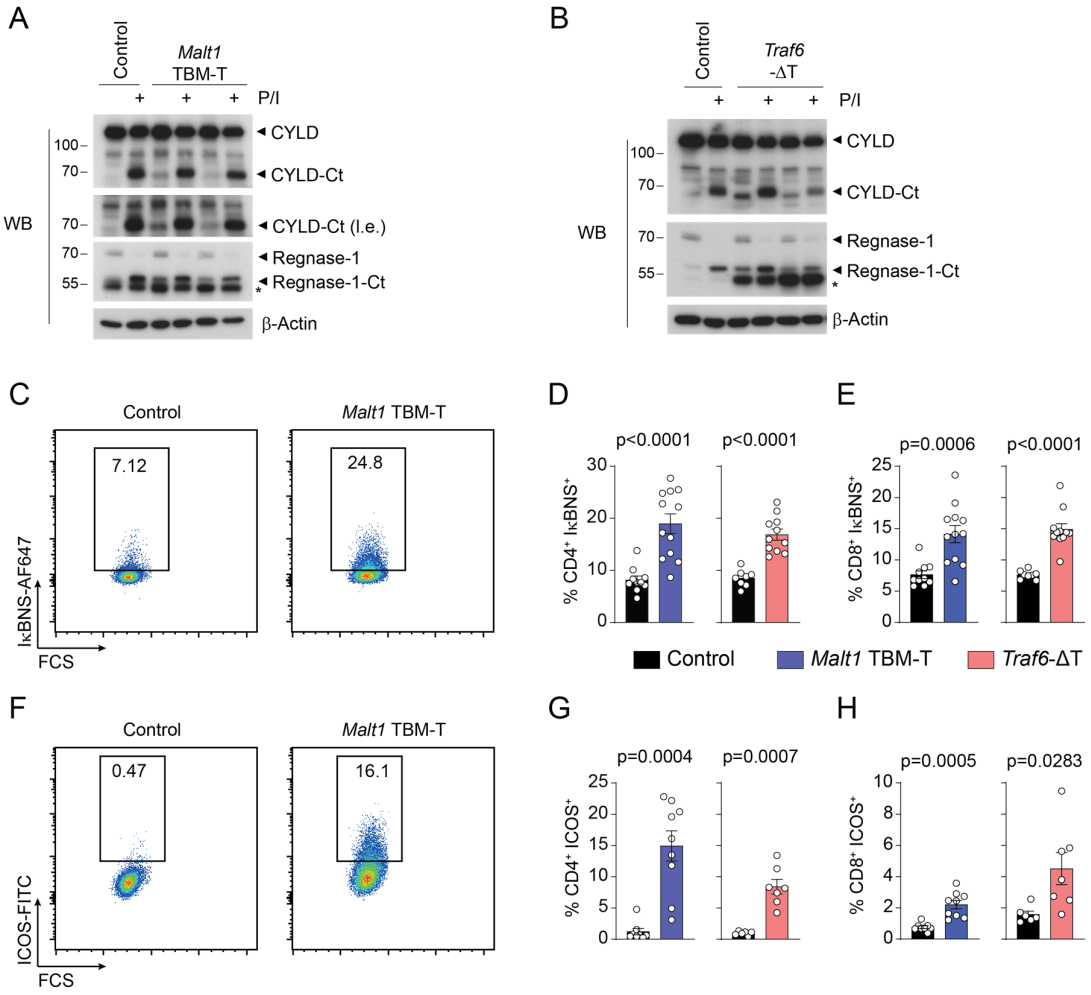

Figure 4-17. Constitutive cleavage of MALT1 substrates in *Malt1* TBM-T and *Traf6*-ΔT mice.
A-B) Immunoblot analysis of MALT1 substrate cleavage in CD4 cells of *Malt1* TBM-T (A) and *Traf6*-ΔT (B) mice after P/I stimulation. Ct: C-terminal cleavage fragment. Asterisks represent non-specific antibody binding. C) Representative plots of CD4+ IκBNS+ T cells in TBM-T and control mice. D,E) Relative populations of IκBNS+ CD4+ (D) and CD8+ (E) T cells in spleen of TBM-T and *Traf6*-ΔT mice. F) Representative plots of CD4+ ICOS+ T cells in TBM-T and control mice. G,H) Relative populations of ICOS+ CD4+ (G) and CD8+ (H) T cells in spleen of TBM-T and *Traf6*-ΔT mice. C-H) Littermate control mice were *Malt1*$^{fl/+}$;*CD4-Cre-*, *Malt1*$^{fl/+}$;CD4-Cre+ and *Malt1*$^{TBM/fl}$;*CD4-Cre-* or *Traf6*-$^{fl/+}$;*CD4-Cre+*,*Traf6*$^{fl/fl}$;*CD4-Cre-* and *Traf6*$^{fl/+}$;*CD4-Cre-* (black) for *Malt1* TBM-T (blue) or *Traf6*-ΔT (pink), respectively. Each dot represents one mouse. All bars show means ± SEM, and p-values were calculated by unpaired t-test with Welch's correction.

4.3 Constitutive MALT1 paracaspase activity relies on CBM formation and an intact TCR

Impaired MALT1-TRAF6 interaction in *Malt1* TBM-T and *Traf6*-ΔT mice leads to autoimmunity with increased T_{EM} populations and enhanced cleavage of MALT1 substrates. However, it was unclear whether constitutive MALT1 paracaspase activation in T cells is a primary and direct consequence of

impaired MALT1-TRAF6 interaction. Therefore, we wanted to build up a heterologous *in vitro* system to investigate potential T cell-intrinsic mechanisms of chronic MALT1 protease activation upon loss of TRAF6 and to exclude potential secondary effects by the systemic inflammation seen *in vivo*. To this end, TRAF6-deficient Jurkat cells were investigated for cleavage of MALT1 substrates. As was the case in *Traf6*-ΔT mice, TRAF6 knockout Jurkat T cells showed constitutive cleavage of the MALT1 substrates CYLD, HOIL-1, Regnase-1, and Roquin-1/2 compared with unstimulated parental cells, which showed no cleavage (Figure 4-18A). This observation suggests that constitutive MALT1 paracaspase activation is due to a T cell-intrinsic mechanism upon loss of MALT1-TRAF6 interaction.

To determine a dependency of the observed constitutive cleavage on upstream mechanisms, we looked at TRAF6-deficient Jurkat cells in settings without CBM complex formation. Interestingly, tandem knockout of TRAF6 and either BCL10 (B10/T6 dKO) or CARD11 (C11/T6 dKO) led to rescue of constitutive MALT1 activity in unstimulated cells, and CYLD, HOIL-1, Regnase-1, and Roquin-1/2 levels did not differ from parental Jurkat cells (Figure 4-18A). Therefore, the 'constitutive MALT1 cleavage mechanism' is dependent upon CBM complex formation, and loss of CBM complex association completely reverts the phenotype of TRAF6-deficient Jurkat cells in steady state.

These results raised the question, whether upstream signals are responsible for constitutive CBM-dependent MALT1 paracaspase activation in Jurkat T cells under steady state cell culture conditions upon loss of MALT1-TRAF6 interaction. To clarify whether the observed constitutive MALT1 paracaspase activity in TRAF6 knockout Jurkat cell was dependent on signals emanating from the T cell receptor, Jurkat T cells lacking both TRAF6 and a functional TCR were created using CRISPR. To this end, exon 1 of the T cell receptor alpha constant (TRAC) region of the *TCRα* gene was targeted to ablate the TCR complex in TRAF6 KO Jurkat cells (Figure 4-18B). Successful knockouts were verified via flow cytometry by loss of both TCRα/β and CD3ε expression on the surface of the Jurkat T cells (Figure 4-18C), both of which are required for a functional TCR (Galetto et al., 2014). Resulting TCRα/TRAF6 dKO cells showed a loss of constitutive MALT1 cleavage compared to TRAF6 KO Jurkat cells (Figure 4-18D). In parental and TRAF6 KO Jurkat cells, cleavage by MALT1 can be stimulated with P/I or CD3/CD28 crosslinking. TCRα/TRAF6 dKO cells could not be stimulated by CD3/CD28, which requires a functional TCR, but importantly could still be stimulated with P/I, which bypasses and therefore does not require the TCR (Figure 4-18E). Thus, constitutive MALT1 activity upon loss of TRAF6 relies on an intact TCR, showing that inducible and constitutive cleavage are reliant upon the same T cell intrinsic mechanisms.

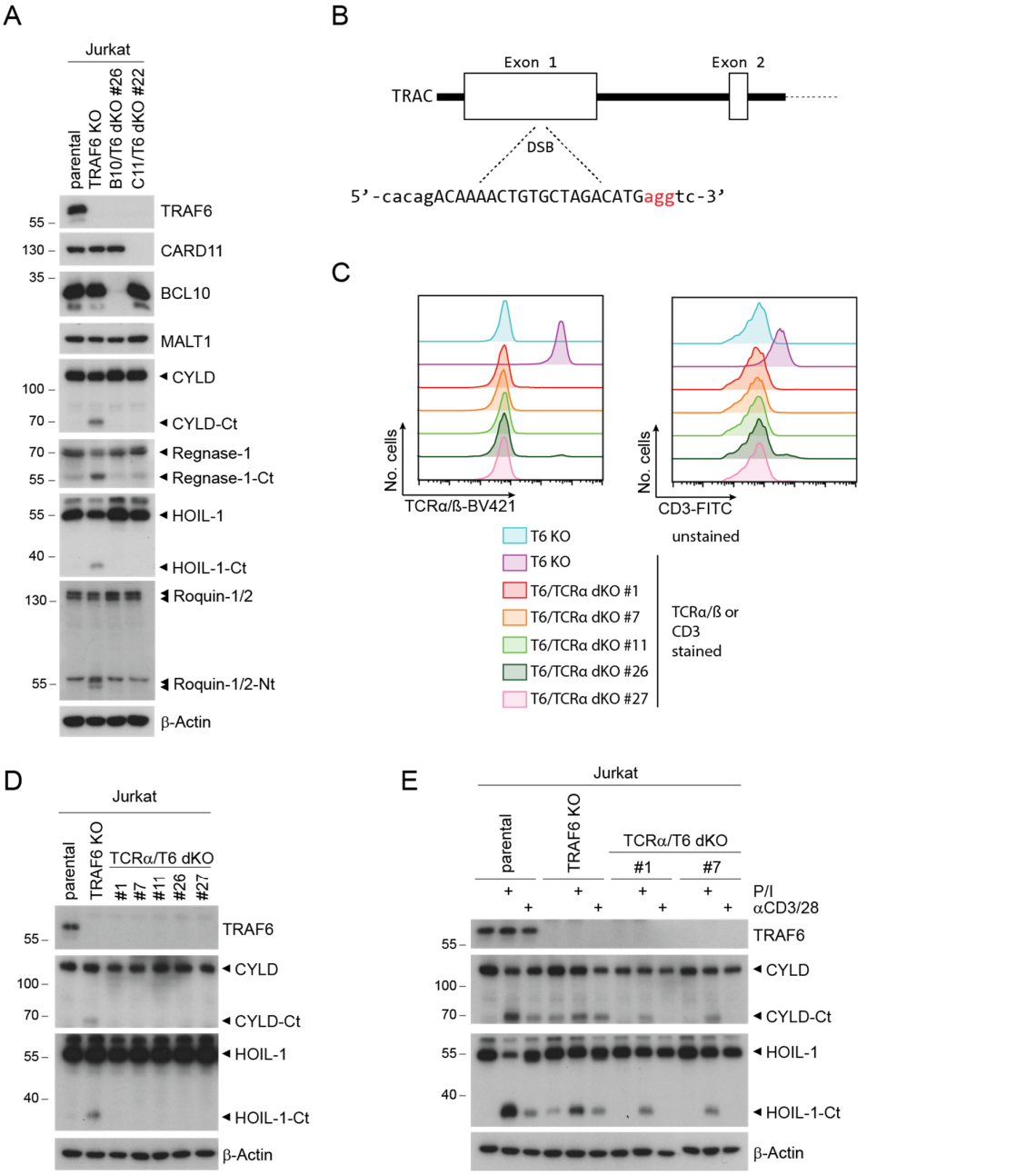

Figure 4-18. Jurkat T cell knockouts.
A) Western Blot showing protein expression of CBM complex members and MALT1 cleavage substrates in parental WT, TRAF6 KO, BCL10/TRAF6 double knockout (dKO), and CARD11/TRAF6 dKO Jurkat cells. B) CRISPR-Cas9 targeting approach for generating *TCRα*-deficient Jurkat clones. C) Immune phenotyping showing TCRα/ß and CD3 expression in TRAF6/TCRα dKO Jurkat clones compared with parental TRAF6 KO Jurkat cells. D) Immunoblot analysis of MALT1 cleavage substrates CYLD and HOIL-1 in TRAF6/TCRα dKO Jurkat clones and parental TRAF6 KO Jurkat cells. E) Immunoblot analysis of MALT1 cleavage substrates CYLD and HOIL-1 in TRAF6/TCRα dKO Jurkat clones after P/I or CD3/CD28 stimulation. A,D,E) Ct: C-terminal cleavage fragment. Nt: N-terminal cleavage fragment.

4.4 Genetic inactivation of MALT1 paracaspase activity

4.4.1 Inactivation of paracaspase activity reverts the *Malt1* TBM phenotype

Malt1 TBM, TBM-T, and *Traf6*-ΔT mice exhibit constitutive MALT1 activity, shown to be dependent upon TCR ligation and CBM complex formation. To investigate the intriguing hypothesis that

persistent MALT1 activity is the cause of fatal, early-onset inflammation, we performed genetic rescue by addition of the C472A paracaspase inactivating mutation (PM) to *Malt1* TBM mice. The resulting mice carry the triple MALT1 mutation E325A, C472A, E814A (henceforth referred to as *Malt1* TBMPM) which lacks both scaffolding (due to TRAF6 binding deficiency) and cleavage function (due to the PM modification) (Figure 4-19A).

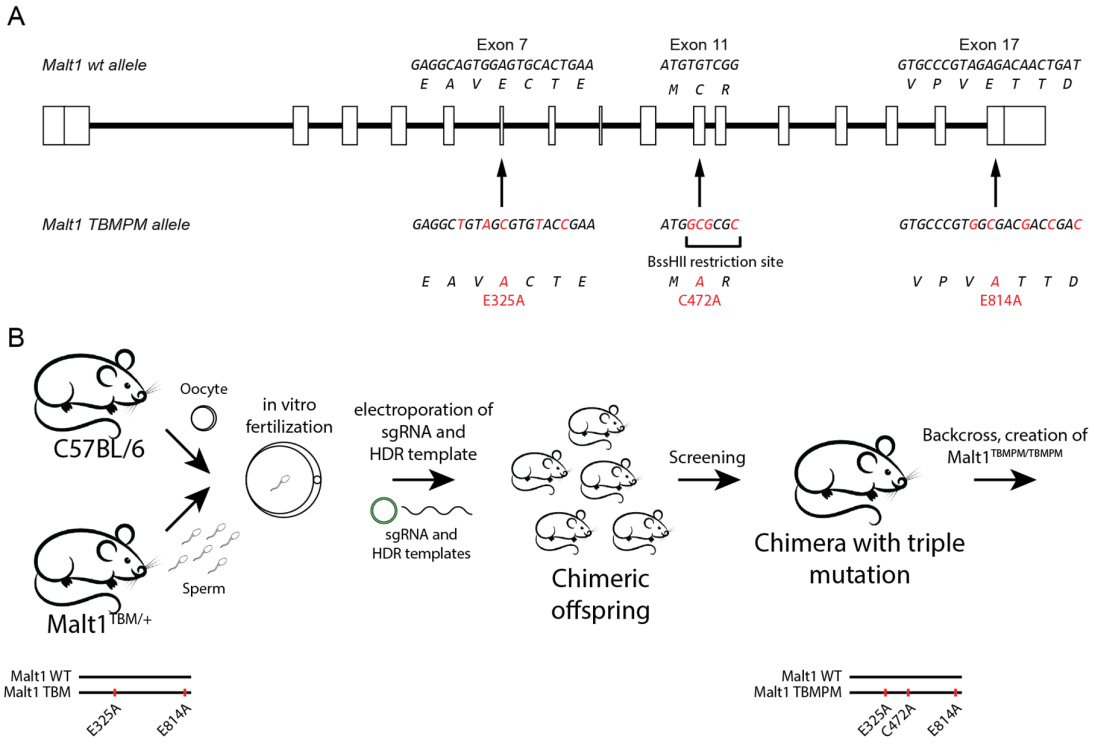

Figure 4-19. Strategy for creation of *Malt1* TBMPM model
Malt1 genomic locus with schematic exon-intron structure and indication of the wildtype sequence (above the scheme) and the mutated sequences (below the scheme) after successful modification of the TBM locus. One additional mutation, C472A (C461A for Malt1 isoform B) within exon 11 was introduced into the *Malt1* gene by CRISPR-Cas9 using an sgRNA and an HDR template. The artificial restriction site BssHII was inserted for downstream screening of mice. All modifications to DNA and amino acid sequences are indicated in red. B) Overview of *Malt1* TBMPM generation. Sperm from *Malt1*$^{TBM/+}$ mice was used for *in vitro* fertilization in C57BL/6 females, and zygotes were electroporated with an sgRNA and HDR template containing C472A and a silent mutation for insertion of the artificial cleavage site BssHII for screening. Offspring were screened using T6BM1/2 mutation-specific primers and BssHII cleavage at the C472 mutation site of exon 11. sgRNA and HDR template sequences are shown in section 7.1.7.2. *in vitro* fertilization was performed by Florian Giesert, Helmholtz Zentrum München.

A workflow for generation of TBMPM mice is depicted in Figure 4-19B. Briefly, sperm from *Malt1*$^{TBM/+}$ mice was used for *in vitro* fertilization with C57BL/6 oocytes; the resulting zygotes were electroporated with a sgRNA and HDR template targeting the paracaspase domain and subsequently transferred into carrier females. Offspring mice were screened and a mouse with all three mutations on one allele was used for backcrossing. Taking advantage of a single nucleotide polymorphism (SNP) close to the C472A mutation site derived from the R1E mES cells (that were used for creation

of the *Malt1* TBM allele), it was possible to verify the C472A mutation to be located on the same allele as the TBM mutations (Fig. 4-20A).

Homozygous *Malt1* TBMPM mice were sequenced and showed correct insertion of the C472A mutation and the silent mutations for the artificial BssHII cleavage site (Figure 4-20A). T6BM alleles could be genotyped using the same primers as for *Malt1* TBM, and BssHII cleavage could accurately distinguish between *Malt1*$^{+/+}$, *Malt1*$^{TBMPM/+}$, and *Malt1*$^{TBMPM/TBMPM}$ (Figure 4-20B). MALT1 protein expression was similar between all genotypes (Figure 4-20C). Importantly, *Malt1* TBMPM homozygous mice did not succumb to the lethal early-onset inflammation that led to a median survival of 27 days in *Malt1*$^{TBM/TBM}$ mice (Figure 4-20D). In fact, *Malt1*$^{TBMPM/TBMPM}$ mice appeared healthy and free of disease up to 15 weeks of age (data not shown).

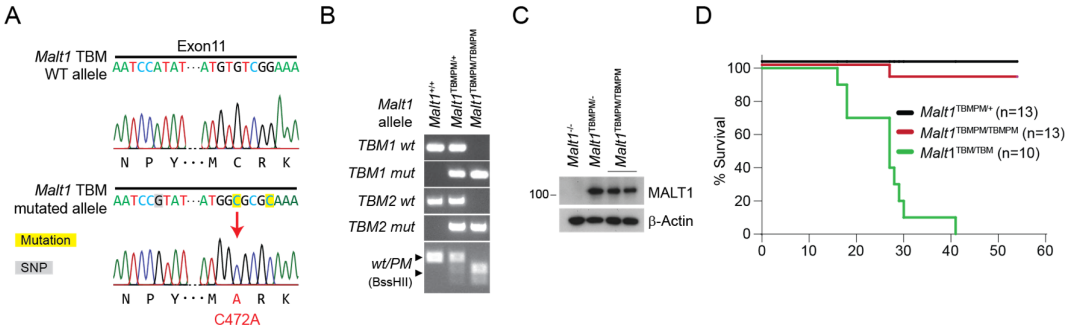

Figure 4-20. *Malt1* TBMPM verification and survival.
A) Sequencing of genomic DNA in exon 11 to verify correct mutagenesis in *Malt1* TBMPM heterozygous mice. Mutated nucleotide residues are highlighted in yellow, altered amino acid sequence is shown in red. B) Genotyping of *Malt1* TBMPM mice to distinguish between *Malt1*$^{TBMPM/TBMPM}$, *Malt1*$^{TBMPM/+}$, and *Malt1*$^{+/+}$. C) Immunoblot analysis showing MALT1 protein expression in *Malt1*$^{TBMPM/TBMPM}$, *Malt1*$^{TBMPM/+}$, and *Malt1*$^{+/+}$ mice. A *Malt1*$^{-/-}$ sample was also analyzed as negative control to prove specificity. D) Survival of *Malt1*$^{TBMPM/TBMPM}$ and *Malt1*$^{TBMPM/+}$ compared with *Malt1*$^{TBM/TBM}$ mice. One *Malt1*$^{TBMPM/TBMPM}$ mouse died at 27 days of age of unknown causes.

Malt1$^{TBMPM/TBMPM}$ mice showed no change in body or spleen weight compared to heterozygous controls (Figure 4-21A). Homozygous *Malt1* TBMPM mice had a very slight reduction in CD3+ and concomitant moderate increase in B220+ cells in spleen but not lymph nodes (Figure 4-21B-C). Similarly, CD4+ and CD8+ T cells were slightly decreased in spleen but not lymph nodes (Figure 4-21D-E). Thus, loss of MALT1 enzymatic function in *Malt1* TBMPM mice completely rescues the early-onset lethality of *Malt1* TBM.

4.4.2 T cells from *Malt1* TBMPM mice are unresponsive to activation

Next, we investigated peripheral lymphocyte activation in *Malt1* TBMPM mice. *Malt1*$^{TBM/TBM}$ mice showed a general increase in inflammation and T cell activation, and a consequence of phenotypic reversion of *Malt1* TBM lethality was hypothesized to be lower accumulation of T_{EM} cells. Indeed, *Malt1*$^{TBMPM/TBMPM}$ mice show a decrease in CD44^{hi}CD62L^{lo} T_{EM} cells in spleen and lymph nodes, and

CD44^{hi}CD62L^{lo}CD8+ T_{EM} cells in lymph nodes, while CD8 T_{EM} cells in spleen were unchanged compared to controls (Figure 4-22A-D). This decrease in T_{EM} populations was met with a relative increase in naïve T cells.

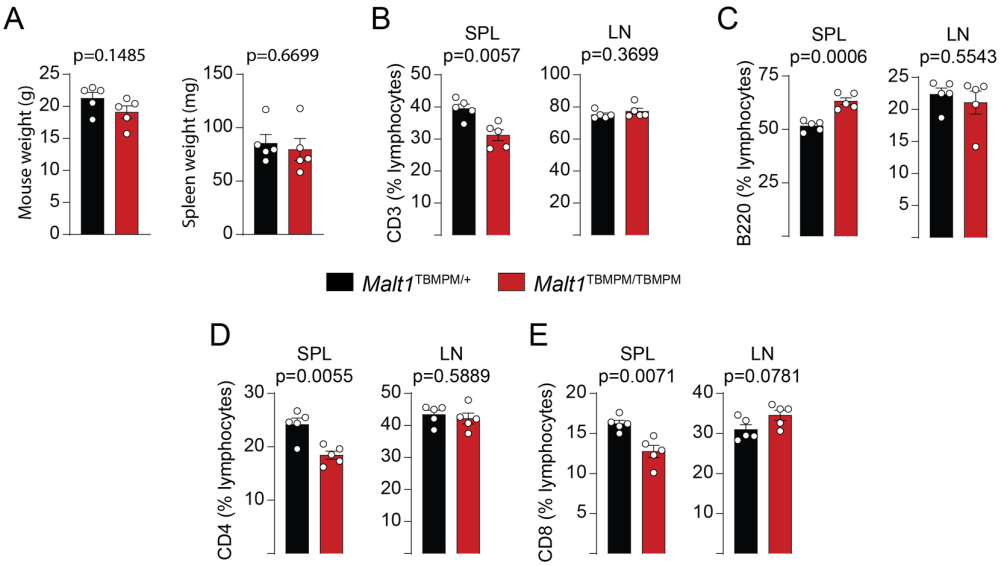

Figure 4-21. T and B cell populations in Cre models.
A-B) Mouse and spleen weight of *Malt1*$^{TBMPM/TBMPM}$ and *Malt1*$^{TBMPM/+}$ mice. B-C) Relative populations of CD3+ T (B) and B220+ B (C) cells in spleen (SPL) and lymph nodes (LN) of *Malt1*$^{TBMPM/TBMPM}$ and *Malt1*$^{TBMPM/+}$ mice. D-E) Relative populations of CD4+ (D) and CD8+ (E) cells in spleen and lymph nodes of *Malt1*$^{TBMPM/TBMPM}$ and *Malt1*$^{TBMPM/+}$ mice. A-E) Mice were analyzed at 8 weeks after birth. Unaffected control *Malt1*$^{TBMPM/+}$ littermates (black) were compared to *Malt1*$^{TBMPM/TBMPM}$ mice (red). Each dot represents one mouse. All bars show means ± SEM, and p-values were calculated by unpaired t-test with Welch's correction.

As observed for CD4+ T cells from *Malt1* TBM-T and *Traf6*-ΔT mice, CD4+ T cells from *Malt1*$^{TBMPM/TBMPM}$ mice showed a severe loss of NF-κB activation compared with OCT-1 control bands, stemming from loss of upstream IκBα phosphorylation and degradation, and deficient p65 phosphorylation after stimulation with P/I (Figure 4-21E). This is due to impaired CBM-TRAF6 scaffold formation. However, as expected due to additional PM modification, no constitutive MALT1 cleavage activity was observed in homozygous TBMPM cells, and cleavage could also not be induced upon P/I stimulation (Figure 4-22E). Consistent with the lower T_{EM} lymphocyte populations in *Malt1* TBMPM, CD3+ CD69+ cells were decreased in spleen and lymph nodes, and B220+ CD69+ cells remained unchanged (Figure 4-22F-G). B220+ CD86+ cells were slightly decreased in spleen but not lymph nodes (Figure 4-22H). Overall, additional catalytic inactivation of MALT1 leads to strong reversion of the activated phenotype of *Malt1* TBM mice.

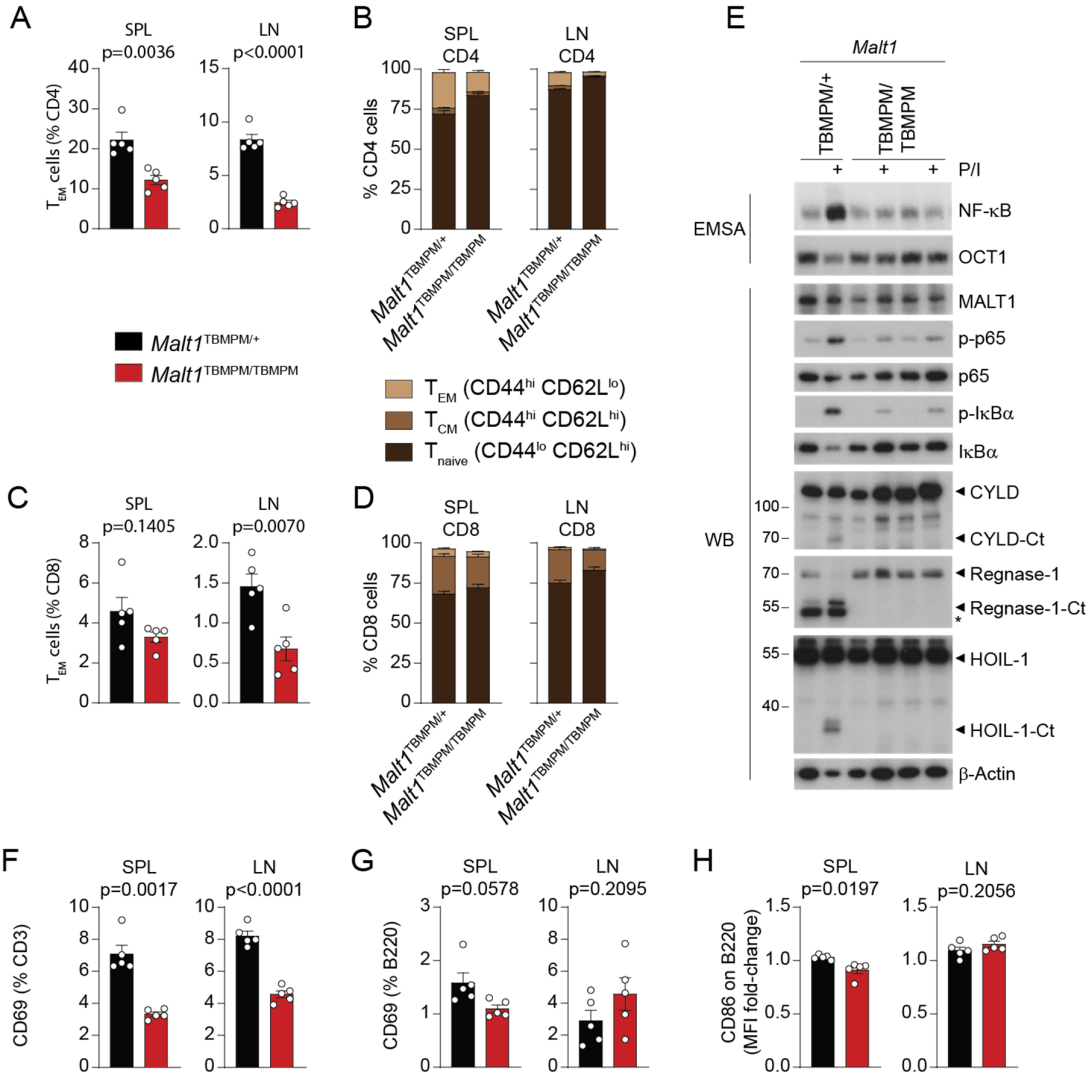

Figure 4-22. Activation phenotype of T and B cells in *Malt1* TBMPM mice.
A-B) Relative populations of CD4+ T_{EM} cells (A) and distribution of CD4+ T_{EM}, T_{CM}, and $T_{Naïve}$ cells (B) in spleen (SPL) and lymph nodes (LN) of *Malt1*$^{TBMPM/TBMPM}$ and *Malt1*$^{TBMPM/+}$ mice. C-D) Relative populations of lo CD8+ T_{EM} cells (C) and distribution of CD8+ T_{EM}, T_{CM}, and $T_{Naïve}$ cells (D) in spleen and lymph nodes of *Malt1*$^{TBMPM/TBMPM}$ and *Malt1*$^{TBMPM/+}$ mice. E) Biochemical analysis of NF-κB DNA binding (EMSA) and canonical NF-κB signaling and MALT1 proteolytic cleavage (WB) for *Malt1*$^{TBMPM/TBMPM}$ and *Malt1*$^{TBMPM/+}$ mice. Ct: C-terminal cleavage fragment. Asterisks represent non-specific antibody binding. F) Relative populations of CD3+ CD69+ T cells in spleen and lymph nodes of *Malt1*$^{TBMPM/TBMPM}$ and *Malt1*$^{TBMPM/+}$ mice. G) Relative populations of B220+ CD69+ B cells in spleen and lymph nodes of *Malt1*$^{TBMPM/TBMPM}$ and *Malt1*$^{TBMPM/+}$ mice. H) Relative expression of CD86 on B220+ B cells in spleen and lymph nodes as MFI fold-change in *Malt1*$^{TBMPM/TBMPM}$ and *Malt1*$^{TBMPM/+}$ mice. A-D; F-H) Mice were analyzed at 8 weeks after birth. Unaffected control *Malt1*$^{TBMPM/+}$ littermates (black) were compared to *Malt1*$^{TBMPM/TBMPM}$ mice (red). Each dot represents one mouse. All bars show means ± SEM, and p-values were calculated by unpaired t-test with Welch's correction.

4.4.3 Loss of MALT1 scaffolding and cleavage function in *Malt1* TBMPM mice phenocopies complete MALT1-deficiency

Next, to better understand the effect of simultaneous loss of MALT1 scaffolding and paracaspase functions, we compared *Malt1* TBMPM and *Malt1* KO mice. A hallmark of *Malt1* KO mice is a complete absence of FoxP3+ Treg cells in lymphoid organs and B1 B cells in the peritoneal cavity (PC). *Malt1* TBMPM homozygous mice showed a phenotype indistinguishable from *Malt1* KO, with

loss of essentially all Treg cells in spleen, lymph nodes, and thymus (Figure 4-23A,D). Additionally, like in *Malt1* KO mice, *Malt1* TBMPM mice had complete loss of PC B1 cells (Figure 4-23B,E). Whereas TBM mice showed a dramatic increase in the cytokines IFNγ and TNFα, *Malt1* TBMPM resembled *Malt1* KO and showed a very mild but negligible increase in IFNγ and no change in TNFα (Figure 4-23C,F). Overall, the phenotype of *Malt1* TBMPM mice was indistinguishable from that of *Malt1* KO mice, and the loss of MALT1 proteolytic function is sufficient for reversion of autoimmunity in *Malt1* TBM mice.

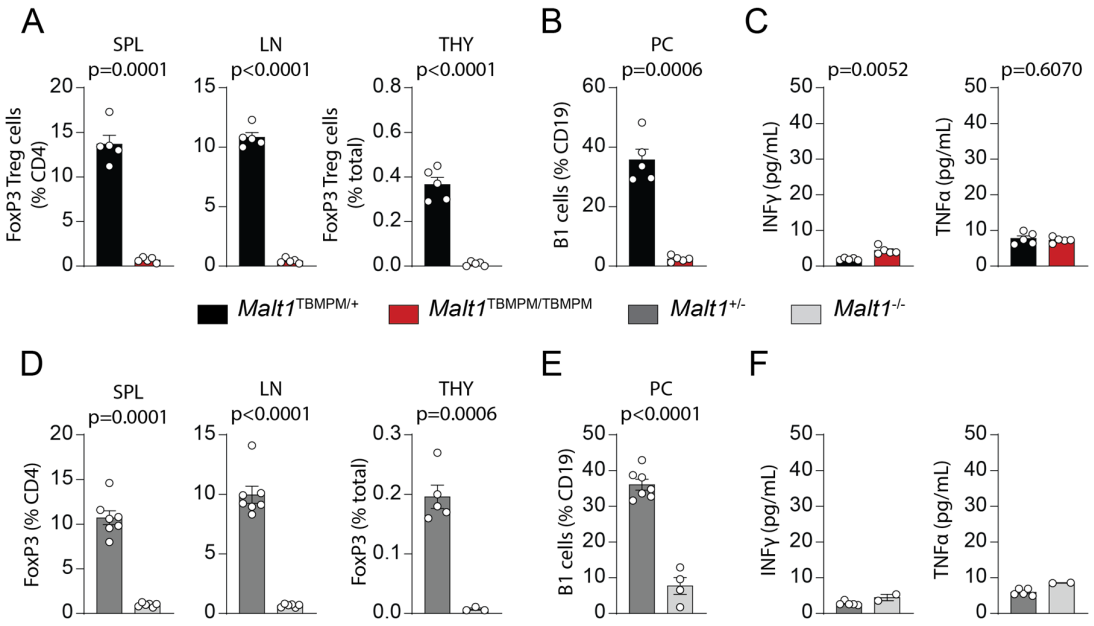

Figure 4-23. Regulatory T cell phenotype in *Malt1* TBMPM mice.
A,D) Relative populations of FoxP3+ Treg cells gated on CD4+ cells in spleen (SPL) and lymph nodes (LN) and FoxP3+ cells gated on total lymphocytes in thymus (THY) of *Malt1* TBMPM (A) and *Malt1* KO (D) mice. B,E) B1 cells (CD19+ B220-) from the peritoneal cavity (PC) of *Malt1* TBMPM (B) and *Malt1* KO (E) mice. C,F) Blood serum levels of indicated cytokines in *Malt1* TBMPM (C) and *Malt1* KO (F) mice. A-F) Mice were analyzed at 8 weeks after birth. Unaffected control *Malt1*$^{TBMPM/+}$ littermates (black) were compared to *Malt1*$^{TBMPM/TBMPM}$ mice (red) and *Malt1*$^{+/-}$ littermates (dark grey) were compared to *Malt1*$^{-/-}$ KO mice (light grey). Each dot represents one mouse. All bars show means ± SEM, and p-values were calculated by unpaired t-test with Welch's correction.

4.4.4 Inactivation of MALT1 paracaspase activity reverts autoimmunity in *Traf6*-ΔT mice

Reversion of the inflammatory phenotype in *Malt1* TBMPM mice gives powerful evidence that constitutive MALT1 activity is responsible for autoimmunity upon loss of TRAF6 interaction. However, to prove that aberrant MALT1 activity drives the autoimmune phenotype of *Traf6*-ΔT mice, inactivation of functional MALT1 enzyme in *Traf6*-ΔT mice was needed. To this end, *Traf6*-ΔT mice were bred with additional conditional loss of MALT1 paracaspase activity under the control of the *CD4-Cre* promotor (*Malt1*$^{PM/flox}$; *Traf6*$^{flox/flox}$; *CD4-Cre*$^{Cre+}$: *Traf6* PM mice). In *Traf6* PM mice, expression of Cre-recombinase in T cells yields *Malt1*$^{PM/-}$ and *Traf6*$^{-/-}$. Littermate controls from *Traf6*

PM breeding allowed for direct comparison to wildtype (*Malt1*$^{fl/+}$; *Traf6*$^{wt/fl}$; CD4-*Cre*$^{Cre+}$), *Traf6*-ΔT (*Malt1*$^{fl/+}$; *Traf6*$^{fl/fl}$; *CD4-Cre*$^{Cre+}$), and *Malt1* PM (*Malt1*$^{PM/fl}$; *Traf6*$^{wt/fl}$; *CD4-Cre*$^{Cre+}$) phenotypes.

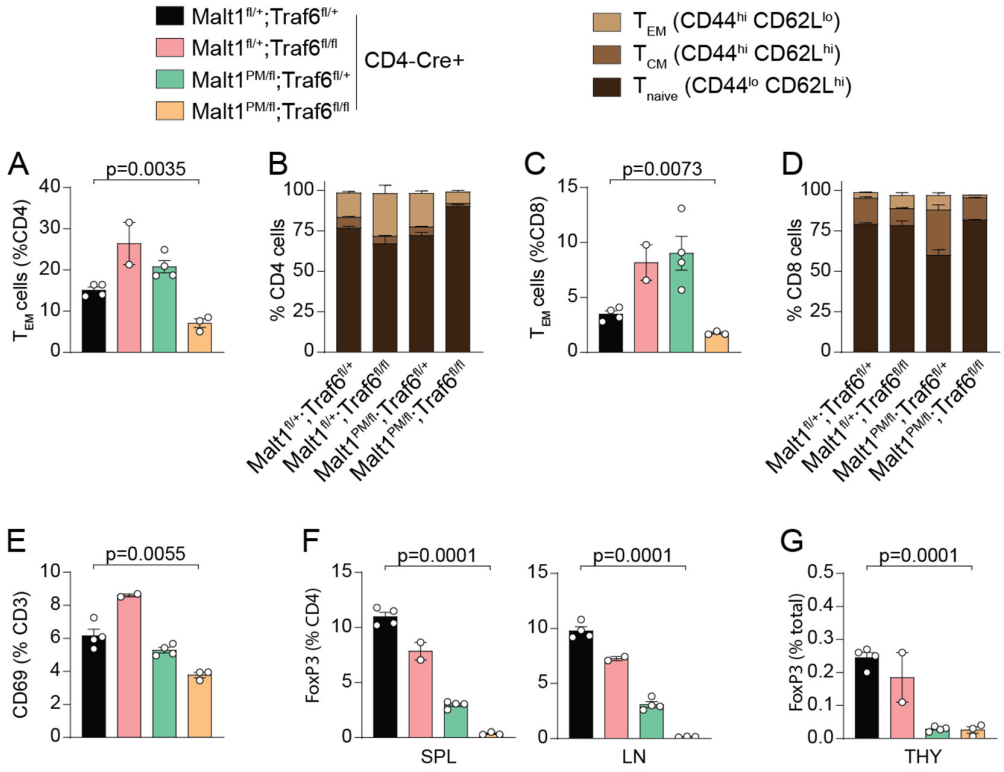

Figure 4-24. Activation phenotype of T cells in *Traf6* PM mice.
A,B) Relative populations of CD4+ T_{EM} cells (A) and distribution of CD4+ T_{EM}, T_{CM}, and $T_{Naïve}$ cells (B) in spleen (SPL) of *Malt1*$^{PM/flox}$; *Traf6*$^{flox/flox}$; *CD4-Cre*$^{Cre+}$ (*Traf6* PM)and control mice. C,D) Relative populations of CD4+ T_{EM} cells (A) and distribution of CD4+ T_{EM}, T_{CM}, and $T_{Naïve}$ cells (B) in spleen of *Traf6* PM and control mice. E) Relative populations of CD3+ CD69+ T cells in spleen of *Traf6* PM and control mice. F,G) Relative populations of FoxP3+ Treg cells gated on CD4+ cells in spleen (F) and FoxP3+ cells gated on total lymphocytes in thymus (G) of *Traf6* PM mice. A-G) Mice were analyzed at 10 weeks after birth. All analyzed mice were positive for CD4-Cre expression. Unaffected control littermates (black) (*Malt1*$^{fl/+}$; *Traf6*$^{wt/fl}$) were compared with *Traf6* PM (orange) (*Malt1*$^{PM/fl}$; *Traf6*$^{fl/fl}$) mice. Additional *Traf6*-ΔT (pink) (*Malt1*$^{fl/+}$; *Traf6*$^{fl/fl}$) and *Malt1* PM (green) (*Malt1*$^{PM/fl}$; *Traf6*$^{wt/fl}$) littermates were analyzed for phenotyping comparison. Each dot represents one mouse. All bars show means ± SEM, and p-values were calculated by unpaired t-test with Welch's correction.

Traf6 PM mice exhibited strong loss of CD4+ and CD8+ T_{EM} cells compared to wildtype controls, showing a reversion of the activated *Traf6*-ΔT phenotype (Figure 4-24A,C). Loss of effector T cell populations was accompanied by an increase in naïve T cells (Figure 4-24B,D). As expected, reduction in T_{EM} populations was accompanied by a reduction in CD3+ CD69+ cells, again indicating lower T cell activation (Figure 4-24E). CD4+ FoxP3+ Tregs were reduced in SPL and LN (Figure 4-24F), as were FoxP3+ Tregs gated on total thymocytes (Figure 4-24G). In general, *Traf6* PM also reverted the phenotype of *Malt1* PM mice, showing a loss of Teff cells and a further reduction in Treg cells than is already caused by loss of paracaspase function alone.

Traf6 PM mice showed a severe loss in NF-κB expression as measured by EMSA compared with OCT-1 control bands (Figure 4-25A). NF-κB was not upregulated in *Traf6* PM or *Traf6*-ΔT mice upon

stimulation with P/I, whereas NF-κB upregulation appeared normal in control and *Malt1* PM mice. In Western Blot, *Traf6*-ΔT mice exhibited constitutive cleavage of MALT1 substrates CYLD, HOIL, and Regnase-1 which was completely reverted in *Traf6* PM mice (Figure 4-25A). *Malt1* PM mice show no substrate cleavage. As shown previously, increased cleavage of Regnase-1 and Roquin-1/2 in *Traf6*-ΔT leads to elevated expression of IκBNS+ and ICOS+ on CD4 T cells (Figure 4-25B,C), and IκBNS and ICOS expression levels in *Traf6* PM were at or below wildtype controls as the result of reverted constitutive cleavage.

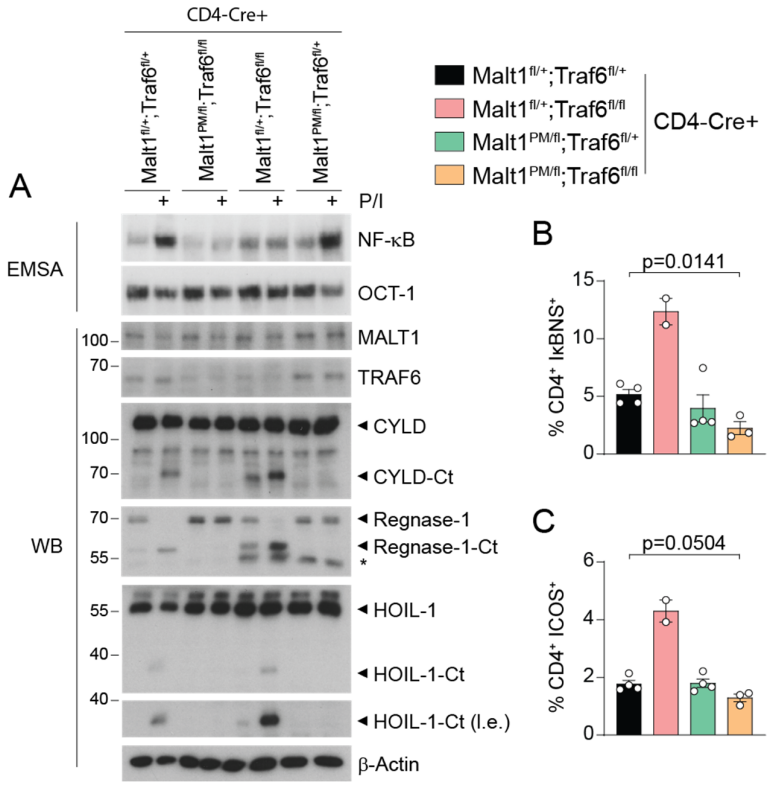

Figure 4-25. MALT1 paracaspase activity in *Traf6* PM mice.
A) Biochemical analysis of NF-κB DNA binding (EMSA) and canonical NF-κB signaling and MALT1 proteolytic cleavage (WB) for *Malt1*$^{PM/flox}$; *Traf6*$^{flox/flox}$ *CD4-Cre*$^{Cre+}$ (*Traf6* PM) mice and littermates. B,C) Relative populations of IκBNS+ (B) and ICOS+ (C) CD4 T cells in spleen of *Traf6* PM mice and littermates. A-C) Mice were analyzed at 10 weeks after birth. All mice were positive for CD4-Cre expression. Unaffected control littermates (black) (*Malt1*$^{fl/+}$; *Traf6*$^{wt/fl}$) were compared with *Traf6* PM (orange) (*Malt1*$^{PM/fl}$; *Traf6*$^{fl/fl}$) mice. Additional *Traf6*-ΔT (pink) (*Malt1*$^{fl/+}$; *Traf6*$^{fl/fl}$) and *Malt1* PM (green) (*Malt1*$^{PM/fl}$; *Traf6*$^{wt/fl}$) littermates were analyzed for phenotype comparison. Each dot represents one mouse. All bars show means ± SEM, and p-values were calculated by unpaired t-test with Welch's correction.

4.4.5 MLT-985 is a potent cellular MALT1 inhibitor

Next, we wanted to test if the phenotype of *Traf6*-ΔT mice could similarly be reverted using a pharmacological approach with allosteric MALT1 inhibitors. The allosteric small molecule MALT1 inhibitor (S)-Mepazine has been shown to have tumor suppressive action in ABC-DLBCL lymphomas, which are dependent upon chronic NF-κB activation (Nagel et al., 2012). Recently, more potent allosteric MALT1 inhibitors, MLT-943 and MLT-985, have been developed with low nanomolar

activity and promising *in vivo* effects (Martin et al., 2020; Quancard et al., 2020). To test the potency and potential efficacy of these inhibitors, we first performed an *in vitro* cleavage assay using purified MALT1 protein. In line with published data, MLT-943 and MLT-985 show low nanomolar inhibition of 5.39 and 3.24 nM, respectively, indicating strong specificity for MALT1 (Figure 4-26A). Next, we tested the effects of MLT-943 and MLT-985 on cellular MALT1 inhibition by comparing constitutive MALT1 cleavage activity in Traf6 KO Jurkat T cells. Both inhibitors showed strong inhibition of MALT1 substrate cleavage following 24-hour incubation with inhibitors, with MLT-985 approximately 2-3-fold more potent than MLT-943, based on the cleavage bands of CYLD and HOIL (Figure 4-23B). Corroborating these results, pharmacokinetic parameters were recently published for each of these compounds, showing that MLT-985 is superior to MLT-943 regarding clearance rate and half-life in mice after intravenous administration (Quancard et al., 2020). Therefore, MLT-985 was chosen for therapeutic treatment of *Traf6*-ΔT mice to investigate if MALT1 protease activity is also responsible for immune activation after loss of TRAF6 expression.

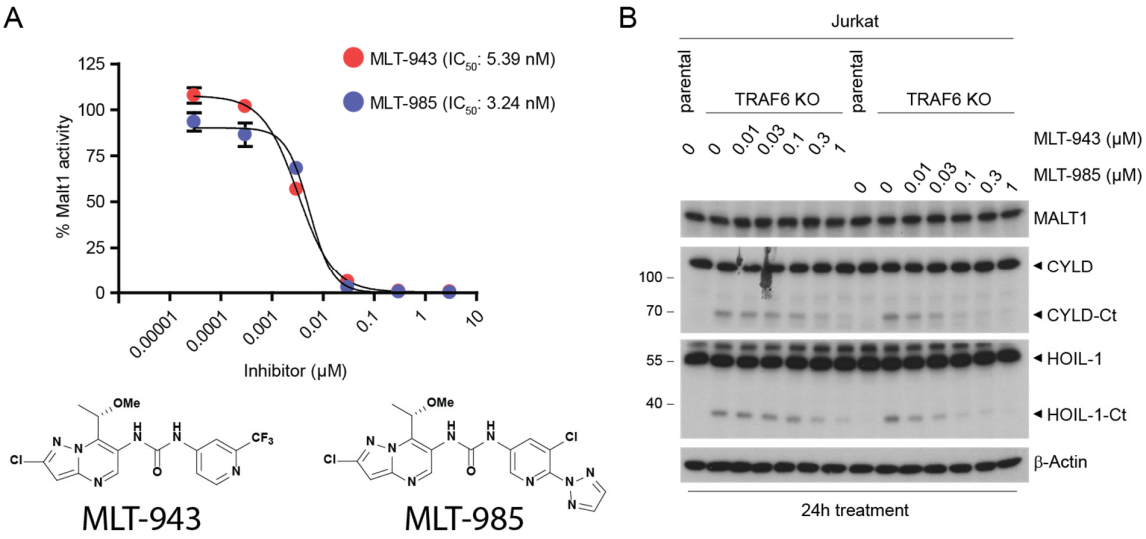

Figure 4-26. *In vitro* testing of allosteric MALT1 inhibitors.
A) Inhibition curves for MLT-943 and MLT-985 and respective IC_{50} values. Structures for the allosteric MALT1 inhibitors MLT-943 and MLT-985 are shown. B) Western Blot showing cellular inhibition of MALT1 with increasing concentrations of MLT-943 and MLT-985. MALT1 substrates CYLD and HOIL-1 are shown. Ct: C-terminal cleavage fragment.

4.4.6 MALT1 inhibitor treatment ameliorates T cell activation caused by TRAF6 ablation in T cells

To determine if MALT1 pharmacological inhibition ameliorates the *Traf6*-ΔT immune activation phenotype, 8 week old *Traf6*-ΔT mice were injected with 16 mg/kg MLT-985 i.p. BID (intraperitoneal, twice daily at 12 hour intervals) over a 10 day period (Figure 4-27A). Mice were analyzed on day 11, and purified CD4+ T cells showed a complete loss of constitutive cleavage of CYLD, HOIL-1, and Regnase-1 compared with vehicle-treated mice (Figure 4-27B). Remarkably, the Roquin targets IκBNS and ICOS returned to untreated control levels following treatment (Figure 4-27C). Activated CD3+

CD69+ cells and CD4+ and CD8+ T_{EM} cells after MLT-985 treatment resembled non-treated control mice (Figure 4-27C-E). As previously reported for MLT-943 treatment (Martin et al., 2020), CD4+ FoxP3+ Tregs were reduced to levels significantly below those of untreated controls, as were the levels of Ox40 on eTregs (Figure 4-27F,G). This reduction is also in agreement with the phenotype of *Malt1* PM mice, where loss of paracaspase activity yields a deficit in FoxP3 Treg cells (Bornancin et al., 2015; Gewies et al., 2014; Jaworski et al., 2014). Reduction in Tregs following 10-day treatment did not visibly compromise the health of the mice. Thus, the high T cell activation and constitutive MALT1 substrate cleavage in *Traf6*-ΔT mice can be completely reverted by 10-day treatment with MALT1 allosteric inhibitors.

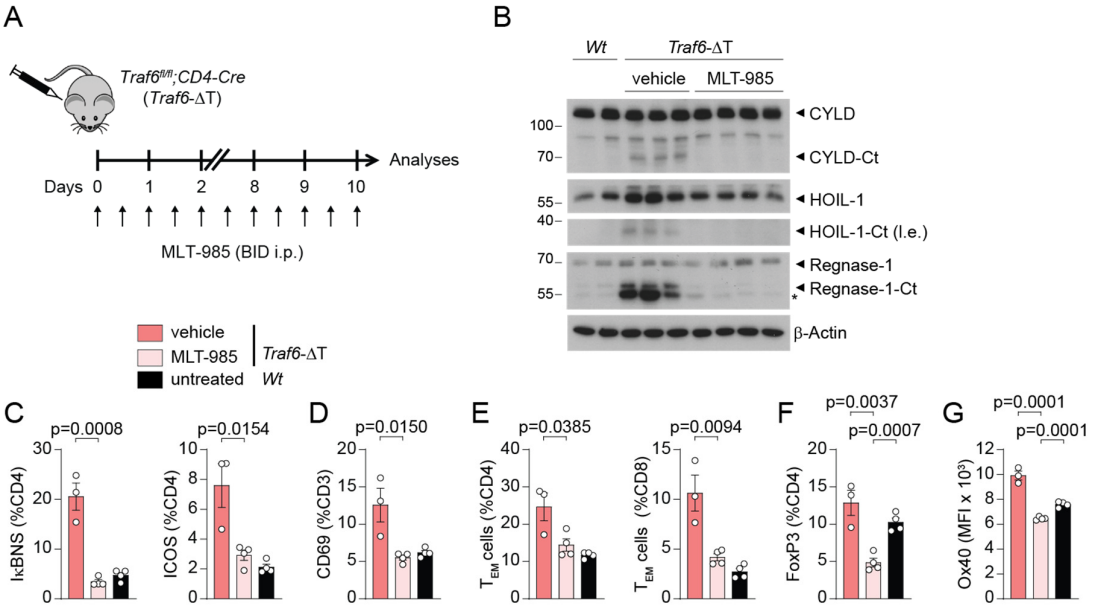

Figure 4-27. *In vivo* treatment of *Traf6*-ΔT mice.
A) Treatment timeline for i.p. BID treatment of *Traf6*-ΔT mice with the allosteric MALT1 inhibitor MLT-985 starting at 8 weeks of age. B) Western Blot showing MALT1 substrate cleavage after *in vivo* treatment of *Traf6*-ΔT mice with MLT-985 or vehicle. Ct: C-terminal cleavage fragment. l.e.: low exposure. C) Relative populations of CD4+ IκBNS and ICOS in MLT-985-treated, vehicle-treated, and untreated *Traf6*-ΔT mice. D) Relative populations of CD3+ CD69+ T cells in MLT-985-treated, vehicle-treated, and untreated *Traf6*-ΔT mice. E) CD4+ and CD8+ T_{EM} populations in MLT-985-treated, vehicle-treated, and untreated *Traf6*-ΔT mice. F) CD4+ FoxP3+ populations in MLT-985-treated, vehicle-treated, and untreated *Traf6*-ΔT mice. G) Ox40 expression in CD4+ FoxP3+ Tregs in in MLT-985-treated, vehicle-treated, and untreated *Traf6*-ΔT mice. C-G) All stains were performed on splenocytes. Untreated control mice were *Traf6$^{wt/fl}$;CD4-Cre+*. Each dot represents one mouse. All bars show the mean ± SEM and p-values were calculated by unpaired t-test.

5 Discussion

Ligation of an antigen to a T cell or B cell receptor initiates downstream signaling and induction of the transcription factor NF-κB which is essential for cell survival, differentiation, proliferation, and cytokine production. Key to responsive NF-κB signaling is the CBM complex, where the paracaspase MALT1 plays a unique dual role as a scaffold and protease. Integral to MALT1 scaffolding function is its interaction with the E3 ligase TRAF6 via two TRAF6-binding motifs (T6BMs). MALT1 recruits TRAF6 to the CBM complex, whereby TRAF6 is activated and mediates post-translational ubiquitination of components of the CBM-IKK signaling hub for promotion of NF-κB activation. Despite our current understanding of this interaction, the precise role of TRAF6 in regulating CBM-dependent NF-κB signaling is not sufficiently understood, largely due to conflicting *in vivo* and *in vitro* results.

Within recent years, several publications have characterized genetically modified mouse models to illuminate the role of MALT1 in signaling and immune functions (Figure 5-1). *Malt1* KO mice clarified that essential immune cell compartments rely upon MALT1 scaffolding and proteolytic activity for development. In MALT1-deficient mice, Treg cells, B1 B cells, and MZ B cells were strongly reduced (Ruefli-Brasse et al., 2003; Ruland et al., 2003). *Malt1* KO mice suffer from immune suppression, but other immune cell compartments maintained normal populations and function. Overall, NF-κB and JNK signaling were impaired in MALT1-deficient B and T lymphocytes resulting in defective proliferation and activation of immune function (Table 5-1) (Ruefli-Brasse et al., 2003; Ruland et al., 2003). To distinguish between the roles played by the dual functions of MALT1 in the immune system, paracaspase-deficient mice (*Malt1* PM) have been developed (Bornancin et al., 2015; Gewies et al., 2014; Jaworski et al., 2014). *Malt1* PM mice express MALT1 protein with intact scaffold function, but which is catalytically inactive (Figure 5-1). *Malt1* PM mice refined our understanding of MALT1 function, showing that development of B cell populations and Treg cells are dependent on MALT1 enzyme activity. *Malt1* PM mice show a partial loss of NF-κB activation (Table 5-1). Further, loss of cleavage of posttranscriptional regulators like Roquin-1/2 and Regnase-1 in *Malt1* PM mice leads to IFNγ overproduction. Due to strongly impaired Tregs, but intact effector cell functions, PM mice eventually develop autoinflammatory syndromes.

5.1 MALT1-TRAF6 interaction is required for cellular homeostasis in mice

Until now, a mouse model with intact MALT1 paracaspase activity but defective scaffold function has been missing. As mentioned above, an integral part of MALT1 scaffold function is defined by the interaction between MALT1 and TRAF6, and this interaction can be disrupted by mutating the two TRAF6-binding motifs in the *Malt1* gene (Meininger et al., 2016). Therefore, mice were generated with the two *Traf6*-binding motifs in MALT1 inactivated by point mutations in exon 7 and exon 17 of

the *Malt1* gene (*Malt1* TBM mice: *Traf6*-Binding Mutant). There was an expectation that, upon loss of MALT1 scaffold function, *Malt1* TBM mice should closely resemble *Malt1* knockout mice due to loss of scaffold-dependent NF-κB signaling. Indeed, signaling could be shown to be disrupted, and *Malt1* TBM mice lack NF-κB activation, supporting the role of TRAF6 as a positive regulator of signaling downstream of the CBM complex (Table 5-1). However, to our surprise homozygous *Malt1*$^{TBM/TBM}$ mice displayed a massive, fatal early-onset phenotype which we prove is driven by aberrant MALT1 enzyme activity.

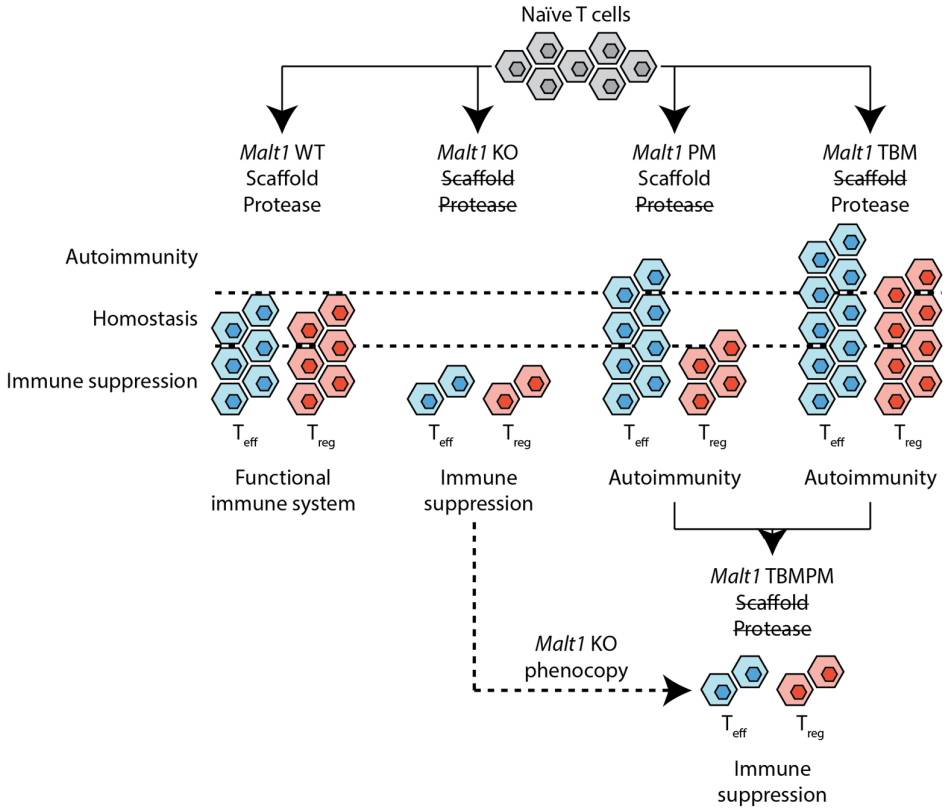

Figure 5-1. Overview of murine MALT1 models.
WT mice have MALT1 with intact scaffold and protease functions (*Malt1* WT), and balanced Teff and Treg functions yield a function immune system. Mice lacking MALT1 expression (*Malt1* KO) have strongly diminished Teff and Treg populations due to defective NF-κB signaling and cleavage of MALT1 substrates, leading to a suppressed immune system. Mice with defective paracaspase function but intact scaffolding function (*Malt1* PM) have a strong reduction in Tregs due to dependency of Treg development on MALT1 enzyme activity. Reduced Tregs are insufficient for the increased Teff activity, leading to autoimmunity. Mice with intact paracaspase function but lacking TRAF6 binding motifs (*Malt1* TBM) have increased Teff and Treg populations, but Tregs are insufficient to combat the increase in Teff cells, yielding autoimmunity. *Malt1* TBM mice with additional inactivation of paracaspase activity (*Malt1* TBMPM) have strongly reduced Teff and Treg populations with immune suppression. *Malt1* TBMPM mutations phenocopy *Malt1* KO in mice.

Strikingly, both *Malt1* TBM and *Malt1* PM mice exhibit autoimmunity and inflammation, but the phenotype of each mouse is driven by distinct mechanisms. In each case, activation of T cell populations occurs, as judged by increased CD4+ and CD8+ T_{EM} populations (Table 5-2). However,

whereas multi-organ autoinflammation in PM mice results primarily from loss of Treg cell numbers and therefore suppressive control over Teff cells, Treg numbers are increased in *Malt1* TBM mice (Figure 5-1). Tregs in TBM mice also exhibit unchanged or increased expression of the suppression markers Ox40 and CTLA-4, indicting normal Treg function (Table 5-2). Nevertheless, TBM Treg cells are insufficient to cope with the massive expansion of immune activating Teff cell. Therefore, in both PM and TBM mice, proliferation and activity of Teff cells exceeds that of Treg cells, yielding loss of peripheral tolerance and autoinflammation. The difference between the two mechanisms driving autoimmunity is also clearly evident when comparing the onset of multiorgan inflammation in each mouse model. While *Malt1* TBM mice succumb to disease at 3-5 weeks due to rapidly increased Teff cells, *Malt1* PM mice have slower disease progression from a strong, but not complete loss of Tregs (Bornancin et al., 2015; Gewies et al., 2014; Jaworski et al., 2014). Overall, relative Teff and Treg cell numbers and function clearly define the outcome of MALT1 mutations *in vivo*.

We hypothesized that autoimmunity in *Malt1* TBM mice is driven by constitutive MALT1 paracaspase activity upon loss of interaction with TRAF6. To prove this, we genetically modified *Malt1* TBM mice to additionally express the paracaspase inactivating mutation C472A. Combination of *Malt1* TBM and PM mutations in these new *Malt1* TBMPM mice led to reversion of autoimmunity, giving strong evidence that the phenotype of TBM mice is driven by overactive paracaspase function (Figure 5-1). In fact, although *Malt1* TBMPM mice express normal levels of MALT1 protein, they exhibit a phenotype indistinguishable from *Malt1* KO mice, with loss of B cell and Treg populations (Table 5-2). Therefore, not only is the TBM phenotype dependent upon MALT1 paracaspase function, the phenotype of *Malt1* PM mice relies on intact MALT1 scaffolding.

	Mouse line							
	***Malt1* TBM**	***Malt1* TBM-T**	***Traf6*-ΔT**	***Malt1* TBM-Treg**	***Malt1* TBMPM**	***Traf6* PM**	***Malt1* KO**	***Malt1* PM**
Inducible NF-κB activation	No	No	No	ND	No	No	No	Yes
Constitutive MALT1 activity	Yes	Yes	Yes	ND	No	No	No	No
Inducible MALT1 activity	Yes	Yes	Yes	ND	No	No	No	No

Table 5-1. NF-κB activation and Inducible and constitutive MALT1 activity in murine models.
Comparison of NF-κB activation and MALT1 paracaspase activity in murine models as measured by EMSA and WB, respectively. Loss of MALT1-TRAF6 interaction leads to abrogated NF-κB activation and constitutive MALT1 activity, which can nonetheless still be induced. Loss of scaffolding and paracaspase function in MALT1 abolishes signaling and substrate cleavage, resembling the phenotype of *Malt1* KO mice. For comparison, characteristic phenotypes of *Malt1* KO and *Malt1* PM mice from literature are shown (Gewies et al., 2014; Ruland et al., 2003). ND = 'Not Determined'.

The early onset of lethal inflammation and strong inflammatory organ infiltration in *Malt1* TBM mice strongly suggests a Treg-independent mechanism that is primarily driven by overshooting of Teff

responses. Additionally, heterozygous expression of TBM mutations in *Malt1*$^{TBM/+}$ mice was sufficient for development of late-onset autoimmunity, arguing for a dominant function of Teff cells and not a loss of Treg function. Expansion of Teff and Treg populations over the lifetime of mice is normal and well described (Goronzy et al., 2007; Jagger et al., 2014), but the presence of heterozygous

	Mouse line						
	Malt1 **TBM**	***Malt1*** **TBM-T**	***Traf6*-ΔT**	***Malt1*** **TBM-Treg**	***Malt1*** **TBMPM**	***Traf6*** **PM**	***Traf6*-ΔT Treatment**
Body condition							
Mouse wt	Normal	Normal	Normal	Normal	Normal	Normal	ND
Spleen wt	**** ↑	* ↑	** ↑	Normal	Normal	Normal	ND
T cells							
CD3	* ↑	Normal	Normal	Normal	** ↓	Normal	ND
CD3 CD69	*** ↑	*** ↑	** ↑	Normal	** ↓	** ↓	* ↓
CD4	** ↑	** ↑	Normal	Normal	** ↓	Normal	ND
CD4 IκBNS	ND	**** ↑	**** ↑	ND	ND	*↓	*** ↓
CD4 ICOS	ND	*** ↑	*** ↑	ND	ND	Normal	ND
CD4 TEM	**** ↑	**** ↑	****↑	Normal	** ↓	** ↓	* ↓
CD8	*** ↑	** ↓	*** ↓	Normal	** ↓	Normal	ND
CD8 IκBNS	ND	*** ↑	**** ↑	ND	ND	Normal	* ↓
CD8 ICOS	ND	*** ↑	* ↑	ND	ND	Normal	ND
CD8 TEM	**** ↑	****↑	***↑	Normal	Normal	** ↓	** ↓
Tregs							
CD4 FoxP3	* ↑	**** ↑	Normal	* ↑	**** ↓	**** ↓	** ↓
eTreg	* ↑	**** ↑	**** ↑	* ↑	ND	ND	ND
Ox40	* ↑	** ↑	* ↑	* ↑	ND	ND	**** ↓
B cells							
B220	**** ↓	Normal	* ↑	Normal	*** ↑	Normal	ND
B220 CD69	**** ↑	**** ↑	** ↑	Normal	Normal	Normal	ND
B220 CD86	**** ↑	* ↑	*** ↑	Normal	* ↓	ND	ND
B1 B cells	ND	ND	ND	ND	**** ↓	ND	ND

Table 5-2. Overview of cell populations determined by immune phenotyping of murine models.
Comparison of important body condition indices, T cell, Treg, and B cell populations analyzed by flow cytometry from mouse lines investigating MALT1-TRAF6 interaction: *Malt1* TBM, *Malt1* TBM-T, *Traf6*-ΔT, *Malt1* TBM-Treg, *Malt1* TBMPM, *Traf6*-ΔT, and inhibitor-treated *Traf6*-ΔT mice. Breedings and relevant controls are shown in section 7.3.6. Stars represent statistical significance ($p<0.05$ (*), $p<0.01$ (**), $p<0.001$(***). ND = 'Not Determined'. Littermate control mice were Malt1$^{TBM/+}$ or *Malt1*$^{fl/+}$*;CD4-Cre-, Malt1*$^{fl/+}$;CD4-Cre+ and *Malt1*$^{TBM/fl}$*;CD4-Cre-* or *Traf6-*$^{fl/+}$*;CD4-Cre+,Traf6*$^{fl/fl}$*;CD4-Cre-* and *Traf6*$^{fl/+}$*;CD4-Cre-* or *Malt1*$^{fl/+}$*;FoxP3-Cre-, Malt1*$^{fl/+}$;FoxP3-Cre+ and *Malt1*$^{TBM/fl}$*;FoxP3-Cre or Malt1*$^{TBMPM/+}$ *or Malt1*$^{fl/+}$*;Traf6*$^{wt/fl}$;CD4-Cre^{+} or vehicle-treated Traf6$^{fl/fl}$;CD4-Cre^{+} for *Malt1* TBM, *Malt1* TBM-T, *Traf6*-ΔT, *Malt1* TBM-Treg, *Malt1* TBMPM, *Traf6* PM, and treated *Traf6*-ΔT, respectively.

mutations greatly exacerbated this increase. Since autoimmunity in TBM mice is driven by constitutive MALT1 protease activity, it appears that presence of WT MALT1 protein counteracts the MALT1 TBM allele, keeping unrestrained catalytic activity to a minimum in young mice. However gradual, this still leads to sufficient protease activation and onset of autoimmunity beyond 6 months of age. Whether the slow disease onset due to presence of WT MALT1 is contingent upon the

dynamics of MALT1 dimerization and CBM complex assembly remains to be determined. However, normal NF-κB levels in *Malt1*$^{TBM/+}$ indicate that CBM filament formation and TRAF6 association with MALT1 are largely intact.

For creation of *Malt1* TBM mice, we used mES cell clones containing faithful homozygous mutations in the T6BM1 and T6BM2 sites of MALT1. Interestingly, *Malt1* TBM chimeras, which have a subset of cells expressing homozygous *Malt1* TBM mutations, showed signs of autoimmunity at 3-5 months of age, with necropsy showing splenomegaly and lymphadenopathy. This inflammatory phenotype and hyperplasia in *Malt1* TBM founder mice argues for clonal outgrowth of homozygous TBM cells. TBM cells likely have a proliferative advantage over wildtype cells which allows them to surpass wildtype cell populations, and mice which developed disease more quickly likely had a higher percentage of chimerism in lymphoid tissue. Clonal outgrowth of TCR clones should be verified by sequencing of the TCR repertoire.

The question arises, how Treg cell populations are able to develop normally in the absence of NF-κB activation, which has been shown to be a major player in development and survival of peripheral Treg cells (Josefowicz & Rudensky, 2009). Treg maturation is clearly dependent upon MALT1 paracaspase activity, apparent from loss of Tregs in *Malt1* KO and *Malt1* PM mice (Bornancin et al., 2015; Gewies et al., 2014; Jaworski et al., 2014). However, it is also contended that Treg function and identity is dependent upon transcriptional targets of NF-κB (Molinero et al., 2009; Schmidt-Supprian et al., 2004). In fact, simultaneous loss of the NF-κB subunits p65 and c-Rel completely depletes FoxP3 Tregs in peripheral and central lymphoid tissue, arguing that NF-κB-regulated genes define Treg function (Grinberg-Bleyer et al., 2017; H. Oh et al., 2017). Nevertheless, cytokine production resulting from advanced inflammation can lead to Treg maturation independent of TCR signaling and CBM complex formation, and Treg suppressive function is independent of NF-κB activation (Rosenbaum et al., 2019). Indeed, presence of FoxP3 Tregs and the suppressive markers CTLA-4 and Ox40 upon loss of MALT1-TRAF6 interaction argues for Treg development independent of MALT1 scaffolding function.

5.2 T cell specific loss of MALT1-TRAF6 interaction drives auto-immune inflammation

Malt1 TBM mice exhibit early-onset autoimmunity and strong induction of cytokines, and it was thus difficult to identify which phenotypic characteristics were primary effects of mutation, and which were secondary effects of systemic autoinflammation. Further, due to the essential role of the MALT1-TRAF6 interaction downstream of TCR signaling, we were interested in the influence of T cells on the *Malt1* TBM phenotype. Therefore, T cell (*Malt1* TBM-T) and Treg-specific (*Malt1* TBM-Treg) Cre-recombinase-dependent models were developed. Interestingly, previous reports on mice

with T cell specific deletion of TRAF6 (*Traf6*-ΔT mice) have described an autoimmune phenotype similar to, but with later onset than *Malt1* TBM mice. Therefore, we used *Traf6*-ΔT mice for phenotypic comparison to our T cell specific TBM models.

Malt1 TBM-T and *Traf6*-ΔT mice exhibit highly similar phenotypes, with strongly increased Teff cell populations at 12 weeks of age (Table 5-2). The T cells of neither *Malt1* TBM-T nor *Traf6*-ΔT mice show activation of NF-κB, indicating that both mutations are sufficient for blocking signaling downstream of MALT1 (Table 5-1). Importantly, no influence was measured on Teff cell populations in *Malt1* TBM-Treg mice, providing evidence that the Teff phenotype of TBM mice is not Treg cell intrinsic. TBM mutations in Tregs alone were sufficient for increased proliferation of Treg populations, hinting at increased signaling in *Malt1* TBM-Treg mice (Table 5-2). Interestingly, reports on Treg-specific *Traf6* KO mice show that TRAF6 ligase function is essential for localization, expansion, and stability of FoxP3, and these mice showed symptoms of autoimmunity (Muto et al., 2013; Ni et al., 2019). However, the reported phenotype is driven by loss of Treg cell numbers and function, which we clearly show is not the case in our models.

Only the inflammatory serum cytokines IL-10 and IFNγ were mildly but significantly increased in *Malt1* TBM-T and *Traf6*-ΔT mice, respectively, arguing that broad, high-level serum cytokines in *Malt1* TBM mice are likely a secondary effect of massive, early onset inflammation. For example, deregulated production of IL-6 can lead to a 'cytokine storm' and fatal autoimmunity, a possible contributing factor to the low survival of *Malt1* TBM (Kishimoto et al., 2015; Tanaka et al., 2016). Likewise, long-term high expression of IFNγ has dire effects on signaling and has been shown to inhibit differentiation of hematopoietic stem cells in the bone marrow, a potential contributor to the massive loss of mature B cells in *Malt1* TBM mice (Qin et al., 2019). Significantly, the high similarity of the phenotypes of *Malt1* TBM-T and *Traf6*-ΔT mice shows that the primary function of TRAF6 in T cells likely depends upon its ability to bind MALT1.

The fact that onset of autoimmunity in *Malt1* TBM-T mice was much milder than that of *Malt1* TBM mice immediately implicates other cell populations in the phenotype of *Malt1* TBM. For example, MALT1-TRAF6 dependent signaling and NF-κB activation is essential for development and activation of B cells (Sasaki & Iwai, 2016). Therefore, the effects of constitutive MALT1 activity should be determined in B cells and could partially explain the decreased B220+ B cells in *Malt1* TBM mice. Additionally, a number of other cell types are dependent upon TRAF6 association to CARD-BCL10-MALT1 complexes. For example, MALT1-BCL10 heterodimers associate with CARD10 in myeloid cells for signaling downstream of PRRs in innate immunity, and CARD14-BCL10-MALT1 complexes transfer signals via Dectin1 and IL-17 receptors of keratinocytes (Ruland & Hartjes, 2019). Defective signaling

in keratinocytes could contribute to autoimmunity and to the dermatitis phenotype we see in TBM-T mice, which has also previously been reported in *Traf6*-ΔT mice (King et al., 2006). Further, TRAF6 deletion could have an effect in signaling pathways in which TRAF6 acts independently of MALT1, for example downstream of IL-1 receptors, TLRs, and IL-17 receptors (Shi & Sun, 2018). Additional Cre-recombinase models will be needed to determine to what extent non-T cell populations play a role in the development of autoimmunity in *Malt1* TBM mice.

Another possible culprit for the milder phenotype of *Malt1* TBM-T mice is gene dosage. *Malt1* TBM-T mice only express one copy of the TBM allele in T cells following Cre-recombination (*Malt1*$^{TBM/-}$). Since the phenotype of TBM mice is hypothesized to be driven by paracaspase activity, a 50% reduction in enzyme concentration could lead to a slower increase in Teff cells. It is also not currently understood whether CBM complex assembly and filament formation acts in a digital, switch-like manner, or if the strength of downstream signaling is analog and heavily dependent upon local protein concentration (David et al., 2018; Kingeter et al., 2010). Assuming that the strength of MALT1 protease activity is dependent upon MALT1 concentration, and that the phenotype in *Malt1* TBM-T is protease-driven, monoallelic expression of MALT1 in TBM-T mice could dampen the onset of autoimmunity by partially impeding CBM filament formation and weakening MALT1 activation. Such a gene-dosage effect could explain the relatively late onset of disease in TBM-T mice and breeding of Cre recombination-independent *Malt1*$^{TBM/-}$ mice would help to clarify these results and should be performed.

5.3 TRAF6 is a positive regulator of NF-κB in primary T cells

It is generally understood that TRAF6 acts as a positive regulator of NF-κB, and loss of TRAF6 expression or interaction with MALT1 in Jurkat T cells leads to impaired NF-κB activation upon TCR stimulation (Meininger et al., 2016; Noels et al., 2007; Oeckinghaus et al., 2007; L. Sun et al., 2004). However, previous data has suggested that TRAF6-deficiency does not impair NF-κB activation in primary murine T cells (King et al., 2006; Motegi et al., 2011). In contradiction to this, we clarify the role of TRAF6 in TCR-induced NF-κB signaling by clearly proving that TRAF6 is essential for CBM-dependent NF-κB activation in primary murine CD4 T cells.

The discrepancy between our data and previous reports is most likely explained by different timing of cell stimulation. In Motegi et al the authors only show NF-κB activation following 24h and 48h TCR/CD28 stimulation. These late time points may induce NF-κB activation from secondary effects, for example as a result of augmented cytokine secretion of activated *Traf6*-ΔT T cells compared to control cells (Motegi et al., 2011). With our detailed biochemical and single cell imaging analyses, we clearly show that early NF-κB activation is strongly impaired in both murine and Jurkat T cells after

TRAF6 ablation and in Jurkat T cells expressing catalytically inactive TRAF6 C70A (Seeholzer, unpublished). In support of our findings, T cell specific loss of the E2-conjugating enzyme Ubc13, which interacts with TRAF6 in the NF-κB pathway, leads to downregulation of NF-κB (Yamamoto et al., 2006). Similarly, cellular inhibition of *Traf6*-Ubc13 interaction with a small molecule inhibitor leads to a reduction in IκBα phosphorylation and NF-κB target gene expression (Brenke et al., 2018). Despite this inconsistency, our results regarding upregulation of activated and effector T cells and general autoimmunity agree with previous reports on TRAF6 ablation in mice (King et al., 2006).

5.4 Loss of MALT1-TRAF6 interaction leads to aberrant paracaspase activity

Induction of constitutive MALT1 cleavage activity in resting T cells is the predominant phenotype of MALT1-TRAF6 ablation *in vivo*. However, it was not clear in the murine setting whether constitutive MALT1 activity is a direct result of aberrant interaction with TRAF6 or a consequence of systemic autoimmunity. Therefore, a heterologous *in vitro* system was developed. TRAF6 KO Jurkat T cells showed complete loss of TCR-dependent NF-κB upregulation, highlighting the essential role that TRAF6 plays in association with the CBM complex as a positive regulator. In fact, NF-κB activation in TRAF6 KO cells closely resembled the phenotype of Jurkat T cells upon loss of MALT1, BCL10, or CARD11 expression (Meininger et al., 2016; Schlauderer et al., 2018; Seeholzer et al., 2018). Jurkat cells lacking expression of TRAF6 or expressing MALT1 with T6BM1/2 mutations (Seeholzer, unpublished) recapitulated the constitutive MALT1 substrate cleavage phenotype of *Traf6*-ΔT and *Malt1* TBM-T mice, with constitutive but still inducible cleavage of MALT1 substrates, providing strong evidence of a cell-autonomous role for TRAF6 as a negative regulator of MALT1 activity under steady state conditions. Inducible MALT1 paracaspase activity has been shown to be dependent upon post-translational modification and protein-protein interaction, namely mono-ubiquitination of MALT1 K644, homodimerization via the paracaspase domain, and an intact MALT1-BCL10 interface (Pelzer et al., 2013; Schlauderer et al., 2018; Wiesmann et al., 2012; Yu et al., 2011). Importantly, constitutive activity in *Malt1* TB6BM1/2 Jurkat T cells was lost upon abrogation of any one of these events, showing that inducible and constitutive MALT1 activities are dependent upon the same mechanisms (Seeholzer, unpublished).

Dependency of constitutive MALT1 activity on CARD11 and BCL10 argues that TRAF6 prevents formation of low level CBM complex activation via mechanisms within or upstream of the CBM complex. While evidence of MALT1 activity independent of CBM complex assembly has been shown under conditions of BCL10 (David et al., 2018; Qiao et al., 2013) or TRAF6 (Bardet et al., 2018) overexpression, our data argues that constitutive cleavage is dependent upon endogenous mechanisms and expression levels. As TRAF6 is required for maintaining homeostasis in resting cells,

it was thought that rather low-level, antigen independent 'tonic' TCR signaling could be culpable for activation of MALT1 upon loss of interaction to TRAF6. While tonic signaling in B cells is well-defined as being essential for B cell survival and maturation (Polic et al., 2001; Srinivasan et al., 2009), it remains controversial in T cells, but would help to explain the essential role of TRAF6 as a negative regulator of MALT1 in resting T cells

Indeed, upon additional deletion of a functional TCRα in TRAF6 KO Jurkat T cells, constitutive activity of MALT1 was lost, and could only be regained by bypassing the TCR with strong, TCR-independent stimulation with P/I. Dependency of the constitutive cleavage phenotype on an intact TCR supports the hypothesis that TRAF6 is required under steady state conditions to prevent MALT1 enzyme activity from being activated by low level, tonic signals (Myers et al., 2017; Roose et al., 2003). These results likely indicate a balance between some currently unknown necessity for tonic TCR signaling and a simultaneous need for keeping downstream signaling pathways (for example NF-κB and JNK) inactive in resting cells to maintain tolerance. Inhibition of MALT1 activity by TRAF6 in resting cells is potentially a mechanism which has evolved to fulfill this need. Further, the fact that TRAF6 holds both a positive and negative position in this mechanism shows a need for rapid, switch like activation of signaling upon antigen stimulation, dependent upon post-translational regulation. However, the benefit of this rapid mode of action clearly means that mutations which inhibit MALT1-TRAF6 interaction have massive consequences to immune regulation. Crossing of *Malt1* TBM mice to *TCR* KO or *MHC-II* knockout mice would help answer the question, whether the TBM phenotype relies on low level, tonic signaling.

5.5 Autoimmunity in *Malt1* TBM and *Traf6*-ΔT mice is driven by MALT1 protease activity

Constitutive MALT1 activity and loss of NF-κB signaling are the primary phenotypic hallmarks upon disruption of MALT1-TRAF6 interaction in murine and cellular models, indicating that TRAF6 plays a role as a negative regulator of MALT1 paracaspase activity in resting cells. By developing two independent genetic approaches, we show that the phenotypes of *Malt1* TBM and *Traf6*-ΔT mice are dependent upon aberrant MALT1 cleavage activity. In *Malt1* TBM mice, combined *in vitro* fertilization with *Malt1*$^{TBM/+}$ sperm and CRISPR-Cas9 targeting of the MALT1 catalytic cysteine-472 yielded *Malt1* TBM mice with additional inactivation of the paracaspase domain on the same allele (*Malt1* TBMPM mice: triple mutant E325A, C472A, E814A). A corresponding approach was taken in *Traf6*-ΔT mice, where loss of TRAF6 expression was combined with the MALT1 PM mutation, both in a T cell-dependent manner (*Traf6* PM mice: *Malt1*$^{PM/fl}$; *Traf6*$^{fl/fl}$; *CD4-Cre*$^{Cre+}$) (see breeding plan, section 7.3.6.5).

Malt1 TBMPM mice faithfully recapitulated the phenotype of complete *Malt1* deficiency, with complete loss of B1 lymphocytes and regulatory T cells, and a suppressed immune response apparent from loss of Teff cell populations (Table 5-2, Figure 5-1) (Bornancin et al., 2015; Gewies et al., 2014; Jaworski et al., 2014; Ruefli-Brasse et al., 2003; Ruland et al., 2003). *Malt1* TBMPM mice provide unequivocal evidence that autoinflammation in *Malt1* TBM mice is dependent upon the catalytic activity of MALT1. Simultaneously, these results provide new evidence for the dependency of the *Malt1* PM phenotype on MALT1 scaffolding and NF-κB activation. *Malt1* TBMPM mice showed no evidence of the PM-triggered autoimmunity, and no weight loss, ataxia, or elevated inflammatory cytokine production was apparent. These results again highlight that, although the autoimmune phenotypes seen in *Malt1* PM and *Malt1* TBM mice are mechanistically distinct, both arise from Teff activity and proliferation in excess of the suppressive ability of Tregs.

The reversion of autoimmunity in *Malt1* TBMPM mice indicates that MALT1 paracaspase activity drives the phenotype of *Malt1* TBM mice. However, this model is MALT1 intrinsic and fails to directly prove that the autoimmunity in *Traf6*-ΔT mice is linked to the same MALT1 cleavage mechanism. We therefore inactivated MALT1 paracaspase activity in *Traf6*-ΔT mice (*Traf6* PM mice). Reversion of autoimmunity, apparent in lower Teff cell populations and loss of Tregs in *Traf6* PM, clearly reflect that the *Traf6*-ΔT phenotype is reliant upon MALT1 activity. In fact, *Traf6* PM mice resemble T cell-specific *Malt1* KO mice, which exhibit the full-body *Malt1* KO phenotype without reduction of MZ and B1 cell populations (Table 5-2) (Demeyer et al., 2019). As was the case in *Malt1* TBMPM mice, *Traf6* PM showed concomitant reversion of the PM phenotype, and mice did not exhibit the weight loss or onset of ataxia which was present in PM controls, arguing that the phenotype of T cell specific paracaspase deficiency is dependent upon TRAF6 ligase activity and NF-κB signaling downstream of the CBM complex (Demeyer et al., 2019).

5.5.1 Therapeutic intervention with a MALT1 inhibitor ameliorates immune activation in the *Traf6*-ΔT mice

We wanted further proof that constitutive MALT1 activity drives autoimmunity in our mouse models. We hypothesized that pharmacological treatment of *Traf6*-ΔT mice with a strong MALT1 inhibitor would reduce MALT1 activity enough to reduce T_{EM} cell populations. Martin et al. showed that 10-day p.o. BID (oral administration, twice daily) treatment of mice with the compound MLT-943 leads to a reduction in Tregs (Martin et al., 2020). This reduction reflects what is seen in *Malt1* PM mice and indicates that this inhibitor can successfully target MALT1 *in vivo* (Bornancin et al., 2015; Gewies et al., 2014; Jaworski et al., 2014). Indeed, 10-day treatment of *Traf6*-ΔT mice with the structurally similar MLT-985 was sufficient to revert Teff cell populations to the level of untreated

wildtype mice (Table 5-2). Furthermore, MALT1 inhibition reverted the constitutive cleavage of Roquin-1/2 and Regnase-1, apparent from reduced translation of their mRNA substrates *icos* and *NFkBID*. These results provide further strong evidence that constitutive paracaspase activity drives autoimmunity. As published by Martin et al., we saw a reduction in CD4+ FoxP3+ Treg cells and the expression of the suppression marker Ox40 upon treatment of *Traf6*-ΔT mice, reflecting the dependence of Treg development on MALT1 activity (Martin et al., 2020). Importantly, severe reduction in Tregs in *Traf6*-ΔT nevertheless does not lead to the PM phenotype, as autoinflammation in PM mice is dependent upon NF-κB activity, which is impaired in *Traf6*-ΔT mice. Our results underscore that changes in Teff cells, not Treg cells, are responsible for the severe immune imbalance caused by TRAF6 ablation or loss of MALT1-TRAF6 interaction

5.6 Constitutive MALT1 cleavage impairs RNA control mechanisms in T cells

Autoimmunity in *Malt1* TBM mice in the absence of NF-κB activation was initially surprising, given that loss of NF-κB signaling upon knockout of individual CBM complex members overwhelmingly leads to immune suppression, not autoimmunity (Egawa et al., 2003; Hara et al., 2003; Ruefli-Brasse et al., 2004). Given that the activated phenotype seen upon loss of MALT1-TRAF6 interaction is dependent upon MALT1 cleavage activity, this clearly implicated a reduction in of one or more MALT1 substrates. Identified MALT1 targets are diverse, with roles as NF-κB regulators, post-transcriptional modulators, and CBM components. NF-κB regulators act in both positive (HOIL-1) and negative (CYLD, A20, and RELB) roles to impact NF-κB activation dynamics. However, the role of constitutive cleavage here is hypothesized to have limited contribution upon MALT1-TRAF6 abrogation, since NF-κB activation is practically non-existent in these mice (Table 5-1). Similarly, constitutive induction of neither MALT1 autocleavage nor BCL10 cleavage was noted upon MALT1-TRAF6 abrogation (Seeholzer, unpublished).

The RNA binding proteins (RBPs) Regnase-1 and Roquin-1/2 are MALT1 cleavage targets which are critical for maintaining peripheral tolerance (Jeltsch et al., 2014; Matsushita et al., 2009; Uehata et al., 2013; Vinuesa et al., 2005; Vogel et al., 2013). Regnase-1 and Roquin-1/2 exert regulation by cleavage of a set of mRNAs coding for, among others, Ox40, c-Rel, IκBNS, ICOS, and IκBζ, and genetic ablation of these RBPs leads to autoimmunity, with splenomegaly, dramatically increased Teff cells, and significantly reduced survival in mice (Matsushita et al., 2009; Uehata et al., 2013; Vogel et al., 2013). IκBNS and ICOS play essential roles in regulation of inflammatory cytokines and cell proliferation, and loss of RBP expression leads to increased expression of proinflammatory cytokines and autoantibodies similar to what is observed in *Malt1* TBM-T and *Traf6*-ΔT mice (Matsushita et al., 2009; Uehata et al., 2013; Vogel et al., 2013). Increased cleavage of Regnase-1 and Roquin-1/2 by

MALT1 would therefore be expected to yield subsequent increased translation from RBP target genes. In line with this, *Malt1* TBM-T and *Traf6*-ΔT mice showed drastically elevated expression of Ox40, ICOS, and IκBNS. Therefore, although there are currently 11 known cleavage substrates of MALT1, we hypothesize that constitutive processing of RBPs is the major driver of inflammation in these mice. Indeed, *Traf6*-ΔT mice treated with MLT-985 or genetically altered by additional MALT1 paracaspase inactivation in *Traf6* PM mice showed a complete rescue of constitutive RBP cleavage, and RBP substrates IκBNS and ICOS returned to or below control levels. Expression of non-cleavable forms of Regnase-1 or Roquin-1/2 in *Malt1* TBM-T or *Traf6*-ΔT mice would be expected to lessen phenotype severity by maintaining RBP activity.

In addition to T and B cell activation, *Malt1* TBM mice show a strong, in some cases complete depletion of B220+ B cells, thought to be a secondary phenotype of systemic inflammation and possibly explaining the lower production of autoantibodies in *Malt1* TBM compared with *Malt1* TBM-T or *Traf6*-ΔT. In support of the hypothesized excessive cleavage of RBPs upon MALT1-TRAF6 ablation, T cell conditional loss of Roquin-1/2 expression also leads to loss of B cell expression and differentiation in the spleen (Matsushita et al., 2009; Vogel et al., 2013), and deletion of Regnase-1 in all cells leads to deficient CD19 B cell differentiation (Mao et al., 2017; Uehata et al., 2013). Thus, loss of B cells in *Malt1* TBM mice is likely a secondary effect of mutation. Roquin-1/2 KO mice also exhibit expansion of T follicular helper (Tfh) and Germinal Center B (GCB) cells. Investigation of Tfh and GCB populations in TBM models would therefore be informative of possible parallels between these models and to demonstrate that dysregulation of RBP cleavage and mRNA stability networks causes autoimmunity.

5.7 Imbalance of MALT1-TRAF6 interaction may account for human immune disorders

The results of inhibitor treatment are of potential relevance to human patients with TRAF6 or MALT1 defects which result in autoimmunity. A recent human T6BM2 E-to-D patient (Kutukculer et al., 2020) shows signs of autoimmunity (lymphadenopathy, dermatitis, and autoantibody production) and immune suppression (infection) with similarities to the phenotype of *Malt1* TBM and *Traf6*-ΔT mice. Our results suggest that a hallmark of this patient may be dysregulated MALT1 paracaspase activity. If this is the case, short term application of therapeutic inhibitors could be beneficial to combat inflammatory episodes, although it is difficult to predict the effects of potential Treg reduction, which could further exacerbate the already prevalent immune imbalance. We show that presence of a single mutated allele in heterozygous *Malt1*$^{TBM/+}$ mice is sufficient to induce late-onset autoimmunity. The parents of the T6BM2 mutation patient are both heterozygous for the E806D mutation, raising the possibility of late-onset autoimmunity which could also potentially be

mitigated by short-term inhibitor treatment. Overall, our results suggest a therapeutic window and it is hoped that MLT-985 or a less potent MALT1 inhibitor could have efficacy in treatment and could potentially reduce effector T cell populations while sparing the conflicting reduction in Tregs.

The human patient only has mutation in the second T6BM and NF-κB signaling is likely still functional in MALT1A protein. However, MALT1B protein expression in human CD4+ T cells is roughly 5-fold higher than that of MALT1A (Kutukculer et al., 2020; Meininger et al., 2016), indicating that the vast majority of MALT1 protein in resting cells cannot interact with TRAF6 to induce NF-κB. The regulation of MALT1 isoform expression is therefore essential to the understanding of this disease, and a MALT1 mutant mouse with only the second T6BM site mutated would be an important model for investigating the processes that contribute to the disease conditions in the patient with MALT1 T6BM2 binding-deficiency.

Pharmacological TRAF6 inhibition has additionally been considered as an approach for reducing proliferation of inflammatory cells by blocking NF-κB signaling. Significant correlation has been found between TRAF6 variants containing single-nucleotide polymorphisms (SNPs) and increased risk of systemic lupus erythematosus and rheumatoid arthritis, two types of autoimmune disease (Namjou et al., 2012; Raychaudhuri et al., 2009). In line with this, a small molecule inhibitor of TRAF6-UBC13 interaction was shown to have potential in the treatment of inflammation in autoimmune psoriasis and rheumatoid arthritis, showing mild reduction of NF-κB and arguing for partial TRAF6 inhibition as a treatment for autoinflammatory disease (Brenke et al., 2018). Our results from *Traf6*-ΔT mice indicate that this approach should be taken with caution, and strong TRAF6 inhibition leading to complete NF-κB abrogation and constitutive MALT1 activity could lead to the opposite of the intended effect, acting rather to further inflammation than as a mitigating factor. Rather, our results from treatment of *Traf6*-ΔT mice indicate a promising potential for the use of MALT1 inhibitors to treat patients with low TRAF6 expression or function.

6 Conclusions and Outlook

In this study, we define and characterize a new role of the TRAF6 E3 ligase as a negative regulator of MALT1, whereupon TRAF6 interaction with MALT1 in resting T cells is essential for maintenance of homeostasis by acting as a brake on MALT1 paracaspase activity (Figure 6-1). Our data from murine and cellular models unravels and explains the paradox how TRAF6 can simultaneously act as a positive regulator of NF-κB activity and as a negative regulator to prevent autoimmunity. Upon antigen ligation to the TCR and assembly of the CBM complex, TRAF6 ligase activity is required for NF-κB signaling, and release of negative regulation of MALT1 leads to full activation of substrate

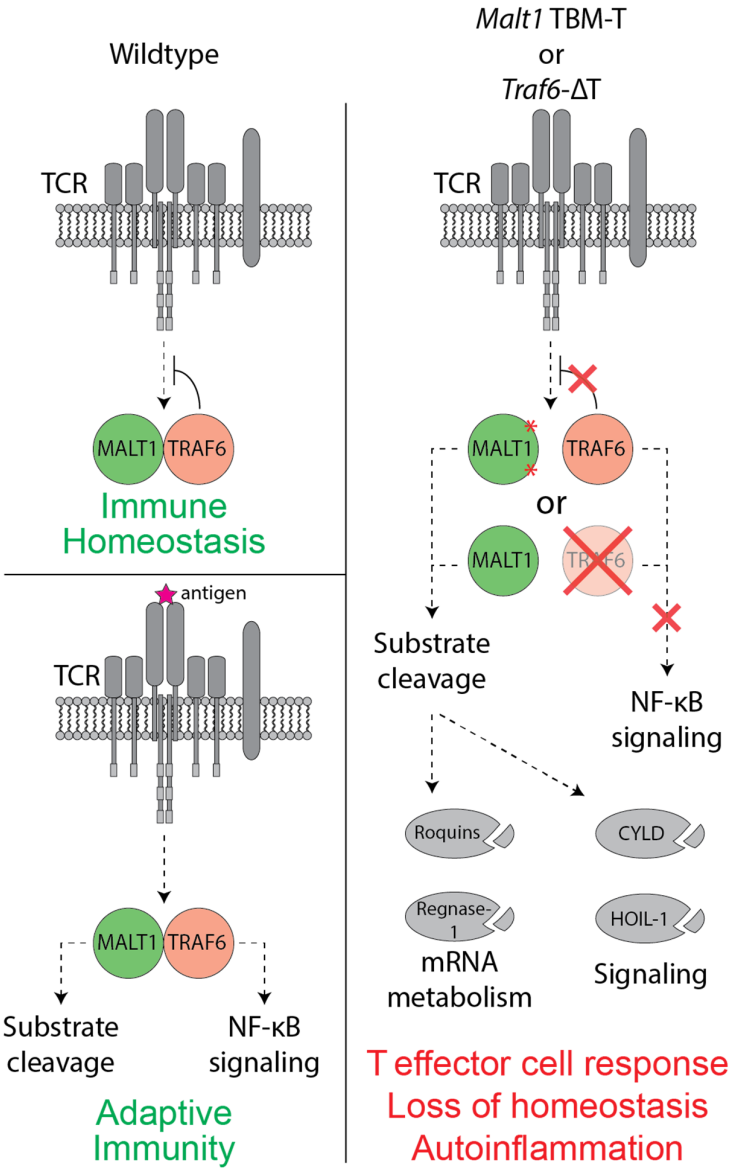

Figure 6-1. Updated model of the MALT1-TRAF6 interaction
An updated model for regulation of MALT1 paracaspase activity by TRAF6. In resting T cells, TRAF6 acts as a negative regulator of MALT1 and maintains paracaspase activity inactive. Upon ligation of an antigen to the TCR, CBM complex formation leads to activation of MALT1 substrate cleavage and downstream NF-κB signaling. Loss of MALT1-TRAF6 interaction via mutation of MALT1 T6BM1/2 or loss of TRAF6 expression in T cells leads to loss of negative regulation by TRAF6 and development of autoimmunity driven by aberrant MALT1 substrate cleavage.

cleavage (Figure 6-1). *Malt1* TBM mice lacking motifs on MALT1 for binding to TRAF6 show severe, fatal autoimmunity due to constitutive MALT1 activity. Additionally, we show the importance of MALT1 scaffolding *in vivo*, and *Malt1* TBM mice have severely reduced NF-κB activation due to a lack of TRAF6 assembly to the CBM complex. In T cells, TBM mutations or loss of TRAF6 expression yield analogous autoimmune phenotypes, arguing for primarily T cell-intrinsic relevance of MALT1-TRAF6 binding (Figure 6-1).

We suggest that the driving force behind development of autoimmunity upon loss of MALT1-TRAF6 interaction is the constitutive cleavage of RBP substrates. Indeed, increased levels of IκBNS, ICOS, and Ox40, all substrates of Regnase-1 and Roquin-1/2, were detected in *Malt1* TBM-T and *Traf6*-ΔT mice. It is hypothesized, but not shown that further RBP substrates should also be upregulated. To this point we lack an unbiased approach in our description of our murine phenotypes. To determine the global effects of *Malt1* TBM mutations, global transcriptomics or proteomics may help to clarify how constitutive MALT1 protease activity affects T cells. Ideally, tamoxifen-inducible models should be utilized to distinguish between primary and secondary effects of MALT1 protease activation. Proteomics may define new MALT1 targets and directly affected proteins, while transcriptomics will indicate changes in transcript regulation and processing. For example, we would expect to see increased mRNA from IκBζ, an atypical IκB protein and Regnase-1 target which controls FoxP3+ Treg differentiation (MaruYama, 2015). Additionally, due to the conspicuous presence of FoxP3+ Tregs despite lack of NF-κB activation, it will be interesting to see if genes and proteins defining Treg identity are strongly modulated in our models.

The MALT1-TRAF6 interaction is essential for signaling downstream of T cell receptors (TCRs), B cell receptors (BCRs), c-type lectin receptors (CLR) in DCs, and in keratinocyte signaling (Dainichi et al., 2019). Receptor signaling through each of these pathways is therefore expected to be abrogated in *Malt1* TBM mice. In later Cre-recombinase dependent models, we attempted to clarify the role of the interaction between MALT1 and TRAF6 specifically in T cells. However, the strong, early onset autoimmune phenotype of *Malt1* TBM mice is likely also dependent upon T cell extrinsic signaling. Differentiation of Ig producing plasma B cells, MZ B cells, B1 B cells, and GCB cell are all dependent upon intact NF-κB signaling downstream of the BCR (Ruland & Hartjes, 2019). NF-κB signaling is also essential for maturation and development of DCs, and defects in DC development can lead to autoimmunity due to defective presentation of self-peptide epitopes during lymphocyte selection (J. Oh & Shin, 2015). Therefore, additional cell types are clearly in need of more detailed analysis.

The focus of this study was on the effect of abrogated MALT1-TRAF6 interaction in T cells, and the strong reduction in B cells seen in *Malt1* TBM mice was attributed to secondary effects of systemic autoinflammation and cytokine production. However, the potential effects of these mutations in B cells should not be overlooked. MALT1 plays an enormous role in homeostatic maintenance in B cells and is a central proto-oncogene in the activation B cell subtype of diffuse large B cell lymphomas (ABC-DLBCLs) (Hailfinger et al., 2009). Survival of ABC-DLBCL cells relies upon MALT1 cleavage activity, and several studies have shown the efficacy of pharmacological intervention with small MALT1 inhibitors (Fontan et al., 2012; Nagel et al., 2012). Therefore, hyperactivity of MALT1 could

lead to chronic BCR signaling and a B-cell driven phenotype. To investigate a potential phenotype in *Malt1* TBM B cells, a B cell-conditional mouse line with the TBM mutations expressed only in CD19 B cells will be bred. CD19 is expressed early in B cells development on pro-B cells and therefore acts as a general B cells marker. It will be important to see if B cells lacking MALT1-TRAF6 interaction will also exhibit constitutive cleavage, and what effect downstream of the BCR this will provoke.

The ability to induce strong effector function in T cells has clear potential use in adoptive T cell therapy. Adoptive T cell therapy uses *ex vivo* modification and reintroduction of autologous T cells to increase anti-tumor effector function. We show that single base-pair mutations within MALT1 T6BMs induces upregulation of CD4+ and CD8+ T_{EM} cells which are hypothesized to possess strong, anti-tumor activity. Overcoming suppression by Tregs in adoptive T cell therapy is difficult and can lead to rapid inactivation of therapeutic T cells (Antony et al., 2005; Antony & Restifo, 2002; Jones et al., 2002). Importantly, we also show that modulated Teff cells are resistant to suppression by Tregs, a common hurdle in T cell therapy. It remains to be seen if *Malt1* TBM T cells retain activity and proliferative capabilities, and if prolonged effector function will lead to T cell exhaustion and loss of function. Nevertheless, the potential efficacy of our system in T cell therapy opens exciting new avenues for research in the direction of human disease.

7 Materials and Methods

7.1 Materials

7.1.1 Instruments and equipment

Instrument/equipment	Source
Adhesive seal sheets	Thermo Fisher Scientific, Waltham, USA
Agarose gel chambers	NeoLab, Heidelberg
Autoclave – VX-95	Systec, Linden
Bacterial culture flasks	Schott, Zwiesel; BD, Heidelberg
Cell-counting chamber Neubauer	NeoLab, Heidelberg
Cell culture flasks/plates	BD, Heidelberg; Nunc, Wiesbaden
Cell viability analyzer – ViCell-XR	Beckman Coulter, Krefeld
Cell strainer (100 µm)	NeoLab, Heidelberg
Centrifuge Beckman Avanti J-26 XP	Beckman Coulter, Krefeld
Centrifuges – 5810R, 5417R, 5471C, 5804	Eppendorf, Hamburg
Chemiluminescence ECL films	GE Healthcare, Freiburg
CO_2 incubators	Binder, Tuttlingen
Cryo tubes	Greiner Bio-One, Frickenhausen
Developer – Optimax	Protec, Oberstenfeld
Electroporation cuvettes – Gene Pulser	Bio-Rad, München
Electroporator – Gene Pulser Xcell System	Bio-Rad, München
NEPA21 electroporator	Nepa Gene Co., Ltd., Japan
CUY501P1-1.5 electrode	Nepa Gene Co., Ltd., Japan
EMSA gel chamber, X952.1	Roth, Karlsruhe
Eppendorf tubes Eppendorf, Hamburg	Eppendorf, Hamburg
Attune Acoustic Focusing Cytometer	Thermo Fisher Scientific, Waltham, USA
Flow cytometry tubes	BD, Heidelberg
Falcon tubes	BD, Heidelberg
Filter pipette tips – TipOne	StarLab, Hamburg
Freezers and Fridges	Liebherr, Ochsenhausen
GST columns – 1 mL	GE Healthcare, Freiburg
Heat blocks	Techne, Burlington, USA
Ice machine – Scotsman AF20	Scotsman Ice Systems, Vernon Hills, USA
ImageStreamX Mark II	Amnis Merck Millipore, Darmstadt
Incubator shaker – I 26	New Brunswick Scientific, Hamburg
Incubators	Sartorius, Göttingen; Heraeus, Hanau
LC system – ÄKTA Purifier System	GE Healthcare, München
LightCycler480	Roche, Mannheim
LightCycler plates 96 well	4titude, Berlin
MACS columns	Miltenyi Biotec, Bergisch Gladbach
MACS magnetic rack	Miltenyi Biotec, Bergisch Gladbach
Magnetic stirrer	NeoLab, Heidelberg
Micro scales, scale	Kern & Sohn, Balingen

Microtiter plate (U- or V-shape), 96-well	Greiner Bio-One, Frickenhausen
Microplate, 384 well	Greiner Bio-One, Frickenhausen
Microscopes	Leica, Wetzlar
Microwave	SHARP, Hamburg
Mouse ear punch	Fine Science Tools, Heidelberg
Petri dishes	Greiner Bio-One, Frickenhausen
pH meter – inoLab pH7110	WTW, Weilheim
Pipette tips	Eppendorf, Hamburg
Pipettes – Reference	Eppendorf, Hamburg
Pipetting aid – accu-jet pro	Brand, Wertheim
Power supplies – EV202, EV243	Consort, Turnhout, Belgium
Precision scale – New Classic MS	Mettler Toledo, Gießen
Rotator – Intelli-Mixer	NeoLab, Heidelberg
SDS-PAGE gel chambers	Roth, Karlsruhe
Shaker – Polymax 1040	Heidolph Instruments, Schwabach
Spectral photometer – Biophotometer	Eppendorf, Hamburg
Syringes – 1 mL	Wagner & Munz, München
Thermocycler – Mastercycler gradient	Eppendorf, Hamburg
Thermomixer comfort	Eppendorf, Hamburg
Ultracentrifuge – Optima MAX	Beckman Coulter, Krefeld
Ultra-pure water system – Milli-Q Plus	Merck Millipore, Darmstadt
Ultrasonic Device – UP200S	Hielscher Ultrasonics GmbH, Teltow
UV-Vis Spectrophotometer – NanoDrop 2000	Thermo Fisher Scientific, Waltham, USA
Vortexer	Heidolph Instruments, Schwabach
Western Blot detection – Amersham Hyperfilm TM ECL	GE Healthcare, München
Western Blot transfer – PVDF-membrane, 0.45 µm	Merck Millipore, Darmstadt
Western Blot transfer – Semi-dry blotter	Peqlab, Erlangen
Western Blot transfer – Whatman paper	Roth, Karlsruhe
96-well PCR plate	Thermo Fisher Scientific, Waltham, USA

7.1.2 Chemicals

7.1.2.1 General

Chemical	**Source**
Ac-LRSR-AMC MALT1 cleavage probe	Peptides International, Louisville, USA
Acrylamide/Bisacrylamide	Roth, Karlsruhe
Agarose	Biozym, Hessisch Oldendorf
Ampicillin	Roth, Karlsruhe
ß-Glycerophosphate	Sigma-Aldrich, Taufkirchen
Bovine serum albumin (BSA)	Sigma-Aldrich, Taufkirchen
Calcium chloride (CaCl2)	Roth, Karlsruhe
CHAPS	Roth, Karlsruhe

Coomassie blue	Bio-Rad, München
cOmplete Tablets, Mini, EDTA-free	Roche, Mannheim
4',6-diamidino-2-phenylindole (DAPI)	Thermo Fisher Scientific, Waltham, USA
Dimethyl sulfoxide (DMSO)	Roth, Karlsruhe
Dithiothreitol (DTT)	Sigma-Aldrich, Taufkirchen
DNA 1kb plus ladder	Thermo Fisher Scientific, Waltham, USA
dNTP-Mix	Thermo Fisher Scientific, Waltham, USA
DPBS (w/o MgCl2 and CaCl2)	Thermo Fisher Scientific, Waltham, USA
Ethanol (EtOH, p. a.)	Merck, Darmstadt
Ethidium bromide (EtBr)	Roth, Karlsruhe
Ethylenediaminetetraacetic acid (EDTA)	Roth, Karlsruhe
Glycerol	Roth, Karlsruhe
Glycine	Roth, Karlsruhe
Glutathione reduced	Sigma-Aldrich, Taufkirchen
HEPES	Roth, Karlsruhe
Ionomycin	Merck, Darmstadt
Isopropyl ß-D-1-thiogalactopyranoside (IPTG)	Thermo Fisher Scientific, Waltham, USA
LB-Agar (Luria/Miller)	Roth, Karlsruhe
LB-Medium (Luria/Miller)	Roth, Karlsruhe
2-(N-morpholino) ethanesulfonic acid (MES)	Sigma-Aldrich, Taufkirchen
Methanol (MeOH, p.a.)	Merck, Darmstadt
$MgCl_2$ x $6H_2O$	Sigma-Aldrich, Taufkirchen
Milk powder	Roth, Karlsruhe
^{32}P-α-dATP	Perkin Elmer, Wiesbaden
^{32}P-γ-dATP	Hartmann, Braunschweig
PageRuler Prestained Protein Ladder	Thermo Fisher Scientific, Waltham, USA
Phorbol 12-myristate 13-acetate (PMA)	Merck, Darmstadt
Potassium chloride (KCl)	Roth, Karlsruhe
Roti-Load 1 – 4x SDS sample buffer	Roth, Karlsruhe
Saccharose/Sucrose	Sigma-Aldrich, Taufkirchen
S.O.C. Medium	Thermo Fisher Scientific, Waltham, USA
Sodium chloride (NaCl)	Roth, Karlsruhe
Sodium dodecyl sulfate (SDS)	Roth, Karlsruhe
Sodium vanadate	Roth, Karlsruhe
TAE buffer (50x)	Omnilab, Bremen
Tetramethylethylenediamine (TEMED)	Roth, Karlsruhe
Tris(hydroxymethyl)-aminomethan (Tris)-HCl	Roth, Karlsruhe
Tri-Na-Citrate	Sigma-Aldrich, Taufkirchen
Tween-20	Roth, Karlsruhe
Western blotting detection (ECL substrate) 20x LumiGlo and 20x Peroxide	Cell Signaling Technology, Frankfurt

7.1.2.2 Cell culture and mice

Name	Description
RPMI (Roswell Park Memorial Institute) 1640	Thermo Fisher Scientific, Waltham, USA
Opti-MEM reduced serum media	Thermo Fisher Scientific, Waltham, USA
Fetal calf serum (FCS)	Thermo Fisher Scientific, Waltham, USA
Penicillin-Streptomycin (10,000 U/ml)	Thermo Fisher Scientific, Waltham, USA
MEM-NEAA	Thermo Fisher Scientific, Waltham, USA
ß-Mercaptoethanol	Roth, Karlsruhe
DPBS	Thermo Fisher Scientific, Waltham, USA
MLT-943	Synthesized by Isabel Hamp Published by Martin et al. (2020)
MLT-985	Synthesized by Isabel Hamp Published by Quancard et al. (2020)
Cas9 protein	Integrated DNA technologies, Coralville, USA

7.1.3 Enzymes and kits

Name	Source
CD4 T cell isolation kit (mouse)	Miltenyi Biotec, Bergisch Gladbach
eFluor 780 Live/Dead stain	Thermo Fisher Scientific, Waltham, USA
Gel extraction kit	Qiagen, Hilden
Phire Tissue Direct PCR Master Mix	Thermo Fisher Scientific, Waltham, USA
Herculase II DNA Polymerase	Agilent Technologies, Waldbronn
LongAmp DNA Polymerase	NEB, Frankfurt
Klenow Polymerase	NEB, Frankfurt
LightCycler 480 SYBR Green I Mastermix	Roche, Mannheim
KAPA SYBR FAST qPCR Mastermix	Peqlab, Erlangen
Plasmid Maxiprep Kit	Qiagen, Hilden
Plasmid Miniprep Kit	Qiagen, Hilden
Fixation kit	Thermo Fisher Scientific, Waltham, USA
Perm/Fix buffer	Thermo Fisher Scientific, Waltham, USA
Red blood cell (RBC) lysis buffer (10x)	Miltenyi Biotec, Bergisch Gladbach
EnGen® sgRNA Synthesis Kit	NEB, Frankfurt
BssHII restriction enzyme	NEB, Frankfurt
Mouse anti-dsDNA Ig's (Total A+G+M) Elisa kit	Alpha Diagnostic International, San Antonio, USA
Mouse enhanced sensitivity master buffer for flex set	BD, Heidelberg
Mouse IFNγ enhanced sensitivity flex set CBA kit	BD, Heidelberg
Mouse IL-4 enhanced sensitivity flex set CBA kit	BD, Heidelberg
Mouse IL-6 enhanced sensitivity flex set CBA kit	BD, Heidelberg
Mouse IL-10 enhanced sensitivity flex set CBA kit	BD, Heidelberg
Mouse IL-17 enhanced sensitivity flex set CBA kit	BD, Heidelberg
Mouse TNFα enhanced sensitivity flex set CBA kit	BD, Heidelberg

7.1.4 Mouse strains

Strain	Description	Source
CD4-Cre	STOCK Tg(Cd4-cre)1Cwi/BfluJ. JAX:017336.	Lee et al., 2001 The Jackson Laboratory
FoxP3-Cre	NOD/ShiLt-Tg(Foxp3-EGFP/cre)1cJbs/J	Xuyu et al., 2008 Gift of Caspar Ohnmacht
Traf6$^{fl/fl}$	ES cells obtained from EUCOMM: Traf6$^{tm2a(EUCOMM)Wtsi}$;	Laboratory of Daniel Krappmann
Malt1 KO/ *Malt1*$^{flox/flox}$	MALT1$^{tm1a(EUCOMM)Hmgu}$ (C57BL/6N-A/a). ES cell clone: HEPD0618_3_D10. Inoculated into foster mice by IDG, HMGU.	Laboratory of Daniel Krappmann
C57BL6/N/J	C57BL6/N/J	Charles River Laboratories, Sulzbach, Germany
Malt1 TBM	ES cells electroporated into mouse embryos by Ronald Naumann, Dresden. mES cell clone: 3-3E10.	Laboratory of Daniel Krappmann
Malt1 TBM-T	CD4-Cre recombinase-dependent *Malt1* TBM	Laboratory of Daniel Krappmann
Malt1 TBM-Treg	FoxP3-Cre recombinase-dependent *Malt1* TBM	Laboratory of Daniel Krappmann
Traf6-ΔT	CD4-Cre recombinase dependent Traf6$^{tm2a(EUCOMM)Wtsi}$	Laboratory of Daniel Krappmann
Malt1 TBMPM	*Malt1* TBM with additional paracaspase inactivation.	Laboratory of Daniel Krappmann
Traf6 PM	*Traf6*-ΔT mice with additional paracaspase inactivation.	Laboratory of Daniel Krappmann
CD1	CD1(ICR) (#022)	Charles River Laboratories, Sulzbach, Germany

7.1.5 Eukaryotic cell lines

Cell line	Information	Source
ES cells, R1/E cells	Murine pluripotent ES cells	Laboratory of Ronald Naumann
MEFs	Murine embryonic feeder cells harvested from C57BL/6 mice	Laboratory of Daniel Krappmann
Jurkat T cells	human T cell line; derived from acute T cell leukemia	Laboratory of Lienhard Schmitz (University of Giessen)
TRAF6-deficient Jurkat T cells	Bardet et al., 2018; This project; made by Thomas Seeholzer	Laboratory of Daniel Krappmann
TRAF6/TCRα-deficient Jurkat T cells	This project	Laboratory of Daniel Krappmann
TRAF6/BCL10-deficient Jurkat T cells	This project; made by Thomas Seeholzer.	Laboratory of Daniel Krappmann
TRAF6/CARD11-deficient Jurkat T cells	This project; made by Thomas Seeholzer.	Laboratory of Daniel Krappmann

7.1.6 Bacteria

Cell line	Information
TOP10	*Escherichia coli*, F-mcrA Δ(mrr-hsdRMS-mcrBC) ϕ80lacZΔM15 ΔlacX74 nupG recA1 araD139 Δ(ara-leu)7697 galE15 galK16 rpsL(StrR) endA1λ-
BL21-CodonPlus Competent cells	Escherichia coli, contain extra copies of rare E. coli argU, ileY, leuW, proL tRNA genes

7.1.7 Plasmids and oligonucleotides

7.1.7.1 Vectors

Name	Description
pX458	Cas9 from S. pyogenes containing EGFP reporter. Addgene #48138
pX458_T6BM1_sgRNA	pX458 containing T6BM1 sgRNA
pX458_T6BM2_sgRNA	pX458 containing T6BM2 sgRNA
pX458_TCRα_sgRNA	pX458 containing TCRα sgRNA
pGEX-6P-1	pGEX-6P-1 vector for protein expression and purification
pGEX-6P-1GST-MALT1 325-760	pGEX-6P-1 vector for GST-MALT1 325-760 expression and purification

7.1.7.2 Guide RNA and homology templates

Name	Sequence (5'-to-3')
T6BM1 sgRNA	GAGGCAGTGGAGTGCACTGA
T6BM2 sgRNA	ATTTCATCAGTTGTCTCTAC
PM sgRNA	TGTTCCTGTTGGATATGTGT
T6BM1 ssODN HDR	TCTCTGTTGACTTAATGACTACCCTTCCTAAGATATGAGTTACAATATGTTCA CATTTGTTTTCTCTAAATAAGGAAGAACAGATGAGGCTGTAGCGTGTACCG AGGTAGTGCAATCCTTTGGTTCAAGACCAAGAGTCCTCATGCTGCATGCTG GTTACTCTGGGGAGAGGTGGAGGTCCTAGCTCACT
T6BM2 ssODN HDR	CCAGACAGGTGTCATTGCAGCCGGACTCCACACACATTCATTTCAAATTATC CCCCCCACCACTACTGCCAGTTTGGTAGATCCAATGTGCCCGTGGCGACGA CCGACGAAATGCCATTCAGTTTTTCTGACAGGCTTATGATTTCTGAAAACTG ACCTTCATGGTTTTGAAAATTAGAATAGTTACAGTAATCT
PM ssODN HDR	CCTGTTGATGCTCCAAATCCATATAGGTCTGAAAATTGCCTATGCGTACAAA ACATACTGAAATTAATGCAAGAAAAGGAGACTGGCCTGAATGTGTTCCTGT TGGATATGGCGCGCAAAAGGTAAAATGTCTCATCTCTCTATCAAGTAGCAA CCTTGACAAAGTCTATGTAAGGCAATTCTGTACGGTGGTAA
TCRα exon 1 sgRNA	ACAAAACTGTGCTAGACATG

7.1.7.3 Genotyping primers

Name	Target	Sequence (5'-to-3')
Malt1 TBM1 genotyping	T6BM1 fwd general	GCAAAGAAACCCTAAACATC
	T6BM1 rev WT-specific	CCTTCAGTGCACTCCACT
	T6BM1 rev Mut-specific	CCTTCGGTACACGCTACA
Malt1 TBM2 genotyping	T6BM2 fwd general	ACGGATAAGAGTGGAGTGAT

	T6BM2 rev WT-specific	ATTTCATCAGTTGTCTCT
	T6BM2 rev Mut-specific	ATTTCGTCGGTCGTCGCC
Malt1 knockout genotyping	Malt1 flox del fwd	CTAGTCAGTCACCAGCTCAG
	Malt1 flox del rev	CTGGCTAACCAATCCTCAAAAC
	Malt1 flox rev	CAGTTCTCAATGCCAACGCAC
Malt1-PM genotyping	F-MALT1-KICA-GT	CCCACTCCCAGGATTGTTATATT
	KI-MALT1-WT-R	GAGACATTTTACCTTTTCCGACAC
	KI-MALT1-CA-F	AATGTGTTCCTGTTGGATATGGCCAG
	R-MALT1-KICA-GT	TGCTCTAGATCCACAGGTGTGGTT
FoxP3-Cre genotyping	FoxP3-Cre TG fwd	CGGGTCAGAAAGAATGGTGT
	FoxP3-Cre TG rev	CAGTTTCAGTCCCCATCCTC
	FoxP3-Cre ctrl fwd	CAAATGTTGCTTGTCTGGTG
	FoxP3-Cre ctrl rev	GTCAGTCGAGTGCACAGTTT
CD4-Cre genotyping	CD4-Cre fwd	ACCAGCCAGCTATCAACTCG
	CD4-Cre rev	TTACATTGGTCCAGCCACC
Traf6 genotyping	Traf6 fwd	CATGGCTTGTTACCTCTGCTC
	Traf6 wt/flox rev	TCCAGCAGTATTTCATTGTCAAC

7.1.7.4 Sequencing primers

Name	**Sequence (5'-to-3')**
T6BM1 fwd	GATCAGCATTCCCTATTGTG
T6BM2 fwd	GCATTTCCATTCCTCTCAG
Malt1 PM fwd	CATCTTTCCTTTCCCCACTC

7.1.7.5 EMSA oligonucleotides

Target	**Sequence (5'-to-3')**
NF-κB (H2K) fwd	GATCCAGGGCTGGGGATTCCCCATCTCCACAGG
NF-κB (H2K) rev	GATCCCTGTGGAGATGGGGAATCCCCAGCCCTG
OCT1 fwd	GATCTGTCGAATGCAAATCACTAGAA
OCT1 rev	GATCTTCTAGTGATTTGCATTCGACA

7.1.8 Antibodies

7.1.8.1 Cell stimulation antibodies

Name	**Source**
Mouse anti-human anti-CD3	BD Pharmigen, Frankfurt am Main
Mouse anti-human anti-CD28	BD Pharmigen, Frankfurt am Main
Rat anti-mouse IgG1	BD Pharmigen, Frankfurt am Main
Rat anti-mouse IgG2	BD Pharmigen, Frankfurt am Main

7.1.8.2 Flow cytometry antibodies

Name	**Clone**	**Source**
mouse anti-CD16/32	93	eBioscience, Frankfurt am Main
mouse anti-CD3-PECy7	UCHT1	eBioscience, Frankfurt am Main

mouse anti-CD45R(B220)-PerCP-Cy5.5	RA3-6B2	Biolegend, San Diego, USA
mouse anti-CD8a-FITC	53-6.7	eBioscience, Frankfurt am Main
mouse anti-CD8a-PE	53-6.7	BD Pharmigen, Frankfurt am Main
mouse anti-CD4-PE	RM4-5	eBioscience, Frankfurt am Main
mouse anti-CD4-PerCP-Cy5.5	RM4-5	eBioscience, Frankfurt am Main
mouse anti-CD25	PC61.5	eBioscience, Frankfurt am Main
mouse anti-CD44-PECy7	IM7	eBioscience, Frankfurt am Main
mouse anti-CD44-FITC	IM7	eBioscience, Frankfurt am Main
mouse anti-CD62L-APC	MEL-14	BD Pharmigen, Frankfurt am Main
mouse anti-CD69-APC	H1.2F3	eBioscience, Frankfurt am Main
mouse anti-CD86-FITC	GL-1	eBioscience, Frankfurt am Main
mouse anti-CD69-APC	H1.2F3	eBioscience, Frankfurt am Main
mouse anti-Ox40-PECy7	OX-86	eBioscience, Frankfurt am Main
mouse anti-CTLA-4-PECy7	UC10-4B9	eBioscience, Frankfurt am Main
mouse anti-CD19-APC	1D3	Biomol, Hamburg
mouse anti-CD23-Biotin	B3B4	eBioscience, Frankfurt am Main
anti-Strepdavadin-APC	-	BD, Heidelberg
mouse anti-CD21-FITC	7G6	eBioscience, Frankfurt am Main
mouse anti ICOS-FITC	C398.4A	eBioscience, Frankfurt am Main
mouse anti-IκBNS	4C1	Core facility monoclonal antibodies HMGU, München
mouse anti-FoxP3-PE	FJK-16s	eBioscience, Frankfurt am Main
mouse anti-rat-AF647	Poly4054	Biolegend, San Diego, USA
mouse anti-PD-1-FITC	J43	eBioscience, Frankfurt am Main
human anti-CD3-FITC	UCHT1	BD Pharmigen, Frankfurt am Main
human anti-TCRα/ß-BV421	IP26	eBioscience, Frankfurt am Main
Rabbit anti-p65	D14E12	Cell Signaling Technology, Frankfurt am Main

7.1.8.3 Immunoblot antibodies

Name	**Clone**	**Source**	**Dilution factor**
Mouse monoclonal anti-CYLD	E10	Santa Cruz Biotechnology	1:1000
Mouse monoclonal anti-HOIL-1	H-1	Santa Cruz Biotechnology	1:1000
Mouse monoclonal anti-Regnase-1/MCPIP1	604421	R&D System	1:1000
Mouse monoclonal anti-ß-Actin	C-4	Santa Cruz Biotechnology	1:10000
Mouse monoclonal anti-MALT1	D-1	Santa Cruz Biotechnology	1:1000
Rabbit monoclonal anti-TRAF6	EP591Y	Abcam	1:1000
Rabbit polyclonal anti-BCL10	H-197	Santa Cruz Biotechnology	1:1000
Mouse monoclonal anti-IκBα	L35A5	Cell Signaling Technology	1:1000
Mouse monoclonal anti-phospho-IκBα (Ser32/36)	5A5	Cell Signaling Technology	1:1000

7.1.8.4 Immunoblot secondary antibodies

Name	Source
HRP-conjugated anti-mouse	Jackson ImmunoResearch
HRP-conjugated anti-rabbit	Jackson ImmunoResearch

7.2 Buffers, solutions, and medium

Name	Components
DNA loading buffer	Glycerol (39% v/v), SDS (0.5% w/v), EDTA (1 mM), bromophenol blue (0.25% w/v), Xylene cyanol (0.25% w/v)
Shift buffer (2x)	20 mM HEPES pH 7.9, 120 mM KCl, 4% Ficoll, 5 mM DTT, 10 µg BSA, 2 µg poly-dI-dC
Annealing buffer	Tris-HCl pH 8.0 (50 mM), NaCl (70 mM)
Blocking buffer	BSA in PBS-T (5 % (w/v))
Blotting buffer	Tris pH 8.3 (48 mM), Glycine (39 mM), Methanol (20 % (v/v)), SDS (0.03 % (w/v))
Co-IP buffer	HEPES pH 7.5 (25 mM), NaCl (150 mM), Glycerol (1 mM), NP- 40 (0.2 % (v/v)), DTT (1 mM), NaF (10 mM), β-Glycerophosphate (8 mM), NaVanadate (300 µM), protease inhibitor mix
flow cytometry buffer	PBS (1x), FCS (3 % (v/v))
LB Agar plates	LB (20 g/l), Agar (15 g/l)
LB medium	LB (20 g/l)
PBS (1x)	NaCl (137 mM), Na2HPO4 (10 mM), KCl (2.7 mM), KH2PO4 (1.7 mM)
PBS-T	PBS, Tween-20 (0.1 % (v/v))
Agarose gel	TAE buffer (1x), Acrylamide/Bisacrylamide (1%)
SDS electrophoresis buffer (1x)	Tris pH 8.8 (25 mM), Glycine (192 mM), SDS (0.1 % (w/v))
5x Separation gel	Tris/HCl pH 8.8 (375 mM), Acrylamide/Bisacrylamide (7.5-11 %), SDS (0.1 %), APS (0.075 %), TEMED (0.05 %)
4x Stacking gel buffer	Tris/HCl pH 6.8 (125 mM), Acrylamide/Bisacrylamide (5 %), SDS (0.1 %), APS (0.1 %), TEMED (0.1 %)
Stripping buffer	Glycine (0.2 M), SDS (0.1 %), Tween-20 (1 % (v/v)), pH 2.2
Malt1 cleavage buffer	MES (50 mM), NaCl (150 mM), Saccharose (10% w/v), CHAPS (0.1%), Tri-Na-Citrate (1 M), DTT (1 mM, added fresh), pH 7.0
Saponin buffer	0.5% saponin (w/v), 1% BSA (w/v), PBS
Protein purification	
Protein Lysis buffer	HEPES pH 7.5 (50 mM), Glycerin (10% v/v), Triton X100 (0.1% v/v), NaCl (150 mM), $MgCl_2$ x $6H_2O$ (2 mM), DTT (1 mM, added fresh), protease inhibitor mix
Protein Wash buffer	Tris (50 mM), NaCl (150 mM), pH 8.0
Protein Elution buffer	Glutathione (15 mM) in Wash buffer
Protein Freezing buffer	Tris-HCl (20 mM), NaCl (500 mM), ß-Mercaptoethanol (20 mM), EDTA (2.5 mM), Saccharose (10% w/v), CHAPS (0.1%), pH 8.0

Cell culture	
Jurkat T cell medium	RPMI 1640 medium, fetal calf serum (10% v/v), penicillin (100 U/mL), streptomycin (100 µg/mL)
Murine T cell medium	RPMI 1640 medium, heat inactivated fetal calf serum (10% v/v), penicillin (100 U/mL), streptomycin (100 µg/mL), HEPES pH 7.5 (10 mM), L-Glutamine (2 mM), Na-Pyruvate (1 mM), MEM-NEAA (1% v/v), ß-Mercaptoethanol (50 mM)
Murine embryonic stem cell medium	DMEM medium, fetal calf serum (18% v/v), β-Mercaptoethanol (50 mM), MEM-NEAA (1% v/v), penicillin (100 U/mL), streptomycin (100 µg/mL), LIF/ESGRO (90 µL)
Murine embryonic feeder cell medium	DMEM medium, ES cell-tested FBS (10% v/v), β-Mercaptoethanol (50 mM), MEM-NEAA (1% v/v), penicillin (100 U/mL), streptomycin (100 µg/mL)

7.3 Methods

7.3.1 *Malt1* TBM mice

7.3.1.1 Design of sgRNA and HDR templates for generation of *Malt1*$^{TBM/TBM}$ mice

Two small guide RNAs (sgRNA) were designed to target T6BM1 and T6BM2 of Malt1. Targeting sequences were chosen using the GPP sgRNA Designer tool from the BROAD Institute (https://portals.broadinstitute.org/gpp/public/analysis-tools/gRNA-design). Guides were inserted into the pX458 vector via BbsI cleavage sites upstream of the sgRNA scaffold. Short single stranded oligodeoxyribonucleotide (ssODNs) homology directed repair (HDR) templates were synthesized spanning each T6BM site (195 nucleotides each). E-to-A point mutations for loss of MALT1-TRAF6 interaction, PAM sequence mutation to prevent multiple Cas9 cleavage events, and artificial cleavage sites for screening were integrated into the homology templates. Additionally, silent mutations around the E-to-A mutations were inserted for utilization of a PCR-based mES cell clone screening method. Guides and homology templates are listed in section 7.1.7.2. Guides were annealed and inserted into the pX458 vector via BbsI cleavage sites upstream of the sgRNA scaffold.

7.3.1.2 ES cell screening

mES cells were electroporated (220 V, 1000 µF) with 7.5 µg of each pX458 vector containing sgRNAs targeting T6BM1 and T6BM2 and each homology template (7.1.7.2). Two days post-transfection, cells were sorted on a MoFlo flow cytometry sorter and enriched on the pX458 EGFP reporter. 2000 GFP-positive cells were plated per 10 cm dish on MEF cells, and after 1 weeks, monoclonal colonies were picked and screened for genetic alteration using mutation-specific primers for the two T6BM loci in RT-PCR (see primers in 7.1.7.3). Potential clones were sequenced, and 2 clones were identified containing all mutations homozygously inserted (2/768 = 0.26% efficiency).

PCR protocol for LightCycler mES cell screening.

Component	Volume (µL)
Template	8
2xKappa mix	10
forward primer (10 mM)	0.4
reverse primer (10 mM)	0.4
water	1.2
total	20

LightCycler settings for mES cell screening.

	Step	Temperature (°C)	Time (sec)	
Denaturation	Initial Melting	95	180	
Amplification	Melting	95	30	40 cycles
	Annealing	58	30	
	Extension	72	30	
Melting curve		95	10	
		50	15	
		95	-	
Cooling	Final Extension	40	∞	

7.3.1.3 Generation of *Malt1* TBM mice

Malt1 TBM mice were created using mES cell clone 3-3E10. Wildtype embryos from C57Bl6/Ncrl wildtype mice (generated from natural matings) were injected at the 8-cell growth phase using laser-assisted injection technology (Poueymirou et al., 2007). After 3 hour incubation, 10-12 embryos were transferred into the oviduct of pseudogravide Crl:CD1(IDR) females. Chimeric mice were born with brown fur color indicating >90% chimerism. Chimeric mice were crossed with C57BL/6 wildtype mice, and germline transmission to offspring (*Malt1*$^{TBM/+}$) was seen in brown fur color in the F1 generation. Heterozygous mice were crossed, and genotypes were verified by differential PCR using mutation and wildtype specific primers for each T6BM site (see section 7.3.6.1). Genomic DNA from homozygous mice was sequenced to verify faithful MALT1 mutations (primers in section 7.1.7.3). Additionally, the entire Malt1 coding sequence was verified to contain no additional mutations.

7.3.2 Generation of *Traf6*-ΔT mice

Frozen embryos of from *Traf6*$^{tm2a(EUCOMM)Wtsi}$ mice (EMMA ID EM:08446; Infrafrontiers Biocenter Oulu) were transferred into foster mothers. Foster mice were crossed with ROSA26-FLPe-deleter mice to delete the IRES-lacZ/Neo cassette. Finally, resulting *Traf6*$^{fl/fl}$ mice were crossed to transgenic CD4-Cre+ recombinase mice for T cell specific knockout of TRAF6 by deletion of exon 4 and 5 in the *Traf6* locus. Genotyping primers are listed in section 7.1.7.2. Breeding plan is in section 7.3.2.

7.3.3 Generation of *Malt1* TBMPM mice

Malt1$^{TBM/+}$ sperm was used for *in vitro* fertilization in C57BL/6N females. Females were superovulated using 5 units of PMSG (Pregnant Mare's Serum Gonadotropin) and 5 units HCG (Human Chorionic Gonadotropin). Guide RNA (200 ng/ µl), HDR template (ssODN, 300 ng/ µl),and Cas9 protein (200 ng µl) were diluted in Opti-MEM buffer, incubated for 10 min at RT and 10 min at 37°C to form an active ribonucleoprotein complex, and electroporated into fertilized one-cell embryos. Zygotes were transferred into pseudopregnant CD1 female mice, and modification in F1 generation mice was detected via cleavage at the artificial restriction site BssHII and via sequencing of genomic DNA. The silent single nucleotide polymorphism (SNP) c.1323A/c.1323G in exon 11, originating from the mES cells used for TBM mouse generation, served as a marker for coexpression of C472A and the T6BM1/2 mutations. Heterozygous mice were backcrossed and intercrossed to yield homozygous Malt1$^{TBMPM/TBMPM}$ mice. Guide and homology template sequence can be found in section 7.1.7.2.

7.3.4 Generation of *Malt1* TBM CD4-Cre and FoxP3-Cre mice

For conditional expression of the *Malt1* TBM allele in T-cells, *Malt1*$^{TBM/+}$ were crossed to CD4-Cre (CD4-Cre (Tg(CD4-cre)1Cwi) (Lee et al., 2001) to yield *Malt1*$^{TBM/+}$; *CD4-Cre*$^{Cre+}$, which were paired to *Malt1*$^{fl/fl}$ mice to yield *Malt1*$^{TBM/fl}$; *CD4-Cre*$^{Cre+}$. For conditional expression of the *Malt1* TBM allele in Treg cells, *Malt1*$^{TBM/+}$ mice were crossed to *FoxP3-Cre* transgenic mice (Tg(Foxp3-EGFP/icre)(Zhou et al., 2008) to yield *Malt1*$^{TBM/+}$*;FoxP3-Cre*$^{Cre+}$, which were paired to *Malt1*$^{fl/fl}$, yielding *Malt1*$^{TBM/fl}$; *FoxP3-Cre*$^{Cre+}$ (*Malt1* TBM-Treg). Cre breeding plans are in section 7.3.6.2.

7.3.5 Generation of *Traf6* PM mice

For conditional CD4 T cell expression of *Malt1* PM in *Traf6*-T mice, *Malt1*$^{fl/fl}$ and *Traf6*$^{fl/fl}$ mice were crossed to yield double floxed *Malt1*$^{fl/fl}$; *Traf6*$^{fl/fl}$ mice. *Malt1* PM heterozygous mice were crossed with *Traf6*$^{wt/fl}$; *CD4-Cre*$^{Cre+}$ mice, giving *Malt1*$^{PM/+}$; *Traf6*$^{wt/fl}$; *CD4-Cre*$^{Cre+}$, which were subsequently crossed with double flox mice to yield Malt1$^{PM/fl}$; Traf6$^{fl/fl}$; *CD4-Cre*$^{Cre+}$ (*Traf6* PM). For controls, Malt1$^{PM/fl}$; Traf6$^{wt/fl}$; *CD4-Cre*$^{Cre+}$ (*Malt1* PM), Malt1$^{+/fl}$; Traf6$^{fl/fl}$; *CD4-Cre*$^{Cre+}$ (*Traf6*-ΔT), and Malt1$^{+/fl}$; Traf6$^{wt/fl}$; *CD4-Cre*$^{Cre+}$ (wildtype control) were used. *Traf6* PM breeding plans are in section 7.3.6.5.

7.3.6 Breeding plans

7.3.6.1 *Malt1* TBM

***Malt1* TBM**

Malt1$^{TBM/+}$	x	*Malt1*$^{TBM/+}$	→	*Malt1*$^{TBM/TBM}$	25%
				Malt1$^{TBM/+}$	50%
				Malt1$^{+/+}$	25%

7.3.6.2 *Malt1* TBM Cre mice

***Malt1* TBM-T**

Step 1					
Malt1$^{TBM/+}$	x	*CD4-Cre*$^{Cre+}$	→	*Malt1*$^{TBM/+}$; *CD4-Cre*$^{Cre+}$	25%
Step 2					
Malt1$^{TBM/+}$; *CD4-Cre*$^{Cre+}$	x	*Malt1*$^{fl/fl}$	→	*Malt1*$^{TBM/fl}$; *CD4-Cre*$^{Cre+}$	25%
				Malt1$^{TBM/+}$; *CD4-Cre*$^{Cre-}$	25%
				Malt1$^{fl/+}$; *CD4-Cre*$^{Cre+}$	25%
				Malt1$^{fl/+}$; *CD4-Cre*$^{Cre-}$	25%

***Malt1* TBM-Treg**

Step 1					
Malt1$^{TBM/+}$	x	*FoxP3-Cre*$^{Cre+}$	→	*Malt1*$^{TBM/+}$; *FoxP3-Cre*$^{Cre+}$	25%
Step 2					
Malt1$^{TBM/+}$; *FoxP3-Cre*$^{Cre+}$	x	*Malt1*$^{fl/fl}$	→	*Malt1*$^{TBM/fl}$; *FoxP3-Cre*$^{Cre+}$	25%
				Malt1$^{TBM/+}$; *FoxP3-Cre*$^{Cre-}$	25%
				Malt1$^{fl/+}$; *FoxP3-Cre*$^{Cre+}$	25%
				Malt1$^{fl/+}$; *FoxP3-Cre*$^{Cre-}$	25%

7.3.6.3 *Traf6*-ΔT mice

***Traf6*-ΔT**

Traf6$^{fl/fl}$	x	*Traf6*$^{wt/fl}$; *CD4-Cre*$^{Cre+}$	→	*Traf6*$^{fl/fl}$; *CD4-Cre*$^{Cre+}$	25%
				Traf6$^{fl/fl}$; *CD4-Cre*$^{Cre-}$	25%
				Traf6$^{wt/fl}$; *CD4-Cre*$^{Cre+}$	25%
				Traf6$^{wt/fl}$; *CD4-Cre*$^{Cre-}$	25%

7.3.6.4 *Malt1* TBMPM mice

***Malt1* TBMPM**

Malt1$^{TBMPM/+}$	x	*Malt1*$^{TBMPM/+}$	→	*Malt1*$^{TBMPM/TBMPM}$	25%
				Malt1$^{TBMPM/+}$	50%
				Malt1$^{+/+}$	25%

7.3.6.5 *Traf6*-PM mice

***Traf6*-PM**

Step 1a

Malt1$^{fl/fl}$	x	*Traf6*$^{fl/fl}$	→	*Malt1*$^{fl/+}$; *Traf6*$^{fl/+}$	100%

Step 1b

Malt1$^{PM/+}$	x	*Traf6*$^{wt/fl}$; *CD4-Cre*$^{Cre+}$	→	*Malt1*$^{PM/+}$; *Traf6*$^{wt/fl}$; *CD4-Cre*$^{Cre+}$	12.5%

Step 2

Malt1$^{fl/+}$; *Traf6*$^{fl/+}$	x	*Malt1*$^{fl/+}$; *Traf6*$^{fl/+}$	→	*Malt1*$^{fl/fl}$; *Traf6*$^{fl/fl}$	6.25%

Step 3

Malt1$^{PM/+}$; *Traf6*$^{wt/fl}$;	x	*Malt1*$^{fl/fl}$; *Traf6*$^{fl/fl}$	→	*Malt1*$^{PM/fl}$; *Traf6*$^{fl/fl}$; *CD4-Cre*$^{Cre+}$	12.5%
CD4-Cre^{Cre+}				*Malt1*$^{PM/fl}$; *Traf6*$^{wt/fl}$; *CD4-Cre*$^{Cre+}$	12.5%
				Malt1$^{fl/+}$; *Traf6*$^{fl/fl}$; *CD4-Cre*$^{Cre+}$	12.5%
				Malt1$^{fl/+}$; *Traf6*$^{wt/fl}$; *CD4-Cre*$^{Cre+}$	12.5%

7.3.7 Mouse genotyping PCR

Genotyping of mice was performed using the Phire Tissue Direct PCR Kit. DNA was extracted using 20 µL of sample diluent and 0.5 µL of DNA release reagent. PCR was run with 10 µL total volume in a 96-well non-skirted PCR plate covered with an adhesive seal. Amplified PCR product was run on a 1% agarose gel in 1x TAE buffer and Ethidium Bromide to visualize DNA bands.

PCR protocol for mouse genotyping.

Component	Volume (µL)
2x Phire direct PCR Master Mix	5
water	4
forward primer (10 mM)	0.25
reverse primer (10 mM)	0.25
DNA	0.5
total	10

PCR cycler setting for mouse genotyping.

Step	Temperature (°C)	Time (sec)	
Initial Melting	95	180	
Melting	95	20	32 cycles
Annealing	primer Tm	20	
Extension	72	20	
Final Extension	72	120	

7.3.8 Sequencing PCR

Primers were designed flanking the target region in murine genomic DNA and PCR was run using LongAmp Polymerase. Genomic DNA was used as prepared for genotyping. Amplified PCR product was run on a 1% agarose gel in 1x TAE buffer and Ethidium Bromide to visualize DNA bands.

PCR protocol for sequencing.

Component	Volume (µL)
LongAmp buffer (5x)	5
dNTP mix	0.75
forward primer (10 mM)	1
reverse primer (10 mM)	1
water	14.85
LongAmp Polymerase	0.4
DNA	2
total	25

PCR cycler settings for sequencing.

Step	Temperature (°C)	Time (sec)	
Initial Melting	95	180	
Melting	95	30	32 cycles
Annealing	primer Tm – 5	30	
Extension	65	30	
Final Extension	72	120	

7.3.9 Cell culture, cultivation and inhibitor treatment of cells

Jurkat T cells were grown in a humidified atmosphere (37°C, 5% CO_2) in Jurkat T cell medium and maintained at a density between 0.5 and 1.5x10^6 cells per mL. Jurkat T-cells were verified by the Authentication Service of the Leibniz Institute (DSMZ). Primary murine T cells were isolated from spleen and treated with red blood lysis solution, and CD4 T cells were purified via a CD4 T cell isolation kit. Purified CD4 T cells were cultured in murine T cell medium. Jurkat T cells were stimulated with Phorbol 12-Myristate 13-Acetate (PMA) (200 ng/ml)/Ionomycin (300 ng/ml) or anti-CD3 (0.3 µg)/CD28 (1 µg) in presence of rat anti-mouse IgG1 and IgG2a (0.5 µg each). Murine CD4 T cells were stimulated with PMA (200 ng/ml)/Ionomycin (300 ng/ml). For *in vitro* treatment of Jurkat T cells with the Malt1 inhibitors MLT-943 (Martin et al., 2020) and MLT-985 (Quancard et al., 2020), cells were plated in 6-well plates and incubated with inhibitors for 24 hours in a humidified atmosphere (37°C, 5% CO_2).

7.3.10 Analysis of cytokines and autoantibodies

Cytokines and autoantibodies were measured from blood serum using kits and relevant manufacturer protocols. Blood was collected via cheek punch from the submandibular vein of mice and allowed to clot at room temperature. Blood was centrifuged at 14000 x g for 10 min and 4°C, and clear blood serum was removed and frozen at -80°C until measurement.

7.3.11 Tissue section preparation and histopathological evaluation

Mouse tissue was fixed in 4% paraformaldehyde, embedded in paraffin, and cut to 4 µm on a microtome. Tissue slices were mounted on glass slides and stained with Hematoxylin and Eosin using an automatic stainer. Slides were scanned at 400x using QuPath v.0.2.3. Histological samples were fixed and embedded at the Helmholtz Zentrum, München, staining and imaging was performed in the lab of Dr. Mark Kriegsmann at the University Hospital Heidelberg.

7.3.12 Generation of knockout Jurkat T cells

Jurkat knockout cells for Malt1, BCL10, and CARMA1 were developed and described prior to this work (Oeckinghaus et al., 2007; Schlauderer et al., 2018; Lijun Sun et al., 2004). Traf6 KO Jurkat cells were generated by Thomas Seeholzer in the lab of Daniel Krappmann (Bardet et al., 2018). TCRα

knockout Jurkat cells were made utilizing CRISPR-Cas9 technology and targeting exon 1 of the TCR alpha constant (TRAC) region (Galetto et al., 2014). Briefly, one sgRNA was designed targeting exon 1 of the T cell receptor alpha common (TRAC) region of the TCRα gene. TRAC sgRNA insert was annealed and inserted into the pX458 vector via BbsI cleavage sites upstream of the sgRNA scaffold. 5 µg of vector was electroporated into Traf6 KO Jurkat T cells using a Gene Pulser X (220 V, 1000 µF), and 2 days later cells were sorted via the pX458 EGFP reporter using a MoFlo cell sorter. Cells were diluted and plated, and monoclonal colonies were expanded and confirmed via anti-TCRα/ß and anti-CD3 staining and flow cytometry.

7.3.13 Preparation of cell lysates

CD4 T cells were isolated from mice using a CD4 T cell isolation kit and negative magnetic activated cell sorting according to manufacturer protocols. Jurkat T cells and murine CD4 T cells were centrifuged (350xg, 4°C, 5 min) and washed once with PBS. Cells were lysed in Co-IP buffer (Western Blot) or Bauerle buffer (EMSA) (4°C, 20 min) and centrifuged (20,000xg, 4°C, 30 min). Supernatant was mixed with 4x SDS loading buffer and boiled at 95°C for 5 min.

7.3.14 Western Blot

Cell lysates were separated on a 9% SDS gel using an electrophoretic semi-dry blotting system and transferred onto PVDF membranes. After transfer, membranes were blocked with 5% BSA or 5% milk in PBS-Tween (0.01% Tween) for 1 hour at RT. Primary antibodies were diluted in 2.5% BSA or Milk in PBS-T and incubated with membranes overnight at 4°C. Membranes were washed 3x 15 min in PBS-T and incubated with HRP-coupled secondary antibodies (1:7000 in 1.25% BSA or milk) for 1 hour. Membranes were washed again 3x 15 min in PBS-T and HRP was detected using an enhanced chemiluminescence detection reagent. Antibodies and dilutions are in sections 7.1.8.3 and 7.1.8.4.

7.3.15 Electrophoretic Mobility Shift Assay

EMSA was performed using double stranded NF-κB and OCT1 control oligonucleotides radioactively labeled with [α-^{32}P] dATP using Klenow Fragments. Whole cell lysates were incubated with shift buffer and radioactively labeled oligonucleotides for 30 min and run on a 5% polyacrylamide gel in TBE buffer. Gels were vacuum-dried and visualized on autoradiography films. DNA binding sequences are shown in 7.1.7.5.

7.3.16 Therapeutic treatment of *Traf6*-ΔT mice with Malt1 inhibitor

8 week old *Traf6*-ΔT mice were treated i.p. BID for 10 days with 16 mg/kg MLT-985. 40 mg/mL stock solution was made in DMSO and diluted 1:20 in sterile PBS prior to each injection to yield a crystalline suspension (5% final DMSO concentration). Suspension was warmed to 37°C before

injection in a volume of 200 µL per 25 g body weight. On the 11th day after injection, lymphocyte populations and protein expression were analysed via flow cytometry and Western Blot.

7.3.17 Immune cell phenotyping by flow cytometry

Flow cytometry analysis was performed using single-cell suspensions prepared from murine organ tissue: spleen, lymph nodes, thymus, bone marrow, and peritoneal cells. Tissue and cells were collected from mice, meshed in RPMI buffer, and treated with red blood cell lysis solution. 1x106 cells were plated to each well of a 96 well, v-bottom plate (one well per staining), washed twice with PBS (350 x g, 5 min, 4°C), and stained with eFluor780 live/dead cell permeable dye (1:1000 in PBS, 30 min, 4°C). Cells were washed in FCM buffer and stained with Fc-block (anti-CD16/CD32). Cells were washed with FCM buffer and stained with fluorescent antibodies (20 min, RT). For intracellular staining of FoxP3, cells were permeabilized and fixed, washed once with permeabilization buffer, and stained with anti-FoxP3 in permeabilization buffer (20 min, RT). Cells were washed the FCM buffer, resuspended in FCM buffer, and measured via flow cytometry. Flow cytometry plots and histogram overlays were generated using FlowJO analysis software.

7.3.18 Analyses of IκBNS and ICOS expression by flow cytometry

For intracellular IκBNS and extracellular ICOS staining, primary murine splenocytes (1x10^6) were collected, centrifuged (300 x g, 5 min, 4 °C) and washed twice with PBS. Cells were stained with eFluor780 live/dead cell permeable dye (1:1000 in PBS, 30 min, 4°C). Cells were washed with PBS and fixed in 2% PFA for 20 mins at RT and permeabilized with 0.5% Saponin buffer. Cells were treated with Fc-block in Saponin buffer for 10 min at 4°C. Samples were incubated with anti-IκBNS antibody in Saponin buffer for 30 min at 4°C, washed once with saponin buffer, and stained with secondary antibody in saponin buffer for 30 min at 4°C. Cells were washed with FCM buffer, stained with surface stains in FCM buffer for 30 min at RT, washed again, and resuspended in FCM buffer for measurement via flow cytometry. Flow cytometry plots and histogram overlays were generated using FlowJO analysis software.

7.3.19 Image stream analysis

Murine splenocytes were stimulated with PMA (200 ng/mL) and Ionomycin (300 ng/mL) for 30 min, 37°C. Control samples were unstimulated. Cells were treated with Fc block for 30 min and stained with surface antibodies for 15 min. Cells were fixed and permeabilized and stained with intracellular antibodies for 1 h at 4°C. Cells were stained with a fluorescein isothiocyanate-coupled anti-rabbit IgG secondary antibody for 30 min at 4°C and nuclei were stained with 4’,6-diamidino-2-phenylindole (DAPI). Cells were measured by ImageStream® analysis and analyzed with IDEAS software. High similarity score (high correlation) represents strong nuclear translocation, low similarity scores

indicate cytoplasmic localization. Histogram overlays were generated using FlowJO analysis software. ImageStream® analysis was done in collaboration with Marc Rosenbaum from the group of Jürgen Ruland, TUM school of medicine, München.

7.3.20 Protein purification

GST MALT1 325-760, containing the paracaspase domain of MALT1, was inserted into the pGEX-6P-1 vector and expressed in BL21-RIPL cells. Bacteria were grown in 1L autoclaved LB medium supplimented with 100 µg/µL Ampicillin at 37°C to an OD600 of 0.6-0.8. Bacteria was grown for a further 30 min at 18°C and mixed with 50 µM IPTG to induce protein production. Cells were grown overnight at 18°C, 160 rpm, collected by centrifugation, and resuspended in 7 mL Lysis Buffer. Cells were lysed by sonication (10 x 30 sec, 30 sec between rounds). Cell lysis was centrifuged (16500 rpm, 30 min, 4°C), and the supernatant was transferred to a new tube a centrifuged again (16500 rpm, 60 min, 4°C). Supernatant was loaded into an ÄKTA fit with a 1 mL GST column, washed with Protein Wash Buffer, and eluted with Protein Elution Buffer. Protein eluate was concentrated to 600 µL using a cellulose membrane filter and concentration was measured via NanoDrop.

7.3.21 In vitro IC_{50} assay

Inhibitor strength was measured using purified GST-MALT1 325-760 and a fluorescent probe coupled to a tetrapeptide MALT1 cleavage susbstrate (Ac-LRSR-AMC). Protein was diluted to 25 ng/18.5 µL in MALT1 cleavage buffer and distributed to a 384-well black plate. 0.5 µL of inhibitor, diluted in DMSO,

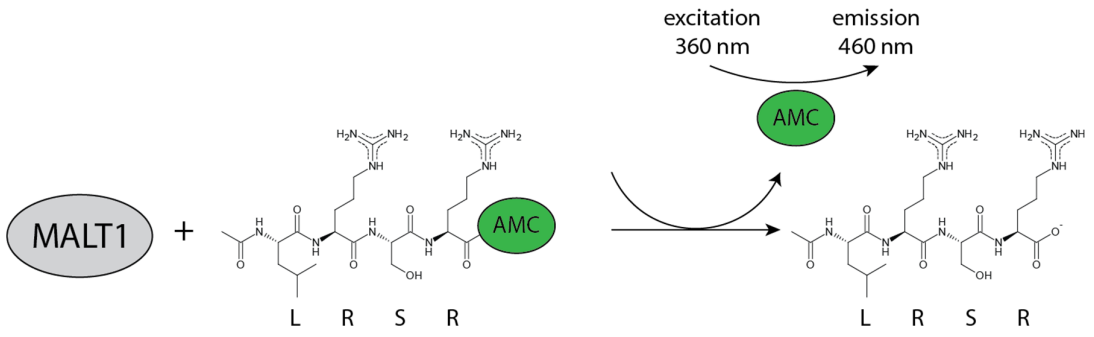

Figure 7-1. Assay for determination of Malt1 inhibitor strength *in vitro*.
MALT1 cleavage assay using purified GST-MALT1 325-760 protein containing the paracaspase domain of MALT1 and a fluorescent cleavage probe containing the MALT1 cleavage site LRSR from BCL10. Upon cleavage by MALT1, the fluorescent AMC probe is released and fluorescence is measured by excitation at 360 nm and emission at 460 nm.

was added to each well and incubated at RT for 30 min. 1 µL of 1 mM Ac-LRSR-AMC fluorescent probe was added to each well, and plate was measured immediately at 360 nm excition, 460 nm emission. Fluorescence was plotted against time, and slope was determined within a linear range

and compared with protein treated with DMSO (blank, 100% activity). Each sample was determined in duplicate.

7.3.22 Statistical analysis

For statistics all experiments in CD4 and Jurkat T cells contained at least three biological replicates and values represent the mean ± standard error of the mean (SEM). Experiments were analysed in by using unpaired Student's t-test with (Figures 4-1 to 4-25) or without (Figure 4-27) Welch's correction. Statistical significance is indicated by p-values. Inhibitor IC_{50} was calculated using a nonlinear regression curve fit. ImageStream results were analyzed using IDEAS software (Amnis Merck Millipore).

8 References

Akira, S., & Takeda, K. (2004). Toll-like receptor signalling. *Nature Reviews Immunology, 4*(7), 499-511. doi:10.1038/nri1391

Akira, S., Uematsu, S., & Takeuchi, O. (2006). Pathogen Recognition and Innate Immunity. *Cell, 124*(4), 783-801. doi:https://doi.org/10.1016/j.cell.2006.02.015

Akiyama, T., Maeda, S., Yamane, S., Ogino, K., Kasai, M., Kajiura, F., . . . Inoue, J. (2005). Dependence of self-tolerance on TRAF6-directed development of thymic stroma. *Science, 308*(5719), 248-251. doi:10.1126/science.1105677

Antony, P. A., Piccirillo, C. A., Akpinarli, A., Finkelstein, S. E., Speiss, P. J., Surman, D. R., . . . Restifo, N. P. (2005). CD8+ T cell immunity against a tumor/self-antigen is augmented by CD4+ T helper cells and hindered by naturally occurring T regulatory cells. *J Immunol, 174*(5), 2591-2601. doi:10.4049/jimmunol.174.5.2591

Antony, P. A., & Restifo, N. P. (2002). Do CD4+ CD25+ Immunoregulatory T Cells Hinder Tumor Immunotherapy? *J Immunother., 25*(3), 202-206.

Arstila, T. P., Casrouge, A., Baron, V., Even, J., Kanellopoulos, J., & Kourilsky, P. (1999). A direct estimate of the human alphabeta T cell receptor diversity. *Science, 286*(5441), 958-961. doi:10.1126/science.286.5441.958

Bacchetta, R., Barzaghi, F., & Roncarolo, M.-G. (2018). From IPEX syndrome to FOXP3mutation: a lesson on immune dysregulation. *Ann. N.Y. Acad. Sci., 1417*, 5–22.

Baens, M., Bonsignore, L., Somers, R., Vanderheydt, C., Weeks, S. D., Gunnarsson, J., . . . Marynen, P. (2014). MALT1 auto-proteolysis is essential for NF-κB-dependent gene transcription in activated lymphocytes. *PLoS One, 9*(8), e103774-e103774. doi:10.1371/journal.pone.0103774

Baens, M., Stirparo, R., Lampi, Y., Verbeke, D., Vandepoel, R., Cools, J., . . . Bornschein, S. (2018). Malt1 self-cleavage is critical for regulatory T cell homeostasis and anti-tumor immunity in mice. *Eur J Immunol, 48*(10), 1728-1738. doi:10.1002/eji.201847597

Bardet, M., Seeholzer, T., Unterreiner, A., Woods, S., Krappmann, D., & Bornancin, F. (2018). MALT1 activation by TRAF6 needs neither BCL10 nor CARD11. *Biochem Biophys Res Commun, 506*(1), 48-52. doi:10.1016/j.bbrc.2018.10.029

Barton, G. M., Kagan, J. C., & Medzhitov, R. (2006). Intracellular localization of Toll-like receptor 9 prevents recognition of self DNA but facilitates access to viral DNA. *Nat Immunol, 7*(1), 49-56. doi:10.1038/ni1280

Bedsaul, J. R., Carter, N. M., Deibel, K. E., Hutcherson, S. M., Jones, T. A., Wang, Z., . . . Pomerantz, J. L. (2018). Mechanisms of Regulated and Dysregulated CARD11 Signaling in Adaptive Immunity and Disease. *Front Immunol, 9*, 2105. doi:10.3389/fimmu.2018.02105

Bennett, C. L., Christie, J., Ramsdell, F., Brunkow, M. E., Ferguson, P. J., Whitesell, L., . . . Ochs, H. D. (2001). The immune dysregulation, polyendocrinopathy, enteropathy, X-linked syndrome (IPEX) is caused by mutations of FOXP3. *Nature Genetics, 27*(1), 20-21. doi:10.1038/83713

Bertin, J., Guo, Y., Wang, L., Srinivasula, S. M., Jacobson, M. D., Poyet, J. L., . . . Alnemri, E. S. (2000). CARD9 is a novel caspase recruitment domain-containing protein that interacts with BCL10/CLAP and activates NF-kappa B. *J Biol Chem, 275*(52), 41082-41086. doi:10.1074/jbc.C000726200

Bertin, J., Wang, L., Guo, Y., Jacobson, M. D., Poyet, J. L., Srinivasula, S. M., . . . Alnemri, E. S. (2001). CARD11 and CARD14 are novel caspase recruitment domain (CARD)/membrane-associated guanylate kinase (MAGUK) family members that interact with BCL10 and activate NF-kappa B. *J Biol Chem, 276*(15), 11877-11882. doi:10.1074/jbc.M010512200

Bidere, N., Snow, A. L., Sakai, K., Zheng, L., & Lenardo, M. J. (2006). Caspase-8 regulation by direct interaction with TRAF6 in T cell receptor-induced NF-kappaB activation. *Curr Biol, 16*(16), 1666-1671. doi:10.1016/j.cub.2006.06.062

Bornancin, F., Renner, F., Touil, R., Sic, H., Kolb, Y., Touil-Allaoui, I., . . . Calzascia, T. (2015). Deficiency of MALT1 paracaspase activity results in unbalanced regulatory and effector T and B cell

responses leading to multiorgan inflammation. *J Immunol, 194*(8), 3723-3734. doi:10.4049/jimmunol.1402254

Brenke, J. K., Popowicz, G. M., Schorpp, K., Rothenaigner, I., Roesner, M., Meininger, I., . . . Hadian, K. (2018). Targeting TRAF6 E3 ligase activity with a small-molecule inhibitor combats autoimmunity. *J Biol Chem, 293*(34), 13191-13203. doi:10.1074/jbc.RA118.002649

Cabalzar, K., Pelzer, C., Wolf, A., Lenz, G., Iwaszkiewicz, J., Zoete, V., . . . Thome, M. (2013). Monoubiquitination and activity of the paracaspase MALT1 requires glutamate 549 in the dimerization interface. *PLoS One, 8*(8), e72051. doi:10.1371/journal.pone.0072051

Charbit-Henrion, F., Jeverica, A. K., Begue, B., Markelj, G., Parlato, M., Avcin, S. L., . . . Group, G. (2017). Deficiency in Mucosa-associated Lymphoid Tissue Lymphoma Translocation 1: A Novel Cause of IPEX-Like Syndrome. *J Pediatr Gastroenterol Nutr, 64*(3), 378-384. doi:10.1097/MPG.0000000000001262

Chiffoleau, E., Kobayashi, T., Walsh, M. C., King, C. G., Walsh, P. T., Hancock, W. W., . . . Turka, L. A. (2003). TNF receptor-associated factor 6 deficiency during hemopoiesis induces Th2-polarized inflammatory disease. *J Immunol, 171*(11), 5751-5759. doi:10.4049/jimmunol.171.11.5751

Coornaert, B., Baens, M., Heyninck, K., Bekaert, T., Haegman, M., Staal, J., . . . Beyaert, R. (2008). T cell antigen receptor stimulation induces MALT1 paracaspase-mediated cleavage of the NF-kappaB inhibitor A20. *Nat Immunol, 9*(3), 263-271. doi:10.1038/ni1561

Dainichi, T., Matsumoto, R., Mostafa, A., & Kabashima, K. (2019). Immune Control by TRAF6-Mediated Pathways of Epithelial Cells in the EIME (Epithelial Immune Microenvironment). *Front Immunol, 10*, 1107. doi:10.3389/fimmu.2019.01107

David, L., Li, Y., Ma, J., Garner, E., Zhang, X., & Wu, H. (2018). Assembly mechanism of the CARMA1-BCL10-MALT1-TRAF6 signalosome. *Proc Natl Acad Sci U S A, 115*(7), 1499-1504. doi:10.1073/pnas.1721967115

Demeyer, A., Skordos, I., Driege, Y., Kreike, M., Hochepied, T., Baens, M., . . . Beyaert, R. (2019). MALT1 Proteolytic Activity Suppresses Autoimmunity in a T Cell Intrinsic Manner. *Front Immunol, 10*, 1898. doi:10.3389/fimmu.2019.01898

Di Pilato, M., Kim, E. Y., Cadilha, B. L., Prussmann, J. N., Nasrallah, M. N., Seruggia, D., . . . Mempel, T. R. (2019). Targeting the CBM complex causes Treg cells to prime tumours for immune checkpoint therapy. *Nature, 570*(7759), 112-116. doi:10.1038/s41586-019-1215-2

Dierlamm, J., Baens, M., Wlodarska, I., Stefanova-Ouzounova, M., Hernandez, J. M., Hossfeld, D. K., . . . Marynen, P. (1999). The Apoptosis Inhibitor Gene API2 and a Novel 18q Gene,MLT, Are Recurrently Rearranged in the t(11;18)(q21;q21) Associated With Mucosa-Associated Lymphoid Tissue Lymphomas. *Blood, 93*(11), 3601-3609. doi:10.1182/blood.V93.11.3601

Douanne, T., Gavard, J., & Bidere, N. (2016). The paracaspase MALT1 cleaves the LUBAC subunit HOIL1 during antigen receptor signaling. *J Cell Sci, 129*(9), 1775-1780. doi:10.1242/jcs.185025

Duwel, M., Welteke, V., Oeckinghaus, A., Baens, M., Kloo, B., Ferch, U., . . . Krappmann, D. (2009). A20 negatively regulates T cell receptor signaling to NF-kappaB by cleaving Malt1 ubiquitin chains. *J Immunol, 182*(12), 7718-7728. doi:10.4049/jimmunol.0803313

Egawa, T., Albrecht, B., Favier, B. t., Sunshine, M.-J., Mirchandani, K., O'Brien, W., . . . Littman, D. R. (2003). Requirement for CARMA1 in Antigen Receptor-Induced NF-κB Activation and Lymphocyte Proliferation. *Current Biology, 13*(14), 1252-1258. doi:10.1016/s0960-9822(03)00491-3

Eitelhuber, A. C., Vosyka, O., Nagel, D., Bognar, M., Lenze, D., Lammens, K., . . . Krappmann, D. (2015). Activity-based probes for detection of active MALT1 paracaspase in immune cells and lymphomas. *Chem Biol, 22*(1), 129-138. doi:10.1016/j.chembiol.2014.10.021

Elton, L., Carpentier, I., Staal, J., Driege, Y., Haegman, M., & Beyaert, R. (2016). MALT1 cleaves the E3 ubiquitin ligase HOIL-1 in activated T cells, generating a dominant negative inhibitor of LUBAC-induced NF-kappaB signaling. *FEBS J, 283*(3), 403-412. doi:10.1111/febs.13597

Essig, K., Hu, D., Guimaraes, J. C., Alterauge, D., Edelmann, S., Raj, T., . . . Heissmeyer, V. (2017). Roquin Suppresses the PI3K-mTOR Signaling Pathway to Inhibit T Helper Cell Differentiation and Conversion of Treg to Tfr Cells. *Immunity, 47*(6), 1067-1082.e1012. doi:10.1016/j.immuni.2017.11.008

Fathman, C. G., & Lineberry, N. B. (2007). Molecular mechanisms of CD4+ T-cell anergy. *Nature Reviews Immunology, 7*(8), 599-609. doi:10.1038/nri2131

Fontan, L., Yang, C., Kabaleeswaran, V., Volpon, L., Osborne, M. J., Beltran, E., . . . Melnick, A. (2012). MALT1 small molecule inhibitors specifically suppress ABC-DLBCL in vitro and in vivo. *Cancer Cell, 22*(6), 812-824. doi:10.1016/j.ccr.2012.11.003

Frizinsky, S., Rechavi, E., Barel, O., Najeeb, R. H., Greenberger, S., Lee, Y. N., . . . Stauber, T. (2019). Novel MALT1 Mutation Linked to Immunodeficiency, Immune Dysregulation, and an Abnormal T Cell Receptor Repertoire. *J Clin Immunol, 39*(4), 401-413. doi:10.1007/s10875-019-00629-0

Fuchs, S., Rensing-Ehl, A., Pannicke, U., Lorenz, M. R., Fisch, P., Jeelall, Y., . . . Ehl, S. (2015). Omenn syndrome associated with a functional reversion due to a somatic second-site mutation in CARD11 deficiency. *Blood, 126*(14), 1658-1669. doi:10.1182/blood-2015-03-631374

Gaide, O., Martinon, F., Micheau, O., Bonnet, D., Thome, M., & Tschopp, J. (2001). Carma1, a CARD-containing binding partner of Bcl10, induces Bcl10 phosphorylation and NF-κB activation1. *FEBS Letters, 496*(2-3), 121-127. doi:https://doi.org/10.1016/S0014-5793(01)02414-0

Galetto, R., Lebuhotel, C., Poirot, L., Gouble, A., Toribio, M. L., Smith, J., & Scharenberg, A. (2014). Pre-TCRα supports CD3-dependent reactivation and expansion of TCRα-deficient primary human T-cells. *Molecular Therapy*.

Gehring, T., Seeholzer, T., & Krappmann, D. (2018). BCL10 - Bridging CARDs to Immune Activation. *Front Immunol, 9*, 1539. doi:10.3389/fimmu.2018.01539

Germain, R. N. (2002). T-cell development and the CD4–CD8 lineage decision. *Nature Reviews Immunology, 2*(5), 309-322. doi:10.1038/nri798

Gewies, A., Gorka, O., Bergmann, H., Pechloff, K., Petermann, F., Jeltsch, K. M., . . . Ruland, J. (2014). Uncoupling Malt1 threshold function from paracaspase activity results in destructive autoimmune inflammation. *Cell Rep, 9*(4), 1292-1305. doi:10.1016/j.celrep.2014.10.044

Giltiay, N. V., Chappell, C. P., & Clark, E. A. (2012). B-cell selection and the development of autoantibodies. *Arthritis Research & Therapy, 14*(4), S1. doi:10.1186/ar3918

Ginster, S., Bardet, M., Unterreiner, A., Malinverni, C., Renner, F., Lam, S., . . . Bornancin, F. (2017). Two Antagonistic MALT1 Auto-Cleavage Mechanisms Reveal a Role for TRAF6 to Unleash MALT1 Activation. *PLoS One, 12*(1), e0169026. doi:10.1371/journal.pone.0169026

Goronzy, J. J., Lee, W. W., & Weyand, C. M. (2007). Aging and T-cell diversity. *Exp Gerontol, 42*(5), 400-406. doi:10.1016/j.exger.2006.11.016

Greil, J., Rausch, T., Giese, T., Bandapalli, O. R., Daniel, V., Bekeredjian-Ding, I., . . . Kulozik, A. E. (2013). Whole-exome sequencing links caspase recruitment domain 11 (CARD11) inactivation to severe combined immunodeficiency. *J Allergy Clin Immunol, 131*(5), 1376-1383 e1373. doi:10.1016/j.jaci.2013.02.012

Grinberg-Bleyer, Y., Oh, H., Desrichard, A., Bhatt, D. M., Caron, R., Chan, T. A., . . . Ghosh, S. (2017). NF-κB c-Rel Is Crucial for the Regulatory T Cell Immune Checkpoint in Cancer. *Cell, 170*(6), 1096-1108.e1013. doi:10.1016/j.cell.2017.08.004

Hachmann, J., Snipas, S. J., van Raam, B. J., Cancino, E. M., Houlihan, E. J., Poreba, M., . . . Salvesen, G. S. (2012). Mechanism and specificity of the human paracaspase MALT1. *Biochem J, 443*(1), 287-295. doi:10.1042/BJ20120035

Hailfinger, S., Lenz, G., Ngo, V., Posvitz-Fejfar, A., Rebeaud, F., Guzzardi, M., . . . Thome, M. (2009). Essential role of MALT1 protease activity in activated B cell-like diffuse large B-cell lymphoma. *Proc Natl Acad Sci U S A, 106*(47), 19946-19951. doi:10.1073/pnas.0907511106

Hailfinger, S., Nogai, H., Pelzer, C., Jaworski, M., Cabalzar, K., Charton, J. E., . . . Thome, M. (2011). Malt1-dependent RelB cleavage promotes canonical NF-kappaB activation in lymphocytes

and lymphoma cell lines. *Proc Natl Acad Sci U S A, 108*(35), 14596-14601. doi:10.1073/pnas.1105020108

Hara, H., Wada, T., Bakal, C., Kozieradzki, I., Suzuki, S., Suzuki, N., . . . Penninger, J. M. (2003). The MAGUK Family Protein CARD11 Is Essential for Lymphocyte Activation. *Immunity, 18*(6), 763-775. doi:10.1016/s1074-7613(03)00148-1

Hayden, M. S., & Ghosh, S. (2008). Shared principles in NF-kappaB signaling. *Cell, 132*(3), 344-362. doi:10.1016/j.cell.2008.01.020

Hayden, M. S., & Ghosh, S. (2012). NF-kappaB, the first quarter-century: remarkable progress and outstanding questions. *Genes Dev, 26*(3), 203-234. doi:10.1101/gad.183434.111

Inoue, J., Ishida, T., Tsukamoto, N., Kobayashi, N., Naito, A., Azuma, S., & Yamamoto, T. (2000). Tumor Necrosis Factor Receptor-Associated Factor (TRAF) Family: Adapter Proteins That Mediate Cytokine Signaling. *Experimental Cell Research, 254*(1), 14-24. doi:10.1006/excr.1999.4733

Isomura, I., Palmer, S., Grumont, R. J., Bunting, K., Hoyne, G., Wilkinson, N., . . . Gerondakis, S. (2009). c-Rel is required for the development of thymic Foxp3+ CD4 regulatory T cells. *J Exp Med, 206*(13), 3001-3014. doi:10.1084/jem.20091411

Jabara, H. H., Ohsumi, T., Chou, J., Massaad, M. J., Benson, H., Megarbane, A., . . . Geha, R. S. (2013). A homozygous mucosa-associated lymphoid tissue 1 (MALT1) mutation in a family with combined immunodeficiency. *J Allergy Clin Immunol, 132*(1), 151-158. doi:10.1016/j.jaci.2013.04.047

Jagger, A., Shimojima, Y., Goronzy, J. J., & Weyand, C. M. (2014). Regulatory T cells and the immune aging process: a mini-review. *Gerontology, 60*(2), 130-137. doi:10.1159/000355303

Jaworski, M., Marsland, B. J., Gehrig, J., Held, W., Favre, S., Luther, S. A., . . . Thome, M. (2014). Malt1 protease inactivation efficiently dampens immune responses but causes spontaneous autoimmunity. *EMBO J, 33*(23), 2765-2781. doi:10.15252/embj.201488987

Jeltsch, K. M., Hu, D., Brenner, S., Zoller, J., Heinz, G. A., Nagel, D., . . . Heissmeyer, V. (2014). Cleavage of roquin and regnase-1 by the paracaspase MALT1 releases their cooperatively repressed targets to promote T(H)17 differentiation. *Nat Immunol, 15*(11), 1079-1089. doi:10.1038/ni.3008

Jones, E., Dahm-Vicker, M., Simon, A. K., Green, A., Powrie, F., Cerundolo, V., & Gallimore, A. (2002). Depletion of CD25+ regulatory cells results in suppression of melanoma growth and induction of autoreactivity in mice. *Cancer Immun, 2*, 1.

Josefowicz, S. Z., & Rudensky, A. (2009). Control of Regulatory T Cell Lineage Commitment and Maintenance. *Immunity, 30*(5), 616-625. doi:https://doi.org/10.1016/j.immuni.2009.04.009

Juilland, M., & Thome, M. (2018). Holding All the CARDs: How MALT1 Controls CARMA/CARD-Dependent Signaling. *Front Immunol, 9*, 1927. doi:10.3389/fimmu.2018.01927

Jun, J. E., Wilson, L. E., Vinuesa, C. G., Lesage, S., Blery, M., Miosge, L. A., . . . Goodnow, C. C. (2003). Identifying the MAGUK Protein Carma-1 as a Central Regulator of Humoral Immune Responses and Atopy by Genome-Wide Mouse Mutagenesis. *Immunity, 18*(6), 751-762. doi:10.1016/s1074-7613(03)00141-9

Kane, L. P., Lin, J., & Weiss, A. (2002). It's all Rel-ative: NF-kappaB and CD28 costimulation of T-cell activation. *Trends Immunol, 23*(8), 413-420. doi:10.1016/s1471-4906(02)02264-0

King, C. G., Kobayashi, T., Cejas, P. J., Kim, T., Yoon, K., Kim, G. K., . . . Choi, Y. (2006). TRAF6 is a T cell-intrinsic negative regulator required for the maintenance of immune homeostasis. *Nat Med, 12*(9), 1088-1092. doi:10.1038/nm1449

Kingeter, L. M., Paul, S., Maynard, S. K., Cartwright, N. G., & Schaefer, B. C. (2010). Cutting edge: TCR ligation triggers digital activation of NF-kappaB. *J Immunol, 185*(8), 4520-4524. doi:10.4049/jimmunol.1001051

Kishimoto, T., Kang, S., & Tanaka, T. (2015). *IL-6: A New Era for the Treatment of Autoimmune Inflammatory Diseases*, Tokyo.

Klein, T., Fung, S. Y., Renner, F., Blank, M. A., Dufour, A., Kang, S., . . . Overall, C. M. (2015). The paracaspase MALT1 cleaves HOIL1 reducing linear ubiquitination by LUBAC to dampen lymphocyte NF-kappaB signalling. *Nat Commun, 6*, 8777. doi:10.1038/ncomms9777

Kobayashi, T., Walsh, P. T., Walsh, M. C., Speirs, K. M., Chiffoleau, E., King, C. G., . . . Choi, Y. (2003). TRAF6 is a critical factor for dendritic cell maturation and development. *Immunity, 19*(3), 353-363. doi:10.1016/s1074-7613(03)00230-9

Krug, A., Rothenfusser, S., Hornung, V., Jahrsdörfer, B., Blackwell, S., Ballas, Z. K., . . . Hartmann, G. (2001). Identification of CpG oligonucleotide sequences with high induction of IFN-alpha/beta in plasmacytoid dendritic cells. *Eur J Immunol, 31*(7), 2154-2163. doi:10.1002/1521-4141(200107)31:7<2154::aid-immu2154>3.0.co;2-u

Kumar, B. V., Connors, T. J., & Farber, D. L. (2018). Human T Cell Development, Localization, and Function throughout Life. *Immunity, 48*(2), 202-213. doi:10.1016/j.immuni.2018.01.007

Kutteh, W. H., Stovall, D. W., & Schust, D. J. (2014). Chapter 14 - Immunology and Reproduction. In J. F. Strauss & R. L. Barbieri (Eds.), *Yen & Jaffe's Reproductive Endocrinology (Seventh Edition)* (pp. 287-307.e283). Philadelphia: W.B. Saunders.

Kutukculer, N., Seeholzer, T., O'Neill, T. J., Graß, C., Aykut, A., Karaca, N. E., . . . Krappmann, D. (2020). Human immune disorder associated with homozygous hypomorphic mutation affecting MALT1B splice variant. *J Allergy Clin Immunol*.

Lam, K. P., Kuhn, R., & Rajewsky, K. (1997). In vivo ablation of surface immunoglobulin on mature B cells by inducible gene targeting results in rapid cell death. *Cell, 90*(6), 1073-1083. doi:10.1016/s0092-8674(00)80373-6

Lamason, R. L., McCully, R. R., Lew, S. M., & Pomerantz, J. L. (2010). Oncogenic CARD11 mutations induce hyperactive signaling by disrupting autoinhibition by the PKC-responsive inhibitory domain. *Biochemistry, 49*(38), 8240-8250. doi:10.1021/bi101052d

Laydon, D. J., Bangham, C. R. M., & Asquith, B. (2015). Estimating T-cell repertoire diversity: limitations of classical estimators and a new approach. *Philosophical transactions of the Royal Society of London. Series B, Biological sciences, 370*(1675), 20140291. doi:10.1098/rstb.2014.0291

Lee, P. P., Fitzpatrick, D. R., Beard, C., Jessup, H. K., Lehar, S., Makar, K. W., . . . Wilson, C. B. (2001). A critical role for Dnmt1 and DNA methylation in T cell development, function, and survival. *Immunity, 15*(5), 763-774. doi:10.1016/s1074-7613(01)00227-8

Lefrancois, L., & Marzo, A. L. (2006). The descent of memory T-cell subsets. *Nat Rev Immunol, 6*(8), 618-623. doi:10.1038/nri1866

Lenz, G., Wright, G., Dave, S. S., Xiao, W., Powell, J., Zhao, H., . . . Staudt, L. M. (2008). Stromal Gene Signatures in Large-B-Cell Lymphomas. *New England Journal of Medicine, 359*(22), 2313-2323. doi:10.1056/NEJMoa0802885

Lobry, C., Lopez, T., Israël, A., & Weil, R. (2007). Negative feedback loop in T cell activation through IκB kinase-induced phosphorylation and degradation of Bcl10. *Proceedings of the National Academy of Sciences, 104*(3), 908-913. doi:10.1073/pnas.0606982104

Lomaga, M. A., Yeh, W.-C., Sarosi, I., Duncan, G. S., Furlonger, C., Ho, A., . . . Mak, T. W. (1999). TRAF6 deficiency results in osteopetrosis and defective interleukin-1, CD40, and LPS signaling. *GENES & DEVELOPMENT, 13*, 1015-1024.

Long, M., Park, S. G., Strickland, I., Hayden, M. S., & Ghosh, S. (2009). Nuclear factor-kappaB modulates regulatory T cell development by directly regulating expression of Foxp3 transcription factor. *Immunity, 31*(6), 921-931. doi:10.1016/j.immuni.2009.09.022

Lu, H. Y., Bauman, B. M., Arjunaraja, S., Dorjbal, B., Milner, J. D., Snow, A. L., & Turvey, S. E. (2018). The CBM-opathies-A Rapidly Expanding Spectrum of Human Inborn Errors of Immunity Caused by Mutations in the CARD11-BCL10-MALT1 Complex. *Front Immunol, 9*, 2078. doi:10.3389/fimmu.2018.02078

Maizels, N. (2005). Immunoglobulin Gene Diversification. *Annual Review of Genetics, 39*(1), 23-46. doi:10.1146/annurev.genet.39.073003.110544

Mao, R., Yang, R., Chen, X., Harhaj, E. W., Wang, X., & Fan, Y. (2017). Regnase-1, a rapid response ribonuclease regulating inflammation and stress responses. *Cell Mol Immunol, 14*(5), 412-422. doi:10.1038/cmi.2016.70

Martin, K., Junker, U., Tritto, E., Sutter, E., Rubic-Schneider, T., Morgan, H., . . . Calzascia, T. (2020). Pharmacological Inhibition of MALT1 Protease Leads to a Progressive IPEX-Like Pathology. *Front Immunol, 11*, 745. doi:10.3389/fimmu.2020.00745

MaruYama, T. (2015). TGF-ß-induced IkB-ζ controls Foxp3 gene expression. *Biochemical and Biophysical Research Communications, 464*, 586-589.

Matsumoto, R., Wang, D., Blonska, M., Li, H., Kobayashi, M., Pappu, B., . . . Lin, X. (2005). Phosphorylation of CARMA1 plays a critical role in T Cell receptor-mediated NF-kappaB activation. *Immunity, 23*(6), 575-585. doi:10.1016/j.immuni.2005.10.007

Matsushita, K., Takeuchi, T., Standley, D. M., Kumagai, Y., Kawagoe, T., Miyake, T., . . . Akira, S. (2009). Zc3h12a is an RNase essential for controlling immune responses by regulating mRNA decay. *Nat, 458*.

McCully, R. R., & Pomerantz, J. L. (2008). The protein kinase C-responsive inhibitory domain of CARD11 functions in NF-kappaB activation to regulate the association of multiple signaling cofactors that differentially depend on Bcl10 and MALT1 for association. *Mol Cell Biol, 28*(18), 5668-5686. doi:10.1128/MCB.00418-08

McKinnon, M. L., Rozmus, J., Fung, S. Y., Hirschfeld, A. F., Del Bel, K. L., Thomas, L., . . . Turvey, S. E. (2014). Combined immunodeficiency associated with homozygous MALT1 mutations. *J Allergy Clin Immunol, 133*(5), 1458-1462, 1462 e1451-1457. doi:10.1016/j.jaci.2013.10.045

Meininger, I., Griesbach, R. A., Hu, D., Gehring, T., Seeholzer, T., Bertossi, A., . . . Krappmann, D. (2016). Alternative splicing of MALT1 controls signalling and activation of CD4(+) T cells. *Nat Commun, 7*, 11292. doi:10.1038/ncomms11292

Meininger, I., & Krappmann, D. (2016). Lymphocyte signaling and activation by the CARMA1-BCL10-MALT1 signalosome. *Biol Chem, 397*(12), 1315-1333. doi:10.1515/hsz-2016-0216

Mills, K. D., Ferguson, D. O., & Alt, F. W. (2003). The role of DNA breaks in genomic instability and tumorigenesis. *Immunological reviews, 194*, 77-95. doi:10.1034/j.1600-065x.2003.00060.x

Molinero, L. L., Yang, J., Gajewski, T., Abraham, C., Farrar, M. A., & Alegre, M. L. (2009). CARMA1 controls an early checkpoint in the thymic development of FoxP3+ regulatory T cells. *J Immunol, 182*(11), 6736-6743. doi:10.4049/jimmunol.0900498

Motegi, H., Shimo, Y., Akiyama, T., & Inoue, J. (2011). TRAF6 negatively regulates the Jak1-Erk pathway in interleukin-2 signaling. *Genes Cells, 16*(2), 179-189. doi:10.1111/j.1365-2443.2010.01474.x

Muto, G., Kotani, H., Kondo, T., Morita, R., Tsuruta, S., Kobayashi, T., . . . Yoshimura, A. (2013). TRAF6 is essential for maintenance of regulatory T cells that suppress Th2 type autoimmunity. *PLoS One, 8*(9), e74639. doi:10.1371/journal.pone.0074639

Myers, D. R., Zikherman, J., & Roose, J. P. (2017). Tonic Signals: Why Do Lymphocytes Bother? *Trends Immunol, 38*(11), 844-857. doi:10.1016/j.it.2017.06.010

Nagel, D., Spranger, S., Vincendeau, M., Grau, M., Raffegerst, S., Kloo, B., . . . Krappmann, D. (2012). Pharmacologic inhibition of MALT1 protease by phenothiazines as a therapeutic approach for the treatment of aggressive ABC-DLBCL. *Cancer Cell, 22*(6), 825-837. doi:10.1016/j.ccr.2012.11.002

Naito, A., Azuma, S., Tanaka, S., Miyazaki, T., Takaki, S., Takatsu, K., . . . Inoue, J. (1999). Severe osteopetrosis, defective interleukin-1 signalling and lymph node organogenesis in TRAF6-deficient mice. *Genes Cells, 4*(6), 353-362. doi:10.1046/j.1365-2443.1999.00265.x

Naito, A., Yoshida, H., Nishioka, E., Satoh, M., Azuma, S., Yamamoto, T., . . . Inoue, J. (2002). TRAF6-deficient mice display hypohidrotic ectodermal dysplasia. *Proc Natl Acad Sci U S A, 99*(13), 8766-8771. doi:10.1073/pnas.132636999

Namjou, B., Choi, C. B., Harley, I. T., Alarcon-Riquelme, M. E., Network, B., Kelly, J. A., . . . Bae, S. C. (2012). Evaluation of TRAF6 in a large multiancestral lupus cohort. *Arthritis Rheum, 64*(6), 1960-1969. doi:10.1002/art.34361

Ni, X., Kou, W., Gu, J., Wei, P., Wu, X., Peng, H., . . . Lu, L. (2019). TRAF6 directs FOXP3 localization and facilitates regulatory T-cell function through K63-linked ubiquitination. *EMBO J, 38*(9). doi:10.15252/embj.201899766

Noels, H., van Loo, G., Hagens, S., Broeckx, V., Beyaert, R., Marynen, P., & Baens, M. (2007). A Novel TRAF6 binding site in MALT1 defines distinct mechanisms of NF-kappaB activation by API2middle dotMALT1 fusions. *J Biol Chem, 282*(14), 10180-10189. doi:10.1074/jbc.M611038200

Oeckinghaus, A., Wegener, E., Welteke, V., Ferch, U., Arslan, S. C., Ruland, J., . . . Krappmann, D. (2007). Malt1 ubiquitination triggers NF-kappaB signaling upon T-cell activation. *EMBO J, 26*(22), 4634-4645. doi:10.1038/sj.emboj.7601897

Oh, H., Grinberg-Bleyer, Y., Liao, W., Maloney, D., Wang, P., Wu, Z., . . . Ghosh, S. (2017). An NF-kappaB Transcription-Factor-Dependent Lineage-Specific Transcriptional Program Promotes Regulatory T Cell Identity and Function. *Immunity, 47*(3), 450-465 e455. doi:10.1016/j.immuni.2017.08.010

Oh, J., & Shin, J. S. (2015). The Role of Dendritic Cells in Central Tolerance. *Immune Netw, 15*(3), 111-120. doi:10.4110/in.2015.15.3.111

Omilusik, K. D., & Goldrath, A. W. (2017). The origins of memory T cells. *Nature, 552*.

Park, H. H. (2018). Structure of TRAF Family: Current Understanding of Receptor Recognition. *Frontiers in Immunology, 9*(1999). doi:10.3389/fimmu.2018.01999

Parkin, J., & Cohen, B. (2001). An overview of the immune system. *Lancet, 357*(9270), 1777-1789. doi:10.1016/s0140-6736(00)04904-7

Pelzer, C., Cabalzar, K., Wolf, A., Gonzalez, M., Lenz, G., & Thome, M. (2013). The protease activity of the paracaspase MALT1 is controlled by monoubiquitination. *Nat Immunol, 14*(4), 337-345. doi:10.1038/ni.2540

Perniola, R. (2018). Twenty Years of AIRE. *Frontiers in Immunology, 9*(98). doi:10.3389/fimmu.2018.00098

Picard, C., Bobby Gaspar, H., Al-Herz, W., Bousfiha, A., Casanova, J. L., Chatila, T., . . . Sullivan, K. E. (2018). International Union of Immunological Societies: 2017 Primary Immunodeficiency Diseases Committee Report on Inborn Errors of Immunity. *J Clin Immunol, 38*(1), 96-128. doi:10.1007/s10875-017-0464-9

Polic, B., Kunkel, D., Scheffold, A., & Rajewsky, K. (2001). How αß T cells deal with induced TCRα ablation. *PNAS, 98*(15), 8744-8749.

Poueymirou, W. T., Auerbach, W., Frendewey, D., Hickey, J. F., Escaravage, J. M., Esau, L., . . . Valenzuela, D. M. (2007). F0 generation mice fully derived from gene-targeted embryonic stem cells allowing immediate phenotypic analyses. *Nat Biotechnol, 25*(1), 91-99. doi:10.1038/nbt1263

Punwani, D., Wang, H., Chan, A. Y., Cowan, M. J., Mallott, J., Sunderam, U., . . . Puck, J. M. (2015). Combined immunodeficiency due to MALT1 mutations, treated by hematopoietic cell transplantation. *J Clin Immunol, 35*(2), 135-146. doi:10.1007/s10875-014-0125-1

Qiao, Q., Yang, C., Zheng, C., Fontan, L., David, L., Yu, X., . . . Wu, H. (2013). Structural architecture of the CARMA1/Bcl10/MALT1 signalosome: nucleation-induced filamentous assembly. *Mol Cell, 51*(6), 766-779. doi:10.1016/j.molcel.2013.08.032

Qin, Y., Fang, K., Lu, N., Hu, Y., Tian, Z., & Zhang, C. (2019). Interferon gamma inhibits the differentiation of mouse adult liver and bone marrow hematopoietic stem cells by inhibiting the activation of notch signaling. *Stem Cell Research & Therapy, 10*(1), 210. doi:10.1186/s13287-019-1311-0

Quancard, J., Simic, O., Pissot Soldermann, C., Aichholz, R., Blatter, M., Renatus, M., . . . Schlapbach, A. (2020). Optimization of the In Vivo Potency of Pyrazolopyrimidine MALT1 Protease

Inhibitors by Reducing Metabolism and Increasing Potency in Whole Blood. *J Med Chem, 63*(23), 14594-14608. doi:10.1021/acs.jmedchem.0c01246

Raphael, I., Nalawade, S., Eagar, T. N., & Forsthuber, T. G. (2015). T cell subsets and their signature cytokines in autoimmune and inflammatory diseases. *Cytokine, 74*(1), 5-17. doi:10.1016/j.cyto.2014.09.011

Raychaudhuri, S., Thomson, B. P., Remmers, E. F., Eyre, S., Hinks, A., Guiducci, C., . . . Plenge, R. M. (2009). Genetic variants at CD28, PRDM1 and CD2/CD58 are associated with rheumatoid arthritis risk. *Nat Genet, 41*(12), 1313-1318. doi:10.1038/ng.479

Rebeaud, F., Hailfinger, S., Posevitz-Fejfar, A., Tapernoux, M., Moser, R., Rueda, D., . . . Thome, M. (2008). The proteolytic activity of the paracaspase MALT1 is key in T cell activation. *Nat Immunol, 9*(3), 272-281. doi:10.1038/ni1568

Reiley, W. W., Jin, W., Lee, A. J., Wright, A., Wu, X., Tewalt, E. F., . . . Sun, S. C. (2007). Deubiquitinating enzyme CYLD negatively regulates the ubiquitin-dependent kinase Tak1 and prevents abnormal T cell responses. *J Exp Med, 204*(6), 1475-1485. doi:10.1084/jem.20062694

Roose, J. P., Diehn, M., Tomlinson, M. G., Lin, J., Alizadeh, A. A., Botstein, D., . . . Weiss, A. (2003). T cell receptor-independent basal signaling via Erk and Abl kinases suppresses RAG gene expression. *PLoS Biol, 1*(2), E53. doi:10.1371/journal.pbio.0000053

Rosebeck, S., Lim, M. S., Elenitoba-Johnson, K. S., McAllister-Lucas, L. M., & Lucas, P. C. (2016). API2-MALT1 oncoprotein promotes lymphomagenesis via unique program of substrate ubiquitination and proteolysis. *World J Biol Chem, 7*(1), 128-137. doi:10.4331/wjbc.v7.i1.128

Rosenbaum, M., Gewies, A., Pechloff, K., Heuser, C., Engleitner, T., Gehring, T., . . . Ruland, J. (2019). Bcl10-controlled Malt1 paracaspase activity is key for the immune suppressive function of regulatory T cells. *Nat Commun, 10*(1), 2352. doi:10.1038/s41467-019-10203-2

Ruefli-Brasse, A. A., French, D. M., & Dixit, V. M. (2003). Regulation of NF-κB–Dependent Lymphocyte Activation and Development by Paracaspase. *Science, 302*, 1581-1584.

Ruefli-Brasse, A. A., Lee, W. P., Hurst, S., & Dixit, V. M. (2004). Rip2 participates in Bcl10 signaling and T-cell receptor-mediated NF-kappaB activation. *J Biol Chem, 279*(2), 1570-1574. doi:10.1074/jbc.C300460200

Ruland, J. (2008). CARD9 signaling in the innate immune response. *Ann N Y Acad Sci, 1143*, 35-44. doi:10.1196/annals.1443.024

Ruland, J., Duncan, G. S., Elia, A., del Barco Barrantes, I., Nguyen, L., Plyte, S., . . . Mak, T. W. (2001). Bcl10 is a positive regulator of antigen receptor-induced activation of NF-kappaB and neural tube closure. *Cell, 104*(1), 33-42. doi:10.1016/s0092-8674(01)00189-1

Ruland, J., & Hartjes, L. (2019). CARD-BCL-10-MALT1 signalling in protective and pathological immunity. *Nat Rev Immunol, 19*(2), 118-134. doi:10.1038/s41577-018-0087-2

Ruland, J., Wakeham, A., Duncan, G. S., & Mak, T. W. (2003). Differential Requirement for Malt1 in T and B Cell Antigen Receptor Signaling. *Immunity, 19*, 749-758.

Sakaguchi, S., Mikami, N., Wing, J. B., Tanaka, A., Ichiyama, K., & Ohkura, N. (2020). Regulatory T Cells and Human Disease. *Annual Review of Immunology, 38*, 541–566.

Sakaguchi, S., Yamaguchi, T., Nomura, T., & Ono, M. (2008). Regulatory T cells and immune tolerance. *Cell, 133*(5), 775-787. doi:10.1016/j.cell.2008.05.009

Sasaki, Y., & Iwai, K. (2016). Roles of the NF-κB Pathway in B-Lymphocyte Biology. *Curr Top Microbiol Immunol, 393*, 177-209. doi:10.1007/82_2015_479

Schlauderer, F., Seeholzer, T., Desfosses, A., Gehring, T., Strauss, M., Hopfner, K. P., . . . Lammens, K. (2018). Molecular architecture and regulation of BCL10-MALT1 filaments. *Nat Commun, 9*(1), 4041. doi:10.1038/s41467-018-06573-8

Schmidt-Supprian, M., Tian, J., Grant, E. P., Pasparakis, M., Maehr, R., Ovaa, H., . . . Rajewsky, K. (2004). Differential dependence of CD4+CD25+ regulatory and natural killer-like T cells on signals leading to NF-kB activation. *PNAS, 101*(13), 4566-4571.

Schmitz, M. L., & Krappmann, D. (2006). Controlling NF-κB activation in T cells by costimulatory receptors. *Cell Death & Differentiation, 13*(5), 834-842. doi:10.1038/sj.cdd.4401845

Schulze-Luehrmann, J., & Ghosh, S. (2006). Antigen-receptor signaling to nuclear factor kappa B. *Immunity, 25*(5), 701-715. doi:10.1016/j.immuni.2006.10.010

Seeholzer, T., Kurz, S., Schlauderer, F., Woods, S., Gehring, T., Widmann, S., . . . Krappmann, D. (2018). BCL10-CARD11 Fusion Mimics an Active CARD11 Seed That Triggers Constitutive BCL10 Oligomerization and Lymphocyte Activation. *Front Immunol, 9*, 2695. doi:10.3389/fimmu.2018.02695

Shi, J. H., & Sun, S. C. (2018). Tumor Necrosis Factor Receptor-Associated Factor Regulation of Nuclear Factor kappaB and Mitogen-Activated Protein Kinase Pathways. *Front Immunol, 9*, 1849. doi:10.3389/fimmu.2018.01849

Sommer, K., Guo, B., Pomerantz, J. L., Bandaranayake, A. D., Moreno-Garcia, M. E., Ovechkina, Y. L., & Rawlings, D. J. (2005). Phosphorylation of the CARMA1 linker controls NF-kappaB activation. *Immunity, 23*(6), 561-574. doi:10.1016/j.immuni.2005.09.014

Srinivasan, L., Sasaki, Y., Calado, D. P., Zhang, B., Paik, J. H., DePinho, R. A., . . . Rajewsky, K. (2009). PI3 kinase signals BCR-dependent mature B cell survival. *Cell, 139*(3), 573-586. doi:10.1016/j.cell.2009.08.041

Staal, J., Driege, Y., Bekaert, T., Demeyer, A., Muyllaert, D., Van Damme, P., . . . Beyaert, R. (2011). T-cell receptor-induced JNK activation requires proteolytic inactivation of CYLD by MALT1. *EMBO J, 30*(9), 1742-1752. doi:10.1038/emboj.2011.85

Stefanová, I., Dorfman, J. R., & Germain, R. N. (2002). Self-recognition promotes the foreign antigen sensitivity of naive T lymphocytes. *Nature, 420*(6914), 429-434. doi:10.1038/nature01146

Stefanová, I., Hemmer, B., Vergelli, M., Martin, R., Biddison, W. E., & Germain, R. N. (2003). TCR ligand discrimination is enforced by competing ERK positive and SHP-1 negative feedback pathways. *Nat Immunol, 4*(3), 248-254. doi:10.1038/ni895

Stepensky, P., Keller, B., Buchta, M., Kienzler, A. K., Elpeleg, O., Somech, R., . . . Warnatz, K. (2013). Deficiency of caspase recruitment domain family, member 11 (CARD11), causes profound combined immunodeficiency in human subjects. *J Allergy Clin Immunol, 131*(2), 477-485 e471. doi:10.1016/j.jaci.2012.11.050

Sun, L., Deng, L., Ea, C.-K., Xia, Z.-P., & Chen, Z. J. (2004). The TRAF6 Ubiquitin Ligase and TAK1 Kinase Mediate IKK Activation by BCL10 and MALT1 in T Lymphocytes. *Molecular Cell, 14*, 289-301.

Sun, L., Deng, L., Ea, C. K., Xia, Z. P., & Chen, Z. J. (2004). The TRAF6 ubiquitin ligase and TAK1 kinase mediate IKK activation by BCL10 and MALT1 in T lymphocytes. *Mol Cell, 14*(3), 289-301. doi:10.1016/s1097-2765(04)00236-9

Swain, S. L. (1995). T-Cell Subsets: Who does the polarizing? *Current Biology, 5*(8), 849-851. doi:https://doi.org/10.1016/S0960-9822(95)00170-9

Swiatczak, B., & Cohen, I. R. (2015). Gut feelings of safety: tolerance to the microbiota mediated by innate immune receptors. *Microbiol Immunol, 59*(10), 573-585. doi:10.1111/1348-0421.12318

Tanaka, T., Narazaki, M., & Kishimoto, T. (2016). Immunotherapeutic implications of IL-6 blockade for cytokine storm. *Immunotherapy, 8*(8), 959-970. doi:10.2217/imt-2016-0020

Taniuchi, I. (2018). CD4 Helper and CD8 Cytotoxic T Cell Differentiation. *Annu Rev Immunol, 36*, 579-601. doi:10.1146/annurev-immunol-042617-053411

Teh, P. P., Vasanthakumar, A., & Kallies, A. (2015). Chapter Seven - Development and Function of Effector Regulatory T Cells. In A. Liston (Ed.), *Progress in Molecular Biology and Translational Science* (Vol. 136, pp. 155-174): Academic Press.

Thome, M., Charton, J. E., Pelzer, C., & Hailfinger, S. (2010). Antigen receptor signaling to NF-kappaB via CARMA1, BCL10, and MALT1. *Cold Spring Harb Perspect Biol, 2*(9), a003004. doi:10.1101/cshperspect.a003004

Tokunaga, F., & Iwai, K. (2012). LUBAC, a novel ubiquitin ligase for linear ubiquitination, is crucial for inflammation and immune responses. *Microbes Infect, 14*(7-8), 563-572. doi:10.1016/j.micinf.2012.01.011

Torres, J. M., Martinez-Barricarte, R., Garcia-Gomez, S., Mazariegos, M. S., Itan, Y., Boisson, B., . . . Perez de Diego, R. (2014). Inherited BCL10 deficiency impairs hematopoietic and nonhematopoietic immunity. *J Clin Invest, 124*(12), 5239-5248. doi:10.1172/JCI77493

Turvey, S. E., Durandy, A., Fischer, A., Fung, S. Y., Geha, R. S., Gewies, A., . . . Warnatz, K. (2014). The CARD11-BCL10-MALT1 (CBM) signalosome complex: Stepping into the limelight of human primary immunodeficiency. *J Allergy Clin Immunol, 134*(2), 276-284. doi:10.1016/j.jaci.2014.06.015

Uehata, T., Iwasaki, H., Vandenbon, A., Matsushita, K., Hernandez-Cuellar, E., Kuniyoshi, K., . . . Akira, S. (2013). Malt1-induced cleavage of regnase-1 in CD4(+) helper T cells regulates immune activation. *Cell, 153*(5), 1036-1049. doi:10.1016/j.cell.2013.04.034

Uren, A. G., O'Rourke, K., Aravind, L., Pisabarro, M. T., Seshagiri, S., Koonin, E. V., & Dixit, V. M. (2000). Identification of Paracaspases and Metacaspases: Two Ancient Families of Caspase-like Proteins, One of which Plays a Key Role in MALT Lymphoma. *Molecular Cell, 6*, 961-967.

Vinuesa, C. G., Cook, M. C., Angelucci, C., Athanasopoulos, V., Rui, L., Hill, K. M., . . . Goodnow, C. C. (2005). A RING-type ubiquitin ligase family member required to repress follicular helper T cells and autoimmunity. *Nature, 435*(7041), 452-458. doi:10.1038/nature03555

Vogel, K. U., Edelmann, S. L., Jeltsch, K. M., Bertossi, A., Heger, K., Heinz, G. A., . . . Heissmeyer, V. (2013). Roquin paralogs 1 and 2 redundantly repress the Icos and Ox40 costimulator mRNAs and control follicular helper T cell differentiation. *Immunity, 38*(4), 655-668. doi:10.1016/j.immuni.2012.12.004

von Boehmer, H., & Fehling, H. J. (1997). Structure and function of the pre-T cell receptor. *Annu Rev Immunol, 15*, 433-452. doi:10.1146/annurev.immunol.15.1.433

Wegener, E., Oeckinghaus, A., Papadopoulou, N., Lavitas, L., Schmidt-Supprian, M., Ferch, U., . . . Krappmann, D. (2006). Essential role for IkappaB kinase beta in remodeling Carma1-Bcl10-Malt1 complexes upon T cell activation. *Mol Cell, 23*(1), 13-23. doi:10.1016/j.molcel.2006.05.027

Wiesmann, C., Leder, L., Blank, J., Bernardi, A., Melkko, S., Decock, A., . . . Renatus, M. (2012). Structural determinants of MALT1 protease activity. *J Mol Biol, 419*(1-2), 4-21. doi:10.1016/j.jmb.2012.02.018

Williams, L. M., & Rudensky, A. Y. (2007). Maintenance of the Foxp3-dependent developmental program in mature regulatory T cells requires continued expression of Foxp3. *Nat Immunol, 8*(3), 277-284. doi:10.1038/ni1437

Willis, T. G., Jadayel, D. M., Du, M. Q., Peng, H., Perry, A. R., Abdul-Rauf, M., . . . Dyer, M. J. (1999). Bcl10 is involved in t(1;14)(p22;q32) of MALT B cell lymphoma and mutated in multiple tumor types. *Cell, 96*(1), 35-45. doi:10.1016/s0092-8674(00)80957-5

Wu, C.-J., & Ashwell, J. D. (2008). NEMO recognition of ubiquitinated Bcl10 is required for T cell receptor-mediated NF-kappaB activation. *Proceedings of the National Academy of Sciences of the United States of America, 105*(8), 3023-3028. doi:10.1073/pnas.0712313105

Xue, L., Morris, S. W., Orihuela, C., Tuomanen, E., Cui, X., Wen, R., & Wang, D. (2003). Defective development and function of Bcl10-deficient follicular, marginal zone and B1 B cells. *Nat Immunol, 4*(9), 857-865. doi:10.1038/ni963

Yamamoto, M., Okamoto, T., Takeda, K., Sato, S., Sanjo, H., Uematsu, S., . . . Akira, S. (2006). Key function for the Ubc13 E2 ubiquitin-conjugating enzyme in immune receptor signaling. *Nat Immunol, 7*(9), 962-970. doi:10.1038/ni1367

Yamasoba, D., Sato, K., Ichinose, T., Imamura, T., Koepke, L., Joas, S., . . . Takeuchi, O. (2019). N4BP1 restricts HIV-1 and its inactivation by MALT1 promotes viral reactivation. *Nat Microbiol, 4*(9), 1532-1544. doi:10.1038/s41564-019-0460-3

Yu, J. W., Jeffrey, P. D., Ha, J. Y., Yang, X., & Shi, Y. (2011). Crystal structure of the mucosa-associated lymphoid tissue lymphoma translocation 1 (MALT1) paracaspase region. *Proc Natl Acad Sci U S A, 108*(52), 21004-21009. doi:10.1073/pnas.1111708108

Zhang, J., Quintal, L., Atkinson, A., Williams, B., Grunebaum, E., & Roifman, C. M. (2005). Novel RAG1 mutation in a case of severe combined immunodeficiency. *Pediatrics, 116*(3), e445-449. doi:10.1542/peds.2005-0369

Zhou, X., Jeker, L. T., Fife, B. T., Zhu, S., Anderson, M. S., McManus, M. T., & Bluestone, J. A. (2008). Selective miRNA disruption in T reg cells leads to uncontrolled autoimmunity. *J Exp Med, 205*(9), 1983-1991. doi:10.1084/jem.20080707

9 Abbreviations

° C	degrees Celsius
ABC	activated B cell-like (DLBCL)
APC	antigen presenting cell
APC	allophycocyanin
BCL10	B cell chronic lymphocytic leukemia/lymphoma 10
BCR	B cell receptor
BENTA	B cell expansion with NF-κB and T cell anergy
BM	bone marrow
bp	base pair
BSA	bovine serum albumin
CARD	caspase-recruitment domain
CARMA1	CARD-containing MAGUK 1 (also known as CARD11)
CARD11	Caspase recruitment domain-containing protein 11
Cas9	CRISPR-associated protein-9
CBM	CARMA1-BCL10-MALT1
CC	coiled coil
Co-IP	Co-immunoprecipitation
CRISPR	Clustered Regularly Interspaced Short Palindromic Repeats
C-terminus	Carboxyl-terminus
CYLD	cylindromatosis
DAG	diacylglycerol
DD	death domain
DLBCL	diffuse large B cell lymphoma
DMEM	Dulbecco's Modified Eagle Medium
DMSO	dimethyl sulfoxide
DNA	deoxyribonucleic acid
dNTP	deoxyribonucleotide triphosphate
ds	double-stranded
DTT	dithiothreitol
DUB	deubiquitinase
ECL	enhanced chemiluminescence
EDTA	ethylenediaminetetraacetic acid
EGFP	enhanced green fluorescent protein
EMSA	electrophoretic mobility shift assay
ES	embryonal stem (cell)
EUCOMM	European Conditional Mouse Mutagenesis Program
FBS	fetal bovine serum
FCS	fetal calf serum
FITC	fluorescein isothiocyanate
FOXP3	forkhead box p3
h	human
HCG	human chorionic gonadotropin
HEPES	2-[4-(2-Hydroxyethyl)-1-piperazino]-ethansulfonic acid

HOIL1	heme-oxidized IRP2 ubiquitin ligase 1
HRP	horseradish peroxidase
ICOS	inducible T cell co-stimulator
IFNγ	interferon γ (gamma)
Ig	immunoglobulin
IKK	IκB kinase
Iono	ionomycin
IP_3	inositol 1,4,5-trisphosphate
IRF	interferon regulatory factors
ITAM	immunoreceptor tyrosine-based activation motif
IκB	inhibitor of κB
JNK	c-Jun N-terminal kinase
kb	kilo base
kDa	kilo Dalton
KH2PO4	potassium hydrogen phosphate
KO	knockout
LAT	linker for activation of T cells
LB	Luria-Bertani (medium)
LN	lymph node
LUBAC	linear ubiquitin chain assembly complex
MACS	magnetic-activated cell sorting
MAGUK	membrane associated guanylate kinase
MALT1	mucosa associated lymphoid tissue lymphoma translocation protein 1
MAPK	mitogen activated protein kinase
mES	murine embryonic stem (cell)
MFI	mean fluorescence intensity
mg	milligram
MgCl2	magnesium chloride
MHC	major histocompatibility complex
min	minute
mL	milliliter
mRNA	messenger RNA
MZ	marginal zone
NaCl	sodium chloride
NaF	sodium fluoride
NEAA	non-essential amino acids
NEMO	NF-κB essential modulator
NFAT	nuclear factor of activated T cells
NF-κB	nuclear factor kappa B
NK	natural killer
ng	nanogram
nm	nanometer
N-terminus	amino-terminus
P/S	penicillin/streptomycin
PBS	phosphate buffered saline

PBS-T	PBS-Tween 20
PCR	polymerase chain reaction
PDK1	phosphoinositide-dependent kinase 1
PDZ	PSD-95/DLG/ZO1 homology
PE	phycoerythrin
PerCP	Peridinin-Chlorophyll-protein
PE-Cy7	phycoerythrin-cyanine 7
PFA	paraformaldehyde
PI3K	phosphoinositide 3 kinase
PIP2	phosphatidyl inositol 4,5-bisphosphate
PIP3	phosphatidyl inositol 3,4,5-trisphosphate
PKC	protein kinase C
PLCγ	phospholipase C γ (gamma)
PM	paracaspase mutant
PMA	phorbol 12-myristate 13-acetate
PMSG	pregnant mare's serum gonadotropin
RNA	ribonucleic acid
rpm	rounds per minute
RT	room temperature
RT-PCR	real-time PCR
sec	second
SDS	Sodium dodecyl sulfate
SDS-PAGE	SDS polyacrylamide gel electrophoresis
SEM	standard error of the mean
SLP76	SH2-domain containing leukocyte protein of 76 kDa
T6BM	TRAF6 binding motif
TAB	TAK1 binding protein
TAK	transforming growth factor beta activated kinase
TAE	Tris-acetate-EDTA
TBM	TRAF6 binding mutant
TBMPM	TRAF6 binding mutant – paracaspase mutant
TCR	T cell receptor
Teff	T effector
TEMED	Tetramethylethylenediamine
TLR	toll like receptor
Tm	melting temperature
TNF	tumor necrosis factor
TRAF	tumor-necrosis factor associated receptor-associated factor
Tconv	conventional T cell
Treg	regulatory T cell
Tris	Tris(hydroxymethyl)-aminomethan
U	Unit
Ubc13	Ubiquitin-conjugating enzyme E2 13
Uev1A	Ubiquitin-conjugating enzyme E2 variant 1A
UTR	untranslated region

mV	millivolt
WB	Western Blot
WT	wildtype
ZAP70	zeta-chain-associated protein 70 kDa
µg	microgram

10 Appendix

10.1 Publications

O'Neill, T. J.*, Seeholzer, T.*, Gewies, A.*, Gehring, T., Giesert, F., Hamp, I., Graß, C., Schmidt, H., Kriegsmann, K., Tofaute, M. J., Demski, K., Poth, T., Rosenbaum, M., Schnalzger, T., Ruland, J., Göttlicher, M., Kriegsmann, M., Naumann, R., Heissmeyer, V., Plettenburg, O., … Krappmann, D. (2021). TRAF6 prevents fatal inflammation by homeostatic suppression of MALT1 protease. Science immunology, 6(65), eabh2095. https://doi.org/10.1126/sciimmunol.abh2095

Hamp, I.*, **O'Neill, T. J.***, Plettenburg, O., & Krappmann, D. (2021). A patent review of MALT1 inhibitors (2013-present). Expert opinion on therapeutic patents, 31(12), 1079–1096. https://doi.org/10.1080/13543776.2021.1951703

Kutukculer, N., Seeholzer, T., **O'Neill, T. J.**, Graß, C., Aykut, A., Karaca, N. E., Durmaz, A., Cogulu, O., Aksu, G., Gehring, T., Gewies, A., & Krappmann, D. (2021). Human immune disorder associated with homozygous hypomorphic mutation affecting MALT1B splice variant. The Journal of allergy and clinical immunology, 147(2), 775–778.e8. https://doi.org/10.1016/j.jaci.2020.07.034

Arlt, E., Fraticelli, M., Tsvilovskyy, V., Nadolni, W., Breit, A., **O'Neill, T. J.**, Resenberger, S., Wennemuth, G., Wahl-Schott, C., Biel, M., Grimm, C., Freichel, M., Gudermann, T., Klugbauer, N., Boekhoff, I., & Zierler, S. (2020). TPC1 deficiency or blockade augments systemic anaphylaxis and mast cell activity. Proceedings of the National Academy of Sciences of the United States of America, 117(30), 18068–18078. https://doi.org/10.1073/pnas.1920122117

van de Plassche, M., **O'Neill, T. J.**, Seeholzer, T., Turk, B., Krappmann, D., & Verhelst, S. (2020). Use of Non-Natural Amino Acids for the Design and Synthesis of a Selective, Cell-Permeable MALT1 Activity-Based Probe. Journal of medicinal chemistry, 63(8), 3996–4004. https://doi.org/10.1021/acs.jmedchem.9b01879

Gehring, T., Erdmann, T., Rahm, M., Graß, C., Flatley, A., **O'Neill, T. J.**, Woods, S., Meininger, I., Karayel, O., Kutzner, K., Grau, M., Shinohara, H., Lammens, K., Feederle, R., Hauck, S. M., Lenz, G., & Krappmann, D. (2019). MALT1 Phosphorylation Controls Activation of T Lymphocytes and Survival of ABC-DLBCL Tumor Cells. Cell reports, 29(4), 873–888.e10. https://doi.org/10.1016/j.celrep.2019.09.040

10.2 Acknowledgements

I would like to thank Daniel Krappmann for guiding me over the last three and a half years with insight and patience, and for providing an excellent working environment.

My further appreciation to the members of my thesis advisory committee and doctoral defense committee for their advice and review of my thesis: Prof. Dr. Oliver Plettenburg, Prof. Dr. Michael Boshart, Prof. Dr. Christof Osman, Prof. Dr. Pascal Falter-Braun, Prof. Dr. Jürgen Soll, and Prof. Dr. Heinrich Leonhardt.

I thank all of my colleagues, past and present, for their support during my PhD. I could not have done it without you! Further thanks to Prof. Dr. Martin Göttlicher and Dr. Andrea Hofmann for their assistance with the mouse databank and Dr. Sibylle Sabrautzki for her work as our Animal Welfare Officer. Additionally, thank you to all of the HMGU animal caretakers who made this work possible.

Finally, I would like to thank my family for their love and support in my decision to pursue this thesis so far from home. A special thank you to Joana for the love and motivation that she gave me on good days and bad, and for her patience through my late evenings and long weekends in the lab.